THE VIBRATIONAL SPECTRA

OF RECTANGULAR PLATES

by

MANSOOR MOHAMMAD HUSSAIN ALI AL-HELALY

Submitted for the degree of

Doctor of Philosophy

at the

University of Aston in Birmingham

Department of Electrical and Electronic Engineering

December 1981

THE VIBRATION SPECTRA OF RECTANGULAR PLATES

M. M. H. ALI AL-HELALY

Summary

The wire drive pulse-echo system has been extensively used to excite and measure modes of vibration of thin rectangular plates. The frequency spectra of different modes have been investigated as a function of the material elastic moduli and the plate geometry. Most of the work was carried out on isotropic materials.

For square plates a wide selection of materials were used. These were made isotropic in their in-plane dimensions where the displacements are taking place. The range of materials enabled the dependence on Poisson's ratio to be investigated. A method of determining the value of Poisson's ratio resulted from this investigation.

Certain modes are controlled principally by the shear modulus. Of these the fundamental has two nodal lines across the plate surface. One of them, which has nodes at the corners, (the Lamé mode) is uniquely a pure shear mode where the diagonal is a full wave length. One controlled by the Young's modulus has been found.

The precise harmonic relationship of the Lamé mode series in square and rectangular plates was established. Use of the Rayleigh-Lamb equation has extended the theoretical support.

The low order modes were followed over a wide range of sides ratios. Two fundamental types of modes have been recognised: These are the longitudinal modes where the frequency is controlled by the length of the plate only and the $2\ell f$ product has an asymptotic value approaching the rod velocity. The other type is the in-plane flexural modes (in effect a flexurally vibrating bar where the ℓ^2/w is the geometrical parameter). Where possible the experimental work was related to theory. Other modes controlled by the width dimension of the plate were followed.

Anisotropic materials having rolled sheet elastic symmetry were investigated in terms of the appropriate theory. The work has been extended to examine materials from welds in steel plates.

Key Words

ACKNOWLEDGEMENTS

The author wishes to express his sincere gratitude to his supervisor, Dr. J. F. W. Bell, for his guidance and encouragement during his study. Thanks are also due to Mr. F. Hunt, Mr. B. Hale and the late Mr. E. Clenton in the departmental workshop for their fruitful help in preparing the samples required for these investigations.

Special thanks to all my colleagues and the technicians in the Department of Electrical and Electronic Engineering for their co-operative and their cheerful characters. Finally, thanks are due to Helen Turner for her patience in typing this thesis.

CONTENTS

LIST OF SYMBOLS

b   half the plate thickness, and its equal to half the width of the strip

ℓ the plate length

w   the plate width

f   the resonant frequency

λ the wave length

$\frac{2\pi}{\lambda}$ the propagation constant $= \gamma$

ω the radial frequency $= 2\pi f$

C_o the rod velocity

C_p the plate velocity

C_s the shear velocity

C_φ the phase velocity $= 2\ell f$

θ $(\frac{C_s}{C_p})^2 = (\frac{1-\sigma}{2})$

σ Poisson's ratio

φ the phase velocity normalised to the shear velocity

       $= (C_\varphi/C_s)$

φ_p the phase velocity normalised to the plate velocity

       $= (C_\varphi/C_p)$

φ_ℓ the phase velocity normalised to the rod velocity

       $= (C_\varphi/C_o)$

LIST OF FIGURES

(x)

CHAPTER ONE

GENERAL INTRODUCTION

The differential equations for in-plane vibrations of thin isotropic plates are well established (Love 1926[50]). Their solutions are particularly difficult for any but the simple circular plate, which in effect has only one boundary. The complete solutions involving all possible modes of vibration were obtained through numerical methods as used by Holland[30].

For the cartesian case of square and rectangular plates, only one satisfactory solution has been obtained. This is the Lamé mode of square plates where the corners are nodes. In this work, which is essentially experimental, a very large number of modes has been studied. Extensive use has been made of the approximate solutions obtained by Holland[31] and Redwood[48,49]. The pulse echo technique used is applicable to all materials and by using these with a wide selection of Poisson's ratio a fresh insight has been obtained.

As stated, for thin plates having rectangular geometries, a general solution of the differential equations of motion is not at present derivable. The difficulty of obtaining the exact solution is due to the restrictions imposed by the boundary conditions of the

straight edges of the plate. Certain related modes with no displacements at the corners have been solved by M. G. Lamé, 1866[45]. Since then, various approximate methods have been developed and employed to obtain the solution of other vibrational modes of rectangular plates. For instance, Ekstein[22] has applied a perturbation method; Mindlin and Medick[69] have developed an approximate plate theory; M. One[78] has approached the problem via an approximate theory based on an energy principle; EerNisse[21] has developed the coupled-mode theory; Lloyd and Redwood[48] have employed the finite difference method to find the solution of different rectangular plate vibrational modes; and recently R. Holland[31] has obtained more accurate results by applying a technique similar to that used by Ekstein. In his work, the frequency spectra for rectangular plate modes have been determined and represented as a function of Poisson's ratio. Extensive theoretical data for the normalised resonant frequencies of different modes as a function of width-to-length ratios and Poisson's ratio values are fully represented in reference (32).

Experimentally, the method employed to excite and to measure these modes has been only partially successful. This is initially due to the finite thickness of the plate, which requires special techniques to excite the different modes. An optical interference method[93] to observe

the displacements on the straight edge of the plate has been used. Other researchers[31,48,49,78] made use of a split-quartz electrode system on the surface of the plate, which required different electrode polarities to excite the different modes of vibration. This method is only applicable to piezoelectric materials.

In recent years, the explosive growth of electronic instruments in the fields of measurements, has made its contribution to measurements of the natural vibrations in response to the demand for material investigations. By determining their elastic and their mechanical properties the stress analysis of high temperature structural designs can be carried out. The wire drive type pulse-echo system has been developed by Bell[5,14] to excite and measure very weak resonant vibrations with high precision under suitable driving conditions. This has been successfully used to excite and measure the different resonant modes of disks[8,9,13] with an accuracy higher than 0.2%. The basic feature of the system and its diagram are illustrated in detail in Chapter Two.

The excellent results obtained from the disk by this method and the high accuracy of measured eigen values have induced further application of this system for the measurement of the frequency spectrum of rectangular plates.

The changes of the square plate resonant frequency

for different Poisson's ratio values have been
extensively investigated through the use of various
materials which were carefully machined to be isotropic
in their in-plane dimensions. It must be noted that the
disk modes have been taken as a reference in determining
the two elastic moduli (Young's modulus and Poisson's
ratio). The full results are covered in detail in
Chapter Three of this thesis.

The type of square plate modes which are principally
dependent on the shear modulus have been identified. The
sensitivity of certain modes towards the anisotropy of
the materials have also been shown through exploring the
nodal patterns of the vibrational modes, which make use
of the magnetostrictive probe.

Modes have been followed to a finite limit dictated
by signal strength of the plate width-to-length ratio.
Two beam vibrational modes have been distinguished: these
are the longitudinal and in-plane flexural modes. Other
modes whose frequencies are controlled by the width
dimension of the plate, have also been found and
investigated. Particularly interesting were modes
associated with end resonance and with purely plate
velocity.

Chapter Four and Chapter Five cover in detail the
full experimental results and the theoretical investigations,

which have employed the theory of the wave motion in the plate to a limited extent.

Further investigations related to the anisotropic measurements of the materials have been carried out in Chapter Six. The results indicate that the longitudinal modes of a long strip are sensitive to the direction of the grains w.r.t the plate length. The method has proved successful in measurement of the elastic constants of materials with this symmetry. The theoretical analysis supports the results and has given excellent identical results.

It is clearly established that the pulse-echo method is a sensitive instrument for measurements related to the materials characterisations and for investigations related to non-destructive testing and evaluations of the materials, which have unhomogeneous properties. Part of Chapter Six demonstrates an industrial application which has recently been published in a periodical journal (see reference (39)).

CHAPTER TWO

THE INSTRUMENTS AND THE TECHNIQUES

OF THE MEASUREMENTS

2.1 INTRODUCTION

For many years the resonance behaviour of structures
has attracted a great deal of attention. The
theoreticians have been engaged to apply different
methods to determine theoretical solutions for certain
modes of vibration under specific geometrical and
boundary conditions. Experimentally many methods have
been employed to excite and measure these vibrational
modes, obtaining the frequency spectrum and the
associated eigen functions.

Shaw (1955),[93] in his work used the optical
intereference method to observe the surface
displacement patterns of the vibrating disks. Others
used a split-quartz electrode system on the surface of
a plate, which required different electrode polarities
to excite different modes of vibration (P. Lloyd et al.,
1966) and (R. Holland, 1968).

With the growth of electronic instruments in recent
years in the field of measurement and as a result of the
demand in non-destructive evaluation of the materials,

the wire drive pulse-echo system used here was developed
to excite the natural vibrations of certain modes, and
can resolve very weak resonances with high precision under
suitable driving conditions.

Basically, the echo system designed for resonant
ultrasonic thermometry by Bell[5,6], since then it has been
used for many other applications, concerning
measurement of elastic constants and internal friction
of refractory materials over a wide temperature range.[8,9,12,13,14]

2.2 THE PULSE ECHO SYSTEM - BASIC FEATURE

The pulse echo system can be considered as two
individiual units; an electronic unit which generates
and receives the signals, and the transmission line.

In the electronics a signal generator produces bursts
of oscillation, the number being controlled manually.
These are coupled to the line with a magnetostrictive
transducer producing longitudinal stress waves. The
echoes reflected from the remote end of the line, where
the resonator is attached, are then amplified and
displayed on an oscilloscope. A schematic diagram for
the system is shown in Fig. 2.1 , the transmission line
is made of nickel wire or telcoseal (nickel-iron alloy)
and should be long enough to accommodate the number of
waves needed to obtain the required echo pattern without
signal overlap. To minimise the attenuation, and the

backward noise and echoes due to the presence of the kinks

in the line, it is important to stretch and anneal a part

of the line which is to be matched at a position about

$\lambda/4$ from the end of the transmission line. The highly

stressed line has low attenuation but poor magnetostrictive

properties. The annealed part of the line has good

magnetostrictive properties and being short does not

contribute excessively to the attenuation. A coil

provides electrical coupling and a magnet is required to

produce a d.c. bias. The coil is tuned by means of a

decade capacitor. The echo pattern forms as a result

of combining the echo signal from the resonator and the

backward signal from the junction. These two signals

are in reverse phase, consequently they form a cross-

over at a stage when the two signals have the same

amplitude. This cross-over or a "null" is a signature

that confirms the vibration of the resonator as it

indicates that the frequency of the transmitted waves

is equal to the natural resonant frequency of the

resonator. It also confirms the coupling to the line

which is jointed to the resonator by a cementing agent.

Figure 2.2 is a typical oscillogram of the echo

pattern. The echo pattern can be regarded as two parts;

the echo signal and the echo decrement which is the

exponential radiation of the stored energy due to the

resonance and it occurs after the echo signal. The

echo signals have an amplitude of the order of one volt

for an input sinusoidal signal of 30 V. peak-to-peak, which is sufficiently strong for background electronic noise to be neglected.

The attractive feature of this system is that the electronic unit is at a far distance from the resonator, so that the spectra of the bodies can be measured at various temperatures. (Chaplain, K. R., 1980).

The electronic unit is designed to generate a square wave signals in the range from 5 kHz to 1 MHz in frequency, the frequency limit of the techniques.

2.3 THE MAGNETOSTRICTIVE PROBE

This is another important part in the instruments used to identify and form the exact vibrational patterns of displacement for the resonator. Figure 2.3 shows a sketch for the magnetostrictive probe, it consists mainly of a thin nickel wire (0.5 mm diameter) terminated with a magnetostrictive coil to pick up the signal. It is tuned usually with an external capacitor, and has an attached magnet to polarize the field. The displacement pattern of the body can be explored by moving the line gently across the surface of the resonator. The probe signal will be zero at the nodal lines. Using a double beam oscilloscope this signal and the echo can be compared. In moving across a nodal line the probe signal reverses

the phase. Thus a precise picture can be built up for
the nodal pattern of a vibrating plate at different
resonant frequencies using this probe.

The probe can also be used to resolve two adjacent
resonant modes by identifying the most convenient
driving point for each individual mode.

2.4 THE VIBRATIONAL NODAL PATTERN IDENTIFICATION

Any individual mode of vibration will have a certain
displacement pattern of vibration (the eigen function).
This simple fact forms the basis for studying the
resonant frequency spectrum for the vibrational mode
of a thin rectangular plate.

Square isotropic plates were first investigated.
A resonance is excited when it has a component of
vibrational parallel to the line at the driving point.
Thus a diagonal corner drive will excite the Mason mode
of Fig. 2.4 which has two nodal lines parallel to the
sides of the plate but not the mode having the nodal
diagonals (Lamé mode).

Nodal patterns were explored using the probe described
in the previous section. In moving across a node the
amplitude goes through zero and the phase reverses. While
nodes at the edges were detected easily, observations of
the nodal lines on the face of the plate were difficult

as the vibrations were in-plane.

Figure 2.4 shows some typical vibrational patterns for simple resonances of a square plate. In the case of disk resonances, the driving point determines the nodal lines position (the mode is degenerate).

In a case where there were two nodes on each edge, giving four nodal lines it was uncertain whether these actually go through the centre giving a node or parallel to the sides giving an anti-node.

It might be important to mention that for higher modes, some nodal lines have a curved shape rather than a normal straight line proposed. This is also true of flexural (Chladni) vibrations.

2.5 THE DRIVING TECHNIQUE

Knowing the vibrational pattern of displacement for the plate resonant modes, a proper drive point could be selected to give an optimum mechanical coupling with the line, so that the echo signals have maximum amplitude at that drive point. This could be of major assistance in identifying and in resolving the different modes of square and rectangular plate, in addition, in following their vibrational spectra. It is obvious that the longitudinal mode requires a drive at the far end parallel to the length of the plate where the maximum displacements

-11-

are taking place. On the other hand, the flexural mode
(in-plane flexure of a rectangular plate) requires
different drive position, so that the displacements have
vectors parallel to the driving line.

Figure 2.5 shows the proper driving positions of
some square and rectangular plate modes. Typical modes
are shown in this figure and their vibrational patterns
are illustrated for several length-to-width ratios.

Maximising the coupling to the line will result in
a more significant form of the echo signals and,
consequently, more precise measured results will be
obtained.

As has been mentioned before, the magnetostrictive
probe can be of great assistance in executing this work,
as it helps to identify the best drive point of the plate
to the line. The coupled modes (modes occur at one
frequency) can be resolved by selecting and driving the
plate at an appropriate position where one of these modes
has maximum vibrational displacements to the line and the
other modes have a node at that point or have less
coupling to the line.
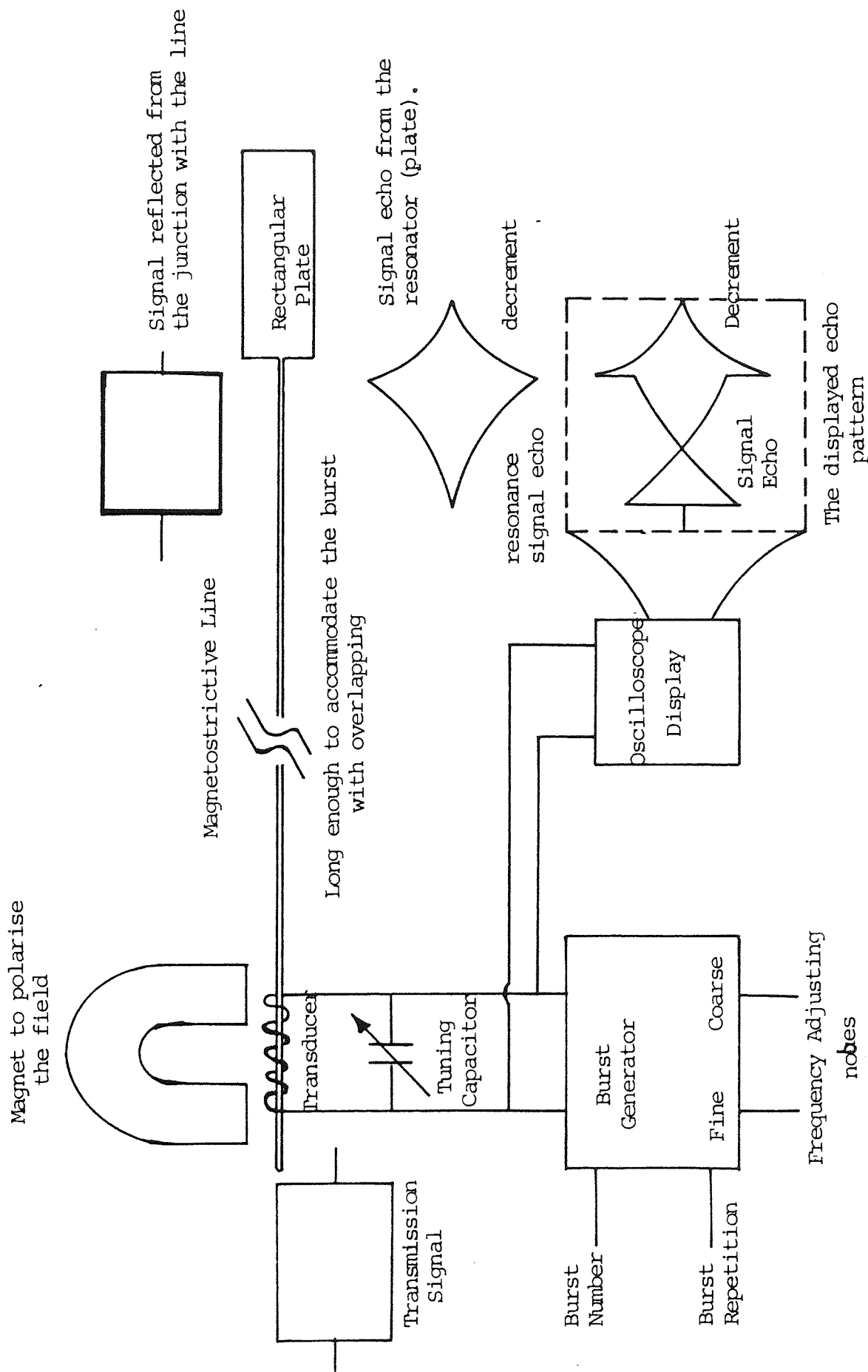
Fig. 2.1 Schematic diagram of the pulse-echo system shows the basic units to generate a transmission burst of certain oscillating numbers and of 30 volts amplitude. This gives an echo of about one volt. The transmission line must be magnetostrictive or part of it at least. It must be long enough to accommodate the number of waves needed to obtain the required echo pattern without signal overlap.

-13-
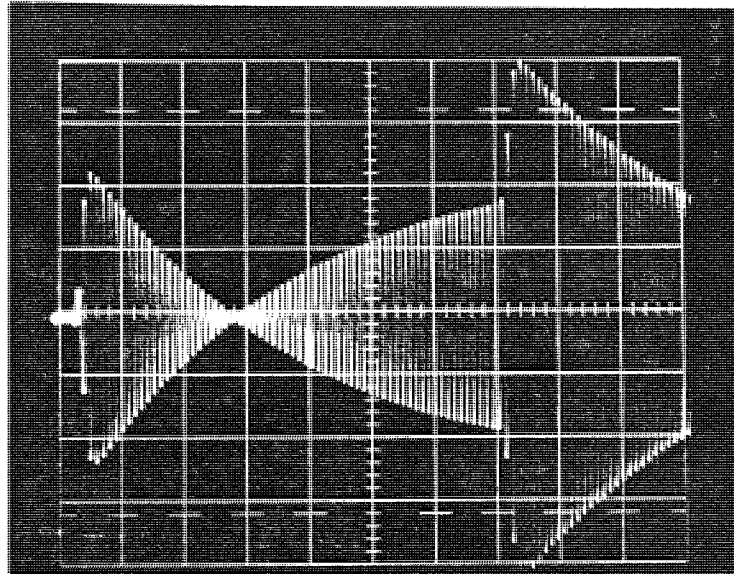
Fig. 2.2   A typical oscillogram of the echo pattern obtained
            as a result of combining the echo signal from
            the resonator and the backward signal from the
            joint of the transmission line. These two signals
            are in a reverse phase. The cross over indicates
            that the frequency of the transmitted waves is
            equal to the natural frequency of the resonator

Oscilloscope Display

A — The Probe Signal

B — The Echo Signal

Nickel wire 0.5 mm

Magnet

The channel (B) of the oscilloscope

The Pulse Echo Line

Plate at Resonance — Light and Lossy Support
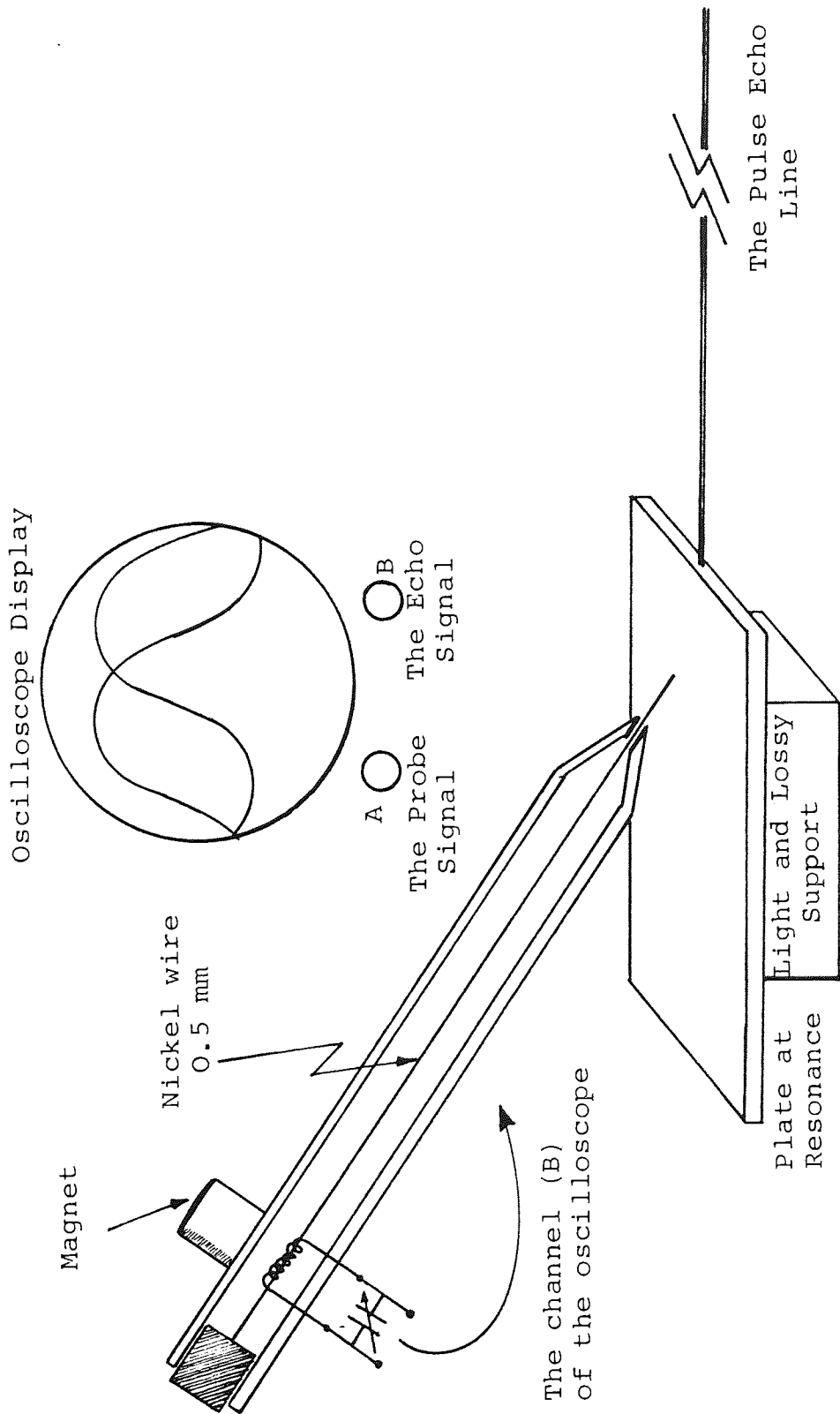
Fig. 2.3 This diagram shows the basic schematic structure of the magnetostrictive probe. The nodal pattern of the resonator can be pictured by displaying the signal of the vibrational displacements and comparing the phase of the motion with the echo signal of the transmission line.

-15-
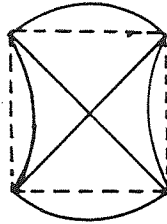
This is the mode first identified
and described by Lamé.

1 - coupled equal

2 - symmetrical vibration

3 - diagonal perfect nodes

4 - analogous to (1,2) disk modes
but drive do not control nodal
pattern.
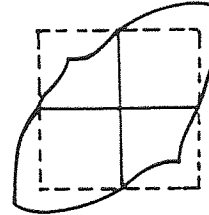
This is the famous Mason mode
which in Quartz has a zero
temperature co-efficient.

1 - equal coupling by diagonal
drive

2 - symmetrical vibration

3 - axes perfect nodes

4 - analogous to (1,2) disk.

(A)   (B)
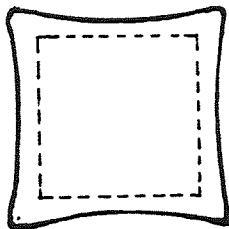
1 - no nodal point

2 - the coupling stronger at the
diagonal drive

3 - symmetrical vibration

4 - analogous to (1,R) disk
(Breathing mode)
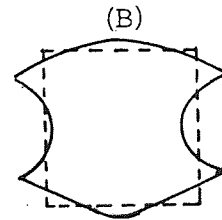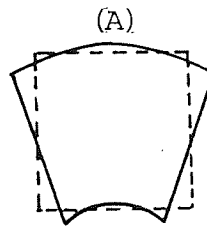
1 - strongly coupled to the edges

2 - (A) is the lowest;
Antisymmetrical vibration,
(B) is the highest;
Symmetrical vibration.

3 - (A) is a flexural type mode,
(B) is dilational tupe mode.

4 - Different dispersion curve,
End resonance mode.

Fig. 2.4   Shows some typical vibration patterns of square plate
resonance.   The mode is excited when it has a component
of vibration parallel to the line at the drive point.
(Dotted line plate at rest).

-16-
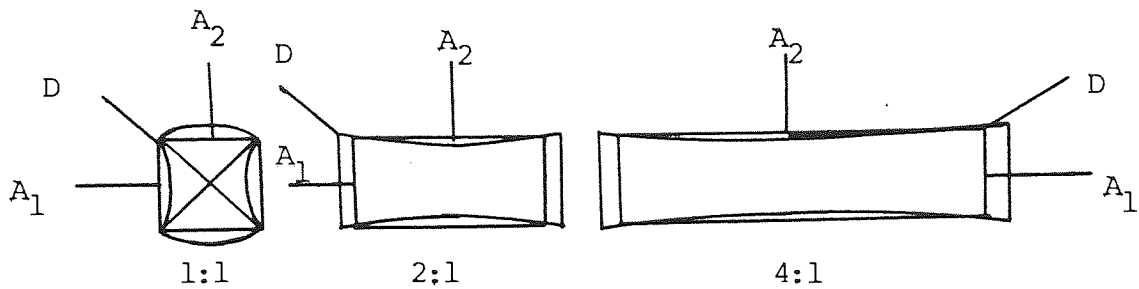
Coupling $A_1 = A_2$

D = Node

A_1 and A_2 out of phase

$A_1 > A_2$

D = significant coupling

A_1 strong

A_2 weak

D significant

(i)
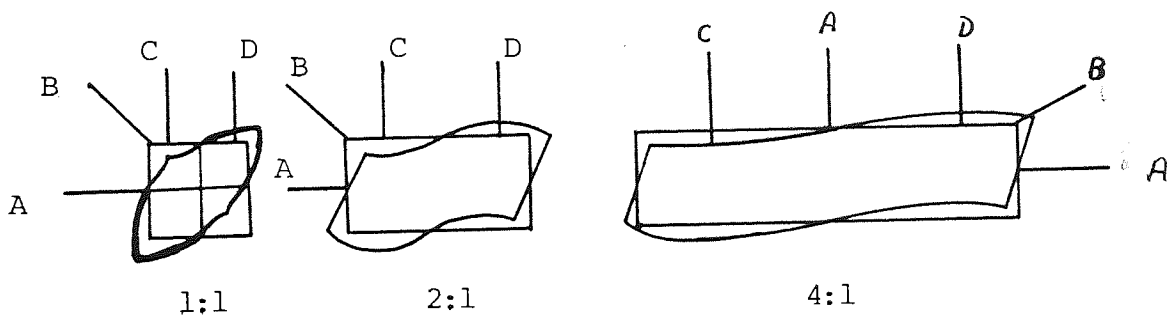
A is a node

Coupling B>C

C and D out of phase

A is a node

C>B

C and D out of phase

A is a node

B is weakly coupled

C and D best drive

C and D out of phase

(ii)

BREATHING MODE

1:1   2:1   4:1

ℓ:w ratio

$A_1 = A_2$ $A_2 > A_1$ Best drive is A or B
$B > A_1$ $B > A_2$ in phase   A and B are in phase.
A_1, A_2 and B are
in phase   (iii)

ℓ:w ratio   1:1   2:1   4:1

A is a node

D>C and D

C and D are out of phase

B and C are out of phase
          (iv)

ℓ:w ratio   1:1   2:1   No Vibration   4:1   No Vibration

(End resonance)   Best drive is when B is at an
                   angle of 45° from the edge.

(v)
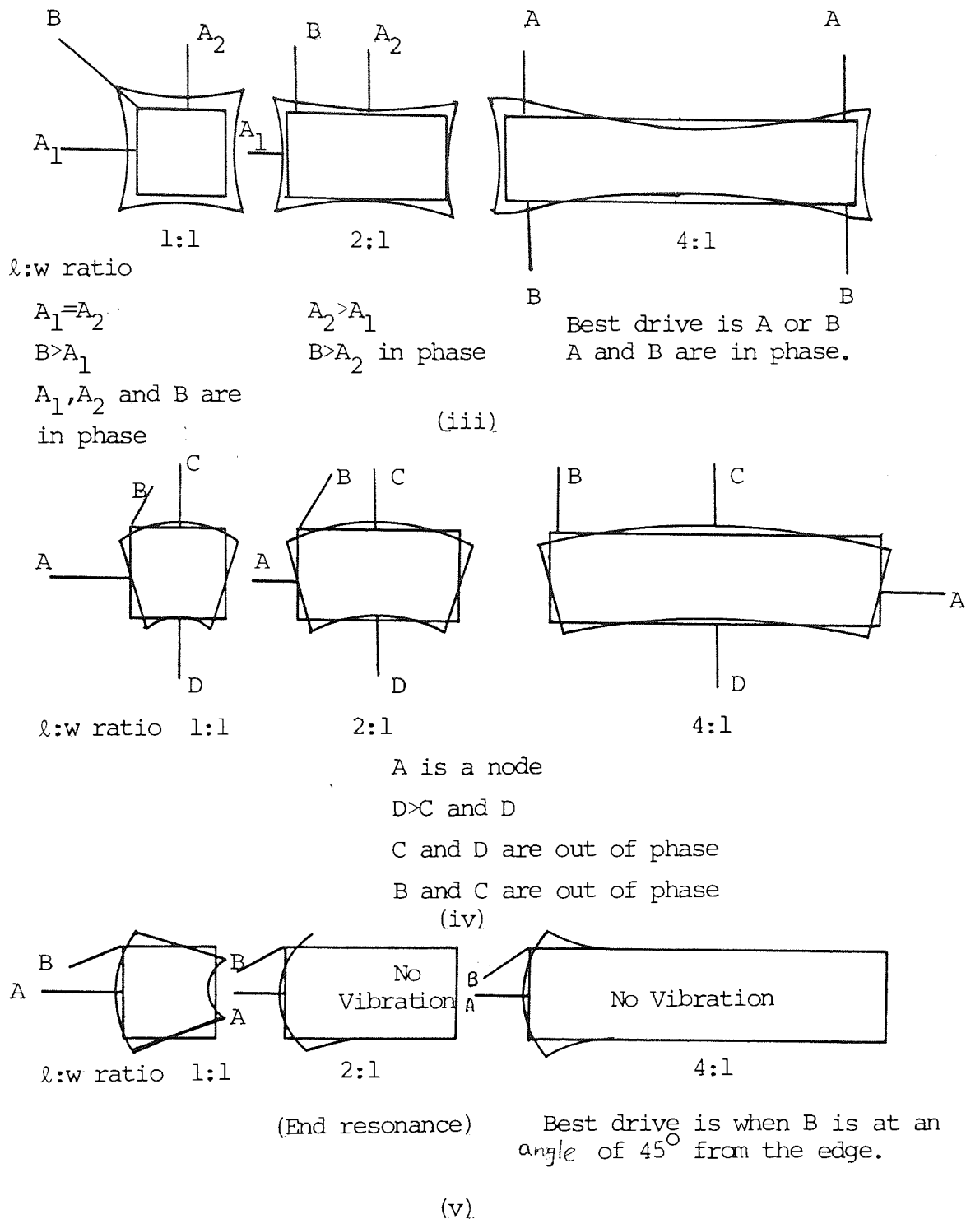
Fig. 2.5   Shows the drive conditions to give maximum coupling of
           the vibration to the line. Typical vibrational patterns
           are shown for different length-to-width ratios.

CHAPTER THREE

THE RESONANT MODES OF SQUARE PLATES

3.1 INTRODUCTION

Problems involving the extensional vibration of circular plates have been solved by Love[50]. Solutions of the differential equations of motion for different modes are available (Holland,1966,Sharp[92]). Experimental measurements on thin isotropic disks show good agreement with these theoretical eigen frequency values. Poisson's ratio and the elastic moduli for isotropic materials can be measured precisely better than 0.2%. Using tabulated eigen values for the various modes, in particular those modes which are governed principally by the shear modulus such as (1,2; 1,3;.....), and those which are more dependent on Young's modulus, e.g. (1,R; 2,1 and 2,R) modes, two moduli can be obtained (Ambati[1], Chaplain[18]). The Poisson's ratio modulus is normally used together with shear, plate or Young's modulus as convenient.

For rectangular plates, no general solution is known, the difficulties of obtaining exact solutions of the equation of motion arise from the restrictions imposed by the boundary conditions on the straight edge of the plates.

Solutions for some modes have been found under

certain limited boundary conditions[45,64]. Modes with zero displacement at the corners have exact solutions, these have been described by Lamé for isotropic elastic plates. He obtained the exact solutions of the equation of motion for these boundary conditions.

Different methods have been attempted to obtain the solutions of the differential equation of motion for different circumstances. Ekstein[22] was first to study the vibrational modes of square plates using variational techniques known as a perturbation method. In this method some extensional modes of square plates were calculated, however his resonant frequencies were only approximate. Then Mähly and Träsch[51] found a method of transforming Ekstein's infinite determinant into a simple transcendental equation which could easily be solved exactly.

Oneo, 1958[78] has studied the modal vibrations of a rectangular plate with variational techniques using trail functions. He reported that an accuracy of better than 1% is obtained for the fundamental longitudinal mode along the length.

Most recently these modes have been studied using finite difference[48,49] and finite element methods[37]. In the work of Lloyd and Redwood, finite difference techniques were applied to transform the differential equation system into an approximate matrix eigen value problem.

They observed that for square and rectangular isotropic plates, there exists four distinct families of modes. They reported that the predicted resonant frequencies are within 2% of experimental values.

More accurate results have been obtained by Holland[31]; using Lagrangian techniques and trail functions similar to those used by Ekstein. By those means, he reduced the differential equation eigen value problem to an approximate matrix characteristic value problem which is more efficient technique than that of Lloyd and Redwood.

Holland has confirmed that rectangular plates can have four types of contour extensional modes: diagonal shear, dilational-type, flexural along the major axes, and flexural along the minor axis.

Extensive theoretical data on the normalised resonant frequencies of different modes of each family is given by Holland and Roark (1967)[32]. They expressed the results using Poisson's ratio and the ratio of length to width as independent variables.

3.2 SOME EXPERIMENTAL CONSIDERATIONS

Solutions of problems in anisotropic elasticity often lead to calculations which are extremely if not

prohibitively difficult. These require some assumptions
to make a solution possible.

To make a comparison between the theoretical results
of the modal resonant frequencies of the square and the
rectangular plates and the experimental results, isotropic
materials have to be used.

Experience with disks is that sliced from drawn rod,
they appear isotropic. In axial directions there is no
stress and effects associated with longitudinal grains
are not present.

In a rod the longitudinal and shear resonances give
the moduli directly. For some materials different values
of moduli are obtained, which indicate radial anisotropy.
Considering anisotropic rods such as carbon or glass
fibre in polymer where the fibres are simply longitudinally
oriented, the longitudinal velocity is high because of
the high elasticity of the fibres but the shear velocity
is small being controlled by the polymer matrix rather
than the fibre.

Materials such as glass and silica (fused quartz)
show identical moduli values whether these results
are obtained from rods or disks cut from the rod.

Disks cut from rolled metal sheets are anisotropic
as is shown by a split in some modes, in particular the
lower order modes. In aluminium and steel the elasticities

differ by a few percent parallel and perpendicular to the direction of the roll. These features have been investigated in detail and are described in Chapter Six.

The isotropic materials which have been measured were prepared by machining a thin slice of a plate from cylindrical rods or bars. They can be considered as a planary isotropic (orthotropic). The grains direction which are longitudinally oriented in the rod, are involved only in the thickness of the plate where no body displacement takes place in it.

3.3 LOW ORDER SQUARE PLATE MODES

To understand the vibrational spectrum of a thin rectangular plate, it is convenient to regard the simplest and easiest geometry in which the vibrations occur - the square plate.

Materials with different Poisson's ratio have been prepared as a thin slice of a plate machined from a cylindrical rod or a bar as described in the previous section.

Precise values for Young's modulus, the shear modulus and Poisson's ratio for the materials used were measured using the disk theory. The vibrational modes of the square plates, which were machined from the isotropic disks, were then investigated using various

driving techniques. Initially the plate was driven at the centre of the side where most of the modes with antinodes at this point will be excited. Modes with a node at this point need different driving positions, ideally parallel to the maximum displacement vector to allow the signal to be picked up and displayed on the screen of the oscilloscope. The modes were soon identified, and the vibrational patterns were drawn using the probe already described. To investigate the nodal pattern for each mode, the probe was extensively used and nodes were identified and followed through a point where the phase of the motion is changing. This is carried out by touching the probe to the surface of the plate at a small angle.

The sketches for the lowest fifteen modes of the square plate resonator are shown in Fig. 3.1 . The vibrational displacements patterns are illustrated for the aluminium plate with their normalised frequencies corresponding to the plate wave velocity.

The resonant modes of the square plate can be classified into groups according to their vibrational patterns. The coupling to the line and the phase of the motion for the opposite sides of the plate must be taken into consideration for this classification. There are mainly three types of the vibrational modes for the

square plate:-

(i)   The dilational type modes - The general feature
is that the displacements at the two opposite sides
of the plate have an equal phase. The mode having
a symmetrical feature of the vibration. The
fundamental of this type is mode (3) in Fig. 3.1 .

(ii) The diagonal shear type modes - These have
nodes at the centre of each side, therefore the
mode requires a different driving position. Mode (1)
represents the fundamental of this type.

(iii) The flexural type modes - These have the
characteristic of "free-free bar" flexural vibrations.
The phase is reversed at the two opposite sides with
maximum coupling at the edges of the plate. These
modes have an antisymmetric vibrational patterns
feature. Mode (2) is the fundamental of this type.

A most interesting feature of the square plate modes
is that, unlike the disk, the mode which has two nodal
diameters is split into two fundamental modes, the lowest
one has nodal lines parallel to the sides and antinodes
at the corners. This mode is historically important
and known in quartz as "Face Shear G.T. Cut" mode
developed by W. P. Mason[54,55]. It gives the low
temperature coefficient quartz resonator which was used

in Radar and LORAN navigation system of W.W.2.

The second fundamental mode has a node at each corner giving nodal lines across the diagonals. This is the original mode described by M. G. Lamé[45] in 1866. Since there is no stress at the corners, this simplified the boundary conditions for the solutions of the equations of motion enabling exact solutions to be achieved. These fundamental modes were found to be the only pure shear modes in square plates.

The breathing mode in the disk (1,R) is associated with one in the square plate vibration. In this mode, the phase of the motion is constant over the whole periphery. The amplitude is higher at the corners than at the centres. The total area of the plate is changing, this means that it is more dependent on Young's modulus, while the other modes are more dependent on the shear modulus because there is a distortion in their shape, and the change in their area is very small.

The breathing mode has a node at its centre if the plate is indefinitely thin, but the resonant frequency requires a correction as in the disk, if the thickness is signficant compared to its length. The displacement in the thickness direction is associated with the lateral contraction due to the Poisson's ratio coupling of the material.

The weakly coupled mode to the driving wire at certain driving positions can always have an alternative position where the vibrations have more significant displacements and consequently the mode will be more tightly coupled to the line.

Some of these modes require an edge drive, while the others require completely different driving conditions. In the case of the edge drive, the lowest of these is mode (2) in Fig. 3.1 . This mode has three nodal lines, two of them are parallel to the sides of the plate and the third is crossing them to form two axial nodes in the plate. The next mode which has three nodal lines is mode (6) of the disk. The three nodal lines are crossing each other at the centre to form an axial node. This was confirmed by clamping the plate at its centre. When the mode has a central node the clamping does not effect it. The feature of modes having non-symmetrical nodal patterns has a special interest in the case of the investigations related to the materials anisotropy, this will be discussed in detail later.

The other modes which have the feature of being tightly coupled at the edges of the plate are modes (4) and (7). These require an angle of 45 degrees with the driving line for optimum excitation. The resonant frequency of mode (4) has been investigated extensively, and it has been found that it is controlled by the Young's

modulus as will be discussed later. This mode with mode (2) were found to combine to form a single resonance (end resonance) when the plate length exceeds twice the width. Maximum coupling again occurs at an angle of 45 degrees between the driving line and the edge of the plate.

Mode (9) was described as a second breathing mode[48]. A close look at its vibrational pattern shows that there are two nodes on each side of the plate indicating by the phase reverse of the motion at the centre and the edge of the plate even their coupling to the line is almost the same. These are forming four nodal lines crossing each other to form a node at the axial centre. This was verified by again clamping the plate at its centre. Nodes on the side of the plate indicate that its shape is changing rather than its area. For this reason it cannot be classified as a breathing mode.

Mode (8) was not unambiguously classified. It has an antinode at the centre indicating that the nodal lines are parallel to the sides. Extensive use of the probe indicated a 2×2 nodal pattern.

Figure 3.2 shows the vibrational nodal patterns for the lowest order modes of the square plate and their corresponding disk modes.

3.4   THE RESONANT FREQUENCY CHARACTERISATION

Isotropic materials ranging from brass with Poisson's ratio of 0.36 to pyrolytic graphite with in-plane value of -0.10 have been used in this investigation. Accurate measurements of Poisson's ratios of the materials and their modulus have been carried out using disk resonators. The disks were then machined to perfect square plate geometries. A set of the samples used in this experimental investigation are shown photographically in Fig. 3.3 .

The different modes of the vibration have been excited using an optimum driving position. The frequency-length product for each mode has been normalised to the plate wave velocity. The complete set of the results is shown for different materials in Table 3.1. The choice of the plate velocity for normalisation is arbitrary but is widely used.

The graphical plot for variations of various modes as a function of Poisson's ratio is shown in Fig. 3.4.

With materials having progressively decreasing Poisson's ratios, all the modes, except one, rise linearly. While the one which is going in opposite direction, like the disk resonant modes, is the breathing mode. The variation of this mode with Poisson's ratio, unlike the others, is not linear. It overlaps with the

Lamé mode and mode (4) at zero Poisson's ratio; i.e. for materials with low Poisson's ratio, the three modes (Lamé, breathing and mode (4)) will be close to each other. This can be used as a reference for calculating the Poisson's ratio for isotropic materials. The frequency ratio between the breathing mode and one of the fundamental modes can be used as a sensitive method for measurement of the elastic modulus of the materials. Table 3.2 shows the frequency ratio of the breathing mode to the Lamé mode for various materials measured. The plate modulus and Poisson's ratio have been measured from the disk. The variation is shown graphically in Fig. 3.5 . Within the limits of observation the frequency ratio varies linearly with Poisson's ratio above (+0.10); then a slight curvature occurs for values below that.

The large change means that observations on square plates give a sensitive measurement of Poisson's ratio and unlike disks present no difficulties in the case of metals with close frequencies of (1,3) and (1,R) modes. This is an important practical application for material studies where square plates can be made available. The accuracy of these measurements, however, depend on an experimental calibration curve, while the corresponding disk method is based on a completely accurate theoretical expression.

3.5   THE MODES OF HARMONIC RELATIONS

Mason and Lamé modes have been investigated extensively, as they are the most common fundamental and simplest resonant modes of square plates. Measurements on square plates with various Poisson's ratio show that these are also modes with frequencies twice and three times the fundamental Lamé mode. This is illustrated in Table 3.3, the frequency is normalised to the shear wave velocity (C_s) which was measured from disk resonators for different materials. These harmonic relationships were accurate to better than ½%. In other words, their resonant frequencies are precise integers of the fundamental Lamé mode regardless of their Poisson's ratio. This is an interesting result as harmonic relationships are not normally encountered in the vibrational spectra of solids. It does not appear to have been explicitly reported to date.

It has been found that all these modes share the same feature of having nodes at their corners. This indicates that they are the modes described and resolved by Lamé. Exact solution for these modes should be obtainable because of having zero displacement at the corners, which satisfy the difficult boundary conditions for the differential equation of motion.

Driving the plate at the centre of the side will excite the odd Lamé modes, i.e. the first, the third,....etc.

modes; while the even modes, because of a node at the centre of their sides, require an intermediate driving position where the maximum displacement occurs.

Figure 3.6 demonstrates the harmonic relationships of the Lamé modes series. It shows the lowest three modal pattern configurations. The simplest explanation is to consider that the second harmonic can be regarded as four Lamé plates of half the fundamental size and twice the frequency. Subsequently the third, fourth,...etc. harmonic have similar considerations.

Lamé mode was found to be the only mode with this feature of being harmonically related. The other fundamental mode, Mason, was found to have no harmonic relationship with any other modes.

Table 3.4 shows the values of the normalised frequency for these two fundamental modes. It can be seen that the first Lamé mode has a constant value of $\sqrt{2}$. The Mason is also considered to be a pure shear mode although an experimental variation for the various materials of about 1% was observed. The results indicate that these two modes are shear type modes with the wavelengths equal to the diagonal of the square plate in the case of Lamé mode.

The graphical plot for the values of the frequency-diagonal product normalised to the shear wave velocity

as a function of Poisson's ratio is shown in Fig. 3.7 .
Modes with no variation or slight variation indicate
that they are governed principally by the shear modulus.
Clearly the breathing mode is the only one which has a large
curvature change with Poisson's ratio comparing to the other
modes.

3.6 THE ROD MODULUS MODES

It is interesting to find some modes which are
controlled by the shear modulus. The dependence of the
two fundamental modes on this modulus was demonstrated
earlier. In the Lamé mode, the shear wave length was
found to form the diagonal of the plate.

Further investigations were carried out concerning
the characterisation of the different resonant modes
with respect to the Young's modulus. Normalising the
frequency-length product for each mode to the rod
velocity shows that mode (4) has a constant value
irrespective of the Poisson's ratio of the materials
being measured.

A complete set of the measurements is given in
Table 3.5, the values of the rod velocity and the
Poisson's ratio were measured to an accurate figure from
the disk. It will be noted that the normalised value of
$2\ell f$ to the rod velocity for all the materials is very
close to unity. Therefore it can be said that this mode

is governed by the rod modulus where the rod wave length
is twice the length dimension of the plate.

It has been thought that the value of $2\ell f$ can be
very close to the rod velocity for infinitely thin plate$s$.
This will reduce the lateral contraction due to the
Poisson's ratio coupling in the thickness direction
of the plate.

The dependence of the other modes on the Young's
modulus can be observed by normalising them to the rod
velocity.   This is shown graphically in Fig.   3.8 .
Modes with slight variation or no variation at all with
the Poisson's ratio indicate that they are governed
principally by the Young's modulus.

3.7   THE ANISOTROPIC EFFECTS OF THE GRAIN ORIENTATIONS
      ON THE RESONANT MODES OF THE SQUARE PLATE

3.7.1   The Symmetrical Modes

In disks cut from rolled metal sheets, which can be
considered as moderately anisotropic,the fundamental
mode which has two perpendicular nodal diameters was
found to be split in two modes[9,19] .   In one, that
with the lower frequency, the nodal lines were
symmetrical about the axis of roll, and in the other they
were at 45 degrees.

A number of square plates of different orientations were cut from rolled metal sheets. The variation of the frequency for the lowest six modes with plate orientation is shown in Fig. 3.9 . The angle is measured relative to the drive position. The cyclical variation of the two fundamental modes can be seen clearly but this does not occur in the flexural modes. The effect is less on the breathing modes. This obviously has an effect on the apparent value of Poisson's ratio. It is shown grahically in Fig. 3.1C . The values of Poisson's ratio were obtained from the ratio of the breathing mode to the Lamé mode using the calibration curve shown in Fig. 3.5 .

3.7.2 THE NON-SYMMETRICAL MODES

Measurements on shim steel square plates show the variation of the two fundamental modes with the plate orientation. These modes, unlike the disk (1,2) modes, have not been split. This is because the modes have symmetrical nodal pattern configurations. On the other hand, modes with non-symmetrical nodal patterns are expected to split as a result of the plate anisotropy.

Mode (2) in Fig. 3.1 was described as the fundamental "free-free bar" vibration. It has three nodal lines forming two axial nodes. This mode becomes double as the existence of the grains remove the mode.

degeneracy. There is a frequency variation of about 3% observed in the measurement of shim steel plates. The best drive to excite the double modes is to drive the plate at the edge where both have displacements. This is demonstrated in Fig. 3.11 .

In general, for any modes of having (n,m) nodal lines; there will be no split if n=m, and the mode will split if n≠m.

3.8   NON-HOMOGENEOUS MATERIALS STUDY

Measurements of the resonant frequencies for anisotropic materials have been carefully investigated. Nuclear graphite, which might be thought to be isotropic, showed anomalous results demonstrating a significant anisotropy. Measurements on square plate, machined out of the disk, show a greater difference between the observations on different sides of the plate. This is shown in spectrum form in Fig. 3.12. The modal frequency was normalised to the fundamental Lamé mode, and the line height represents the normalised coupling. The breathing mode was found to be split into two separate modes, while the fundamental Lamé has no significant effect. This will show two different values of Poisson's ratio, one at (-0.05) when the drive is at (A), and (+0.10) when it is at (B) side.

Since the two fundamental modes have not been affected significantly by the drive position, this indicates that the shear modulus has just a unique value for this material.

Fig. 3.1   Sketches for the lowest fifteen vibrational

resonant patterns of square plate (After

Holland, R. reference 31).

The frequency-length product is normalised

to the plate wave velocity in an Aluminium

plate of Poisson's Ratio (0.338).

Mason
Mode
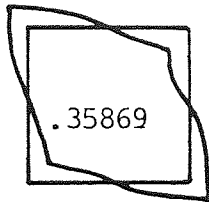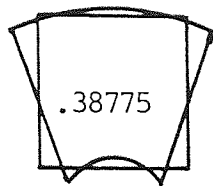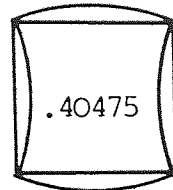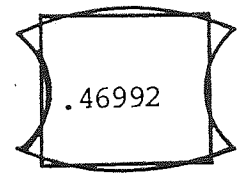
.35869

1

Edge
Mode 1

.38775

2

Lamé
Mode 1

.40475

3

Edge
Mode 2

.46992

4

The Breathing
Mode

.55407

5

Edge Mode 3
Mode (1,3)

.57834

6

Edge
Mode 4

.67677

7

.77916

8

Mode (2,2)

.78604

9

Lamé
Mode 2

.81328

10

.82262

11

.94629

12

.95600

13

1.02187

14

1.07693

15

DISK MODES | SQUARE PLATE MODES

Mason Mode   Lamé Mode

Mode
(1,2)

Mode
(1,2)
Square

Flexural 1   Flexural 2

Mode
(1,3)

Mode
(1,3)
Square

Mode
(1,R)

Breathing
Mode
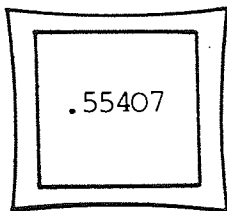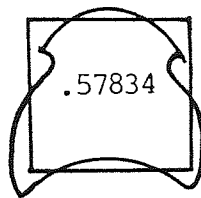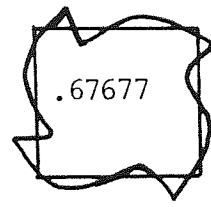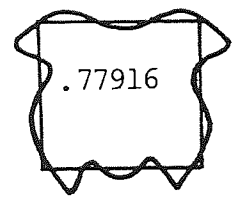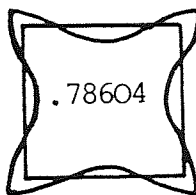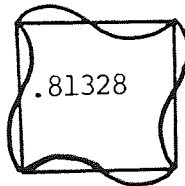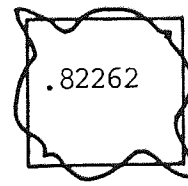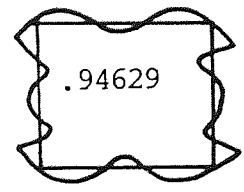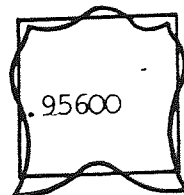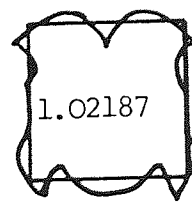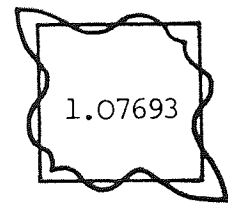
Mode
(1,4)
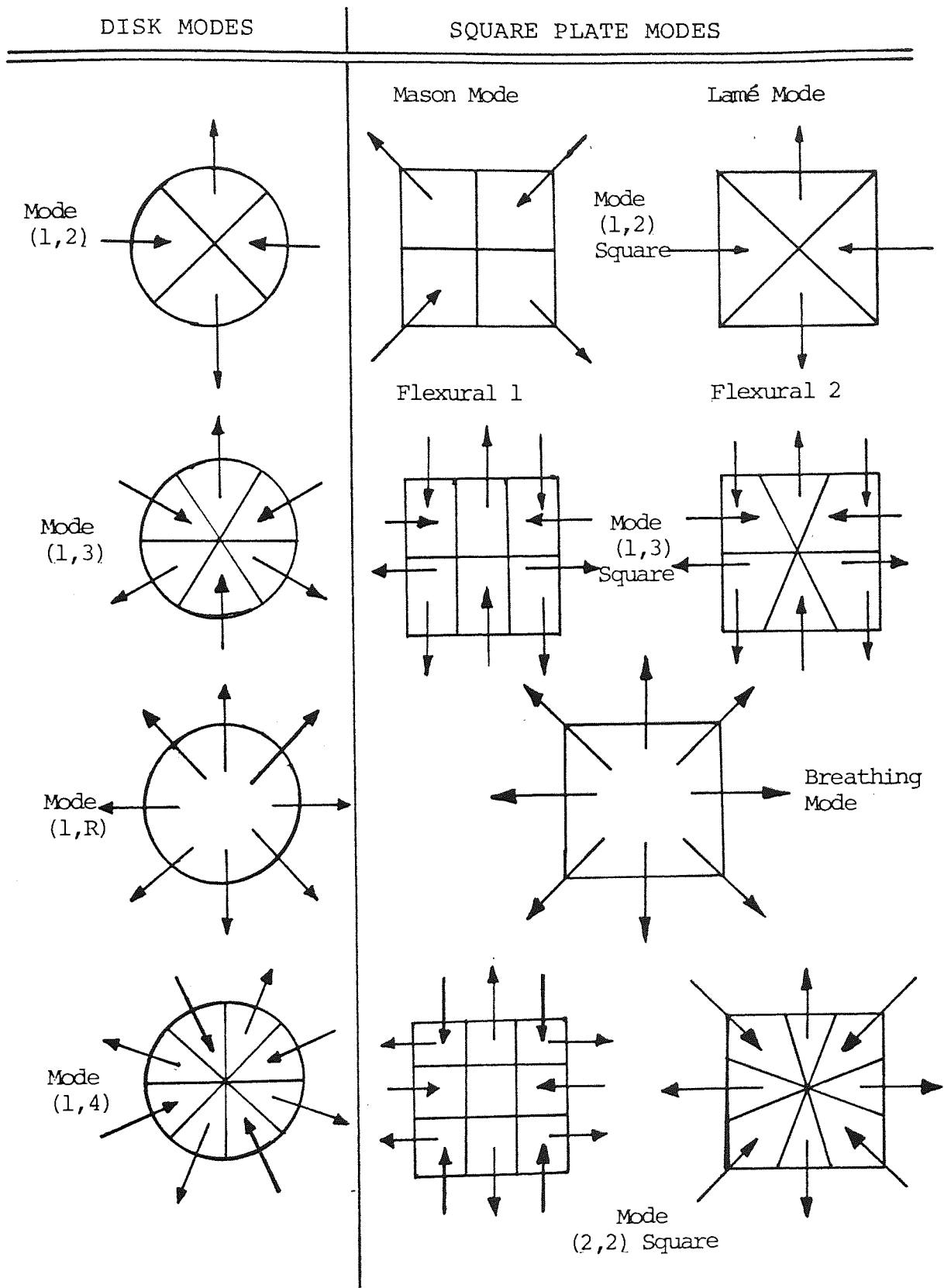
Mode
(2,2) Square

Fig. 3.2   The vibrational nodal pattern configurations for the
lowest modes of square plate and their corresponding
disk modes.

Fig. 3.3   The photographical display shows the set of

samples used in this investigations. These

have been machined in square plate geometries

from disks. The materials shown are ranging

from Brass with Poisson's ratio = 0.357 to

Pyrolytic Graphite of an in-plane Poisson's

ratio = -0.075. The values of Poisson's ratio

and the plate modulus have been obtained from

the disk measurements.

Fig. 3.4 Graphical plot of the variations of the
frequency-length products normalised to the
plate wave velocity for the lowest ten modes
of the square plate as a function of Poisson's
Ratio and C_p were measured from the disk.
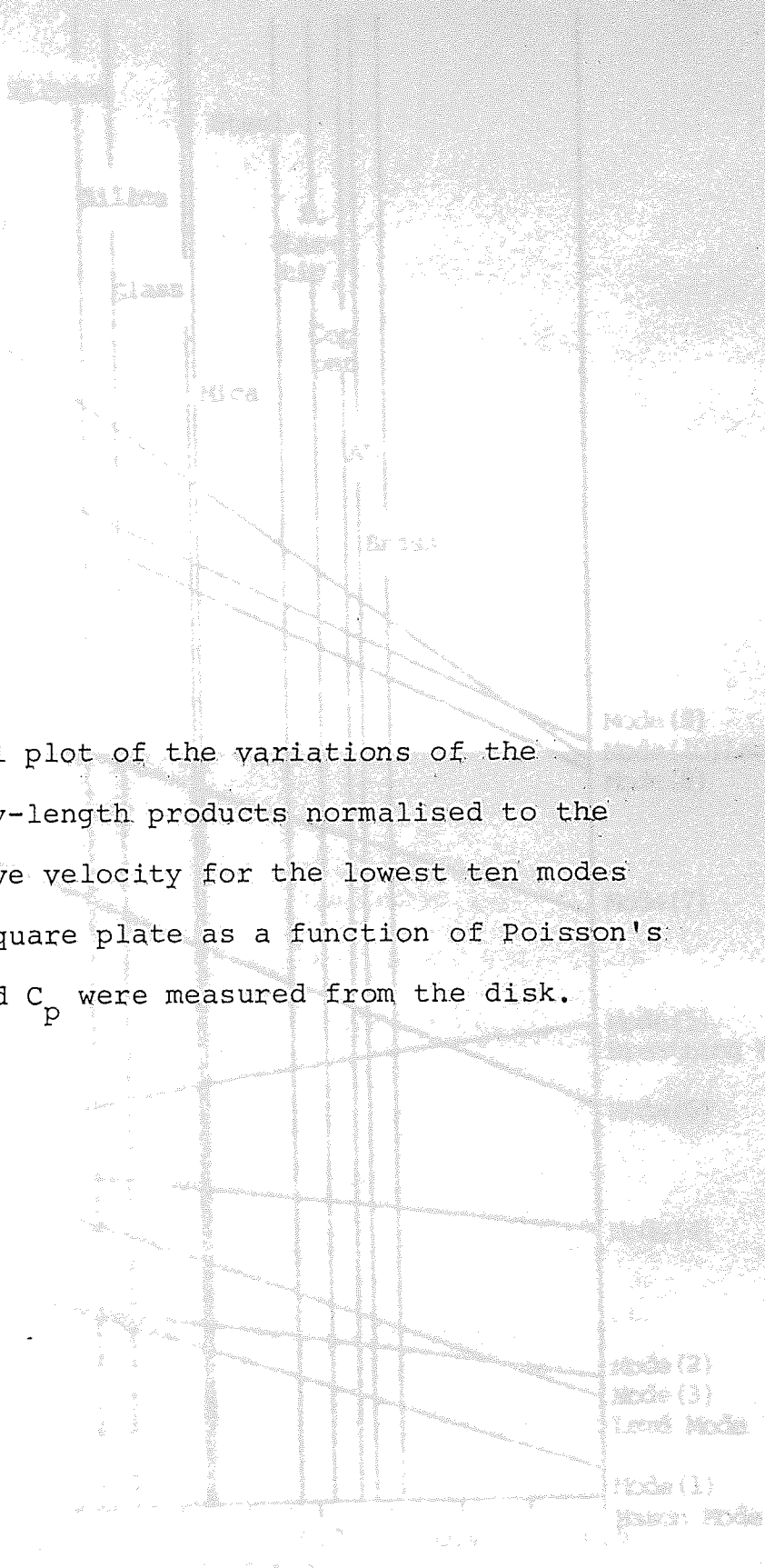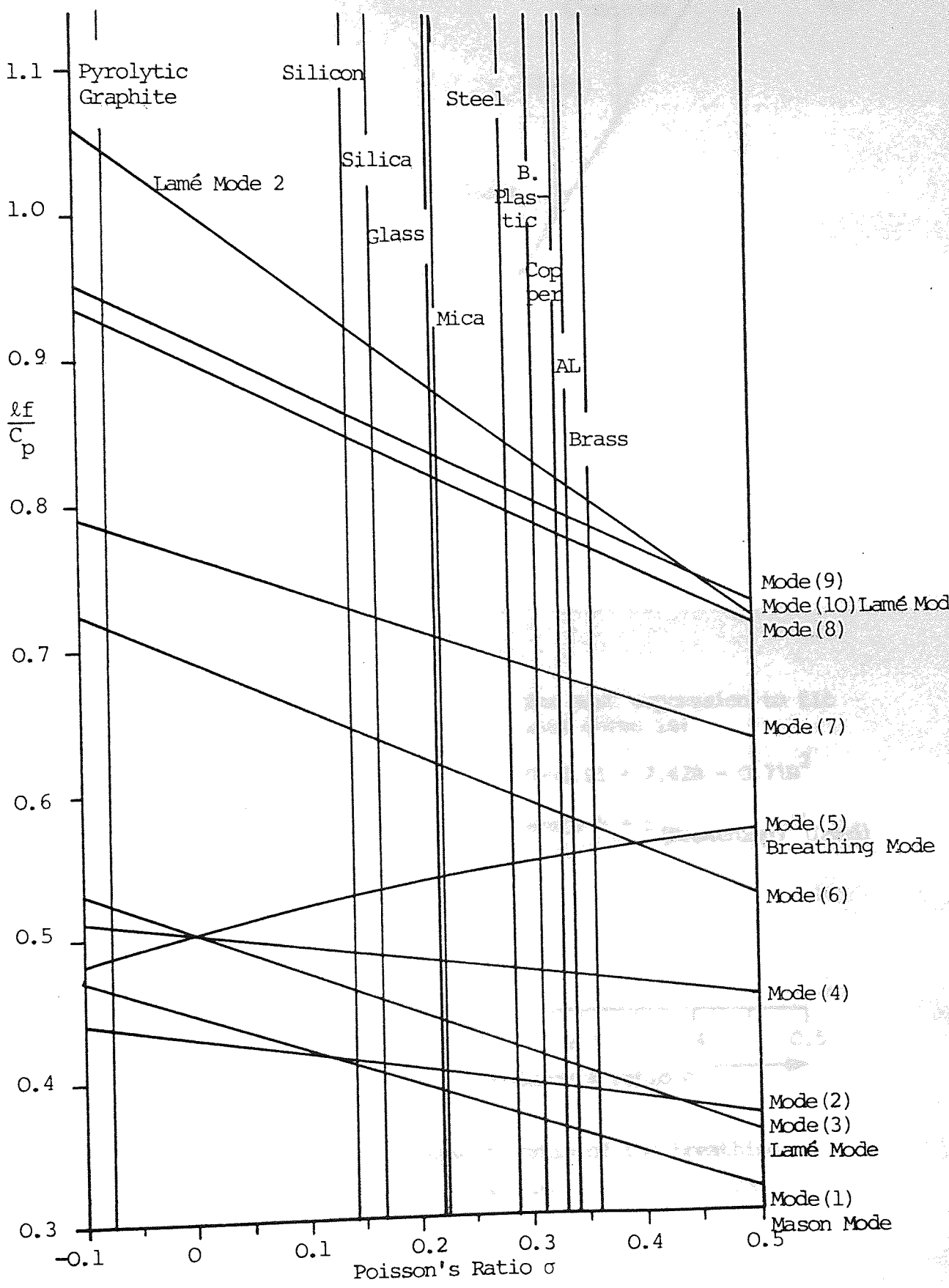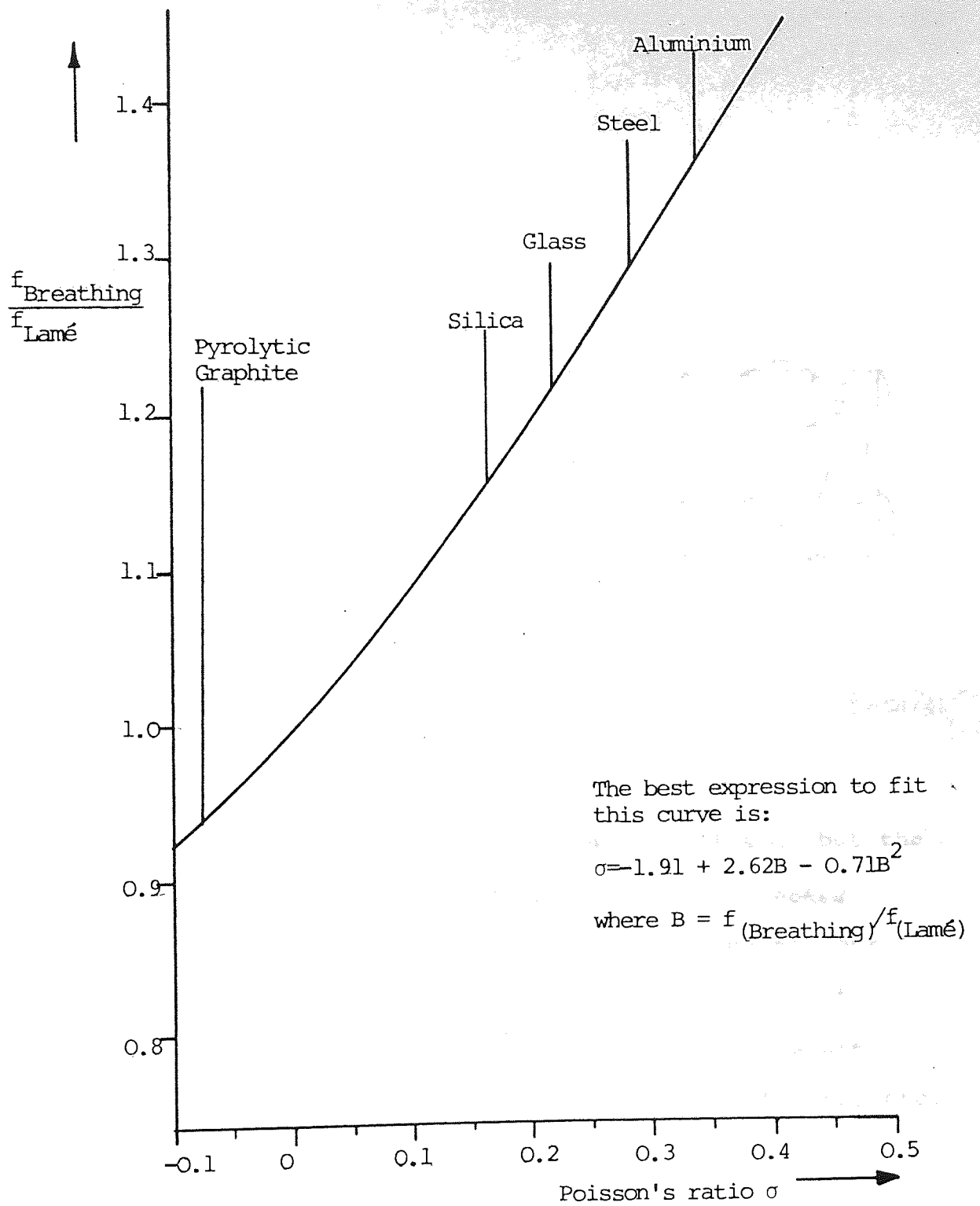
Fig. 3.5   The variation of the frequency ratio of the breathing mode to the Lamé mode as a function of Poisson's ratio.

f_O

(Fundamental Lamé
Mode)

$2f_O$

$3f_O$
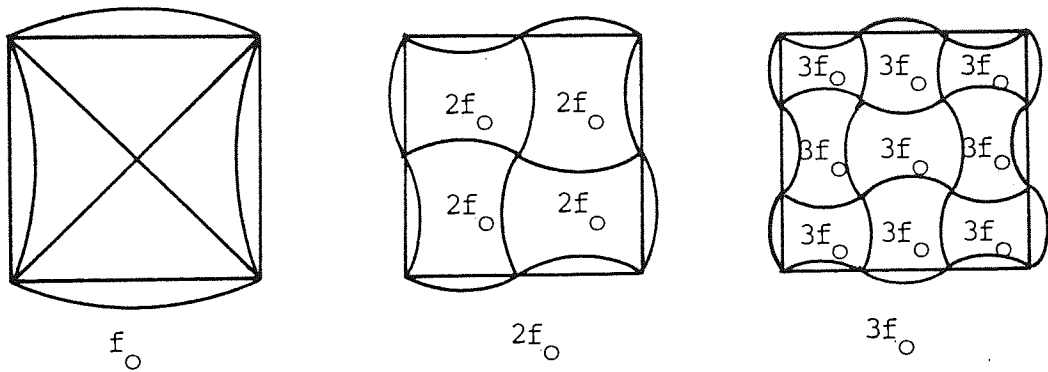
Fig. 3.6   This configuration was given by Holland, but the
harmonic relationship apparently overlooked.
The second harmonic can be considered as four
Lamé plates of half the fundamental size at
twice the frequency. Subsequent results are
determined by considering the third, fourth, etc.
harmonic Lamé modes.
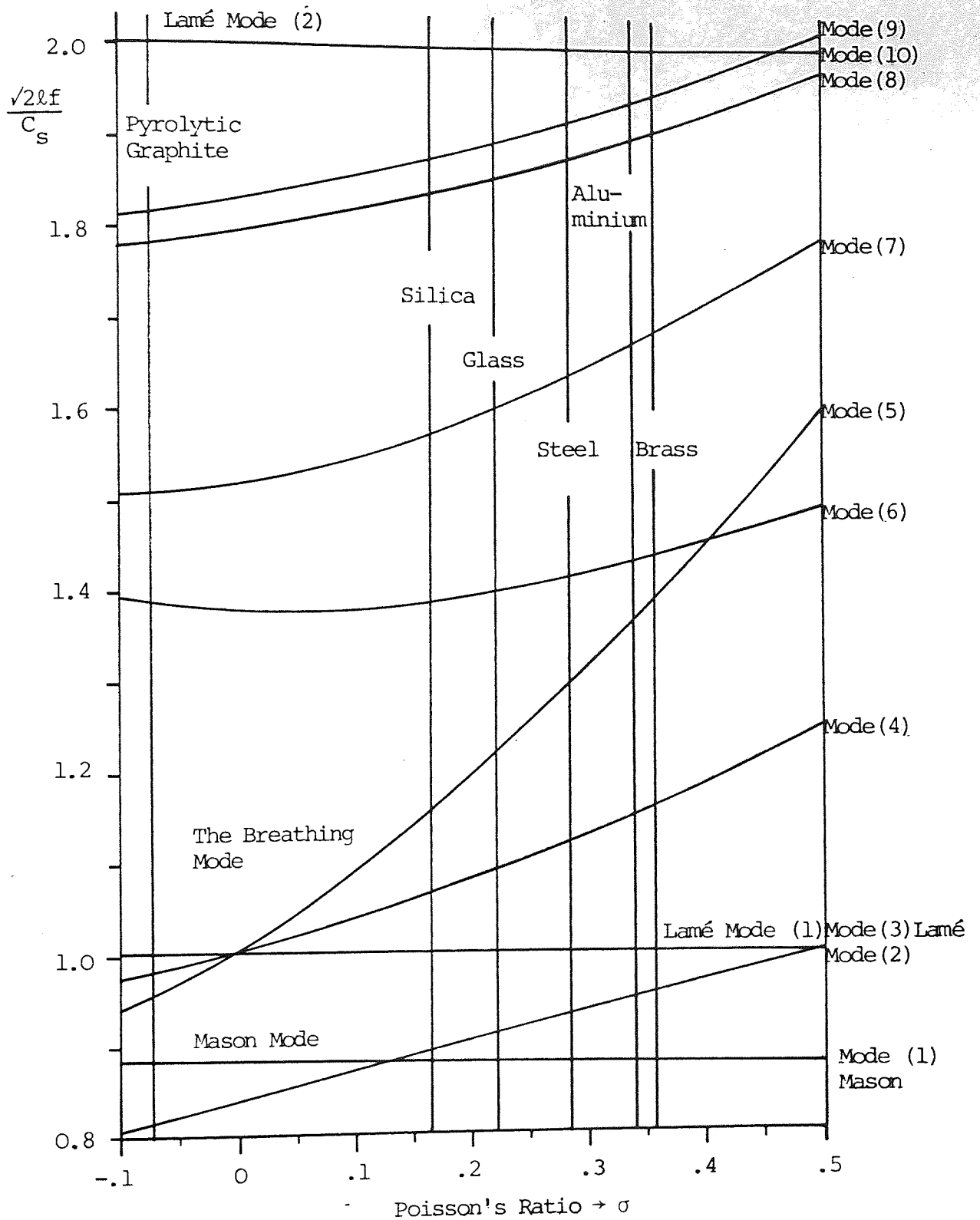
Fig. 3.7 Graphical plot for the values of the frequency-diagonal
products normalised to the shear velocity as a function
of the Poisson's ratio for the lowest ten square plate
modes.

Fig. 3.8   The graphical plot for the variations of the

frequency-length products normalised to the

rod velocity (C_0) as a function of the

Poisson's ratio for the lowest ten square

plate modes.

Figure with vertical axis labeled $\frac{\ell f}{C_0}$ ranging from .3 to 1.1, and horizontal axis labeled "Poissons Ratio σ" ranging from -.1 to .5.

Material labels (top): Pyrolytic Graphite, Silica, Silicon, Steel, Glass & Mica, B, Plastics, AL, Copper, Brass

Curve labels (right): Mode 10, Mode 9, Mode 8, Mode 7, Mode5 (Breathing Mode), Mode 6, Mode 4, Mode 3 (Lamé Mode), Mode 2, Mode 1
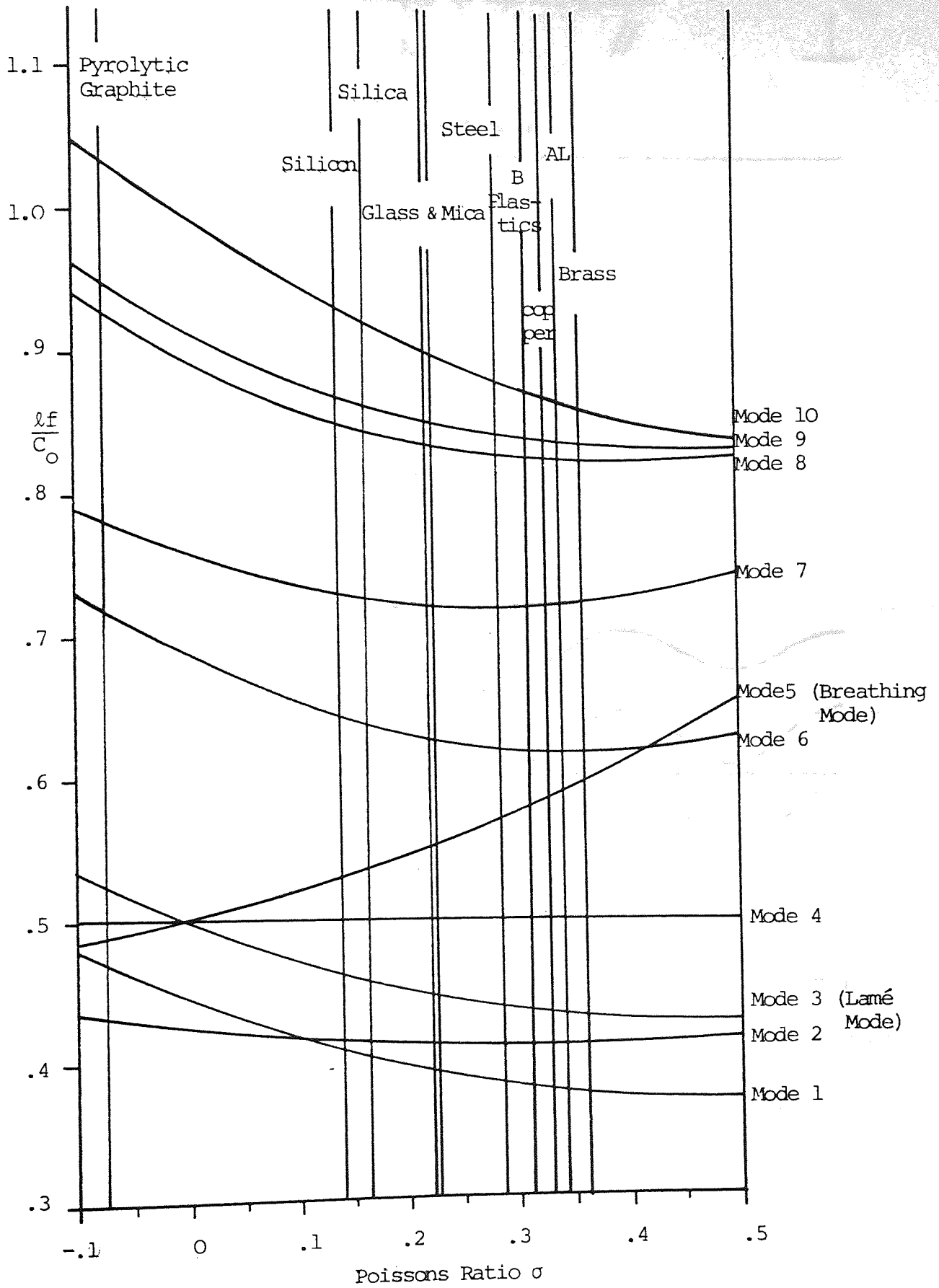
Shim Steel

Grains direction is corresponding to the drive line.
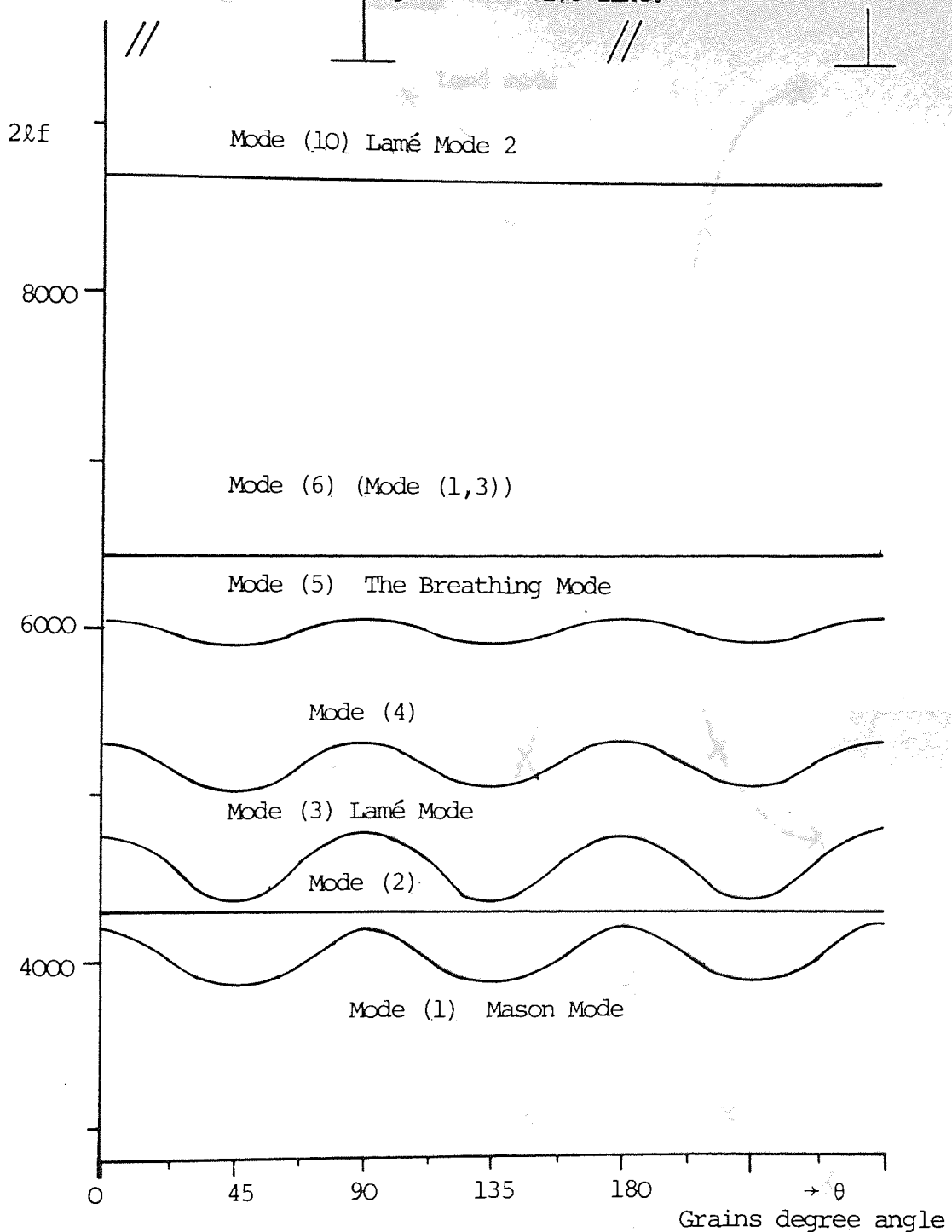
Fig. 3.9   Graphical plot for the variation of different square
            plate modes with the grains direction for shim steel.
            Grain orientation angle is corresponding to the drive
            line.
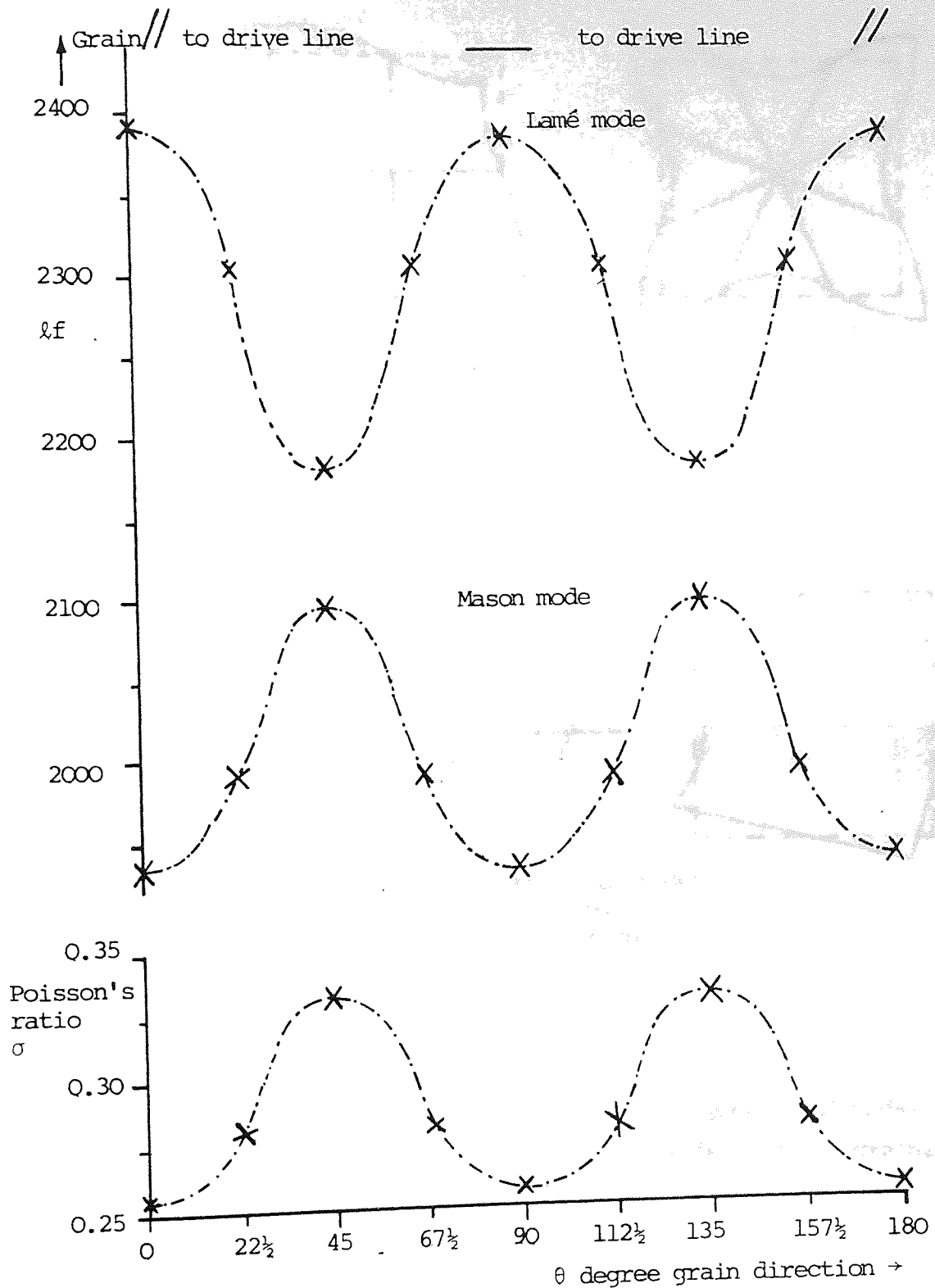
Fig. 3.10 Graphical plates represent the variation of the two
fundamental square plate modes with the grain directions.
The effect of this on the apparent value of Poisson's ratio
is also shown. This has been found from the calibration
curve of Fig. 3.5.

Grains
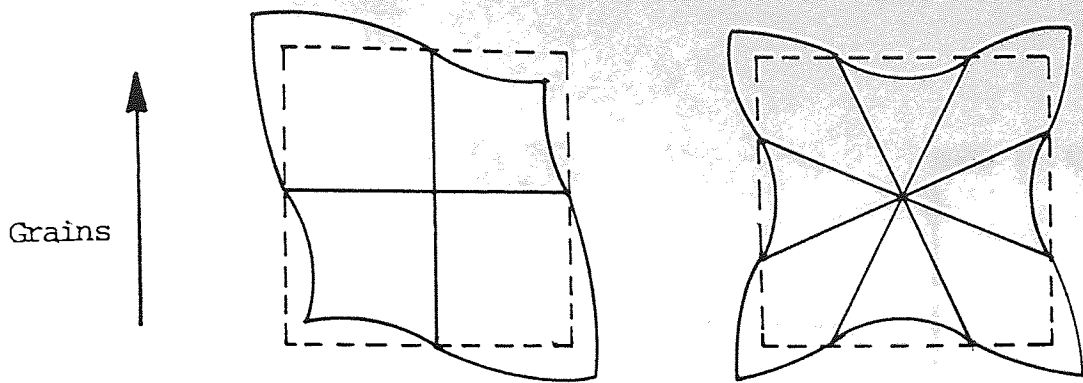
Symmetrical Modes
No Splitting

Grains

$\neq$
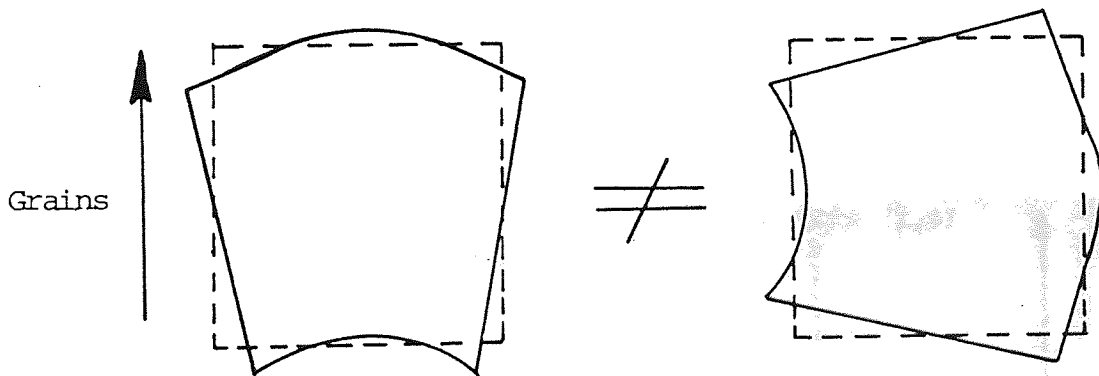
Non-Symmetrical Modes
Splitting
(about 3% for shim steel)

(n,m)   if n=m   No splitting
        if n≠m   Splitting

Fig. 3.11 Sketches for the symmetrical and non-symmetrical modal
patterns configuration showing the effect of the grains
orientation on the modes splitting.

Normalised
Coupling

Fundamental
Lamé Mode

Mode (1,4)

1.0

Breathing

0.5

Mode (1,3)

A drive ⟶

B drive

1.0   Normalised Frequency   2.0

A drive

Normalised
Coupling

Fundamental
Lamé Mode

Mode (1,4)

1.0

B drive ⟶

Mode (1,3)

0.5

Breathing

1.0   Normalised Frequency   2.0
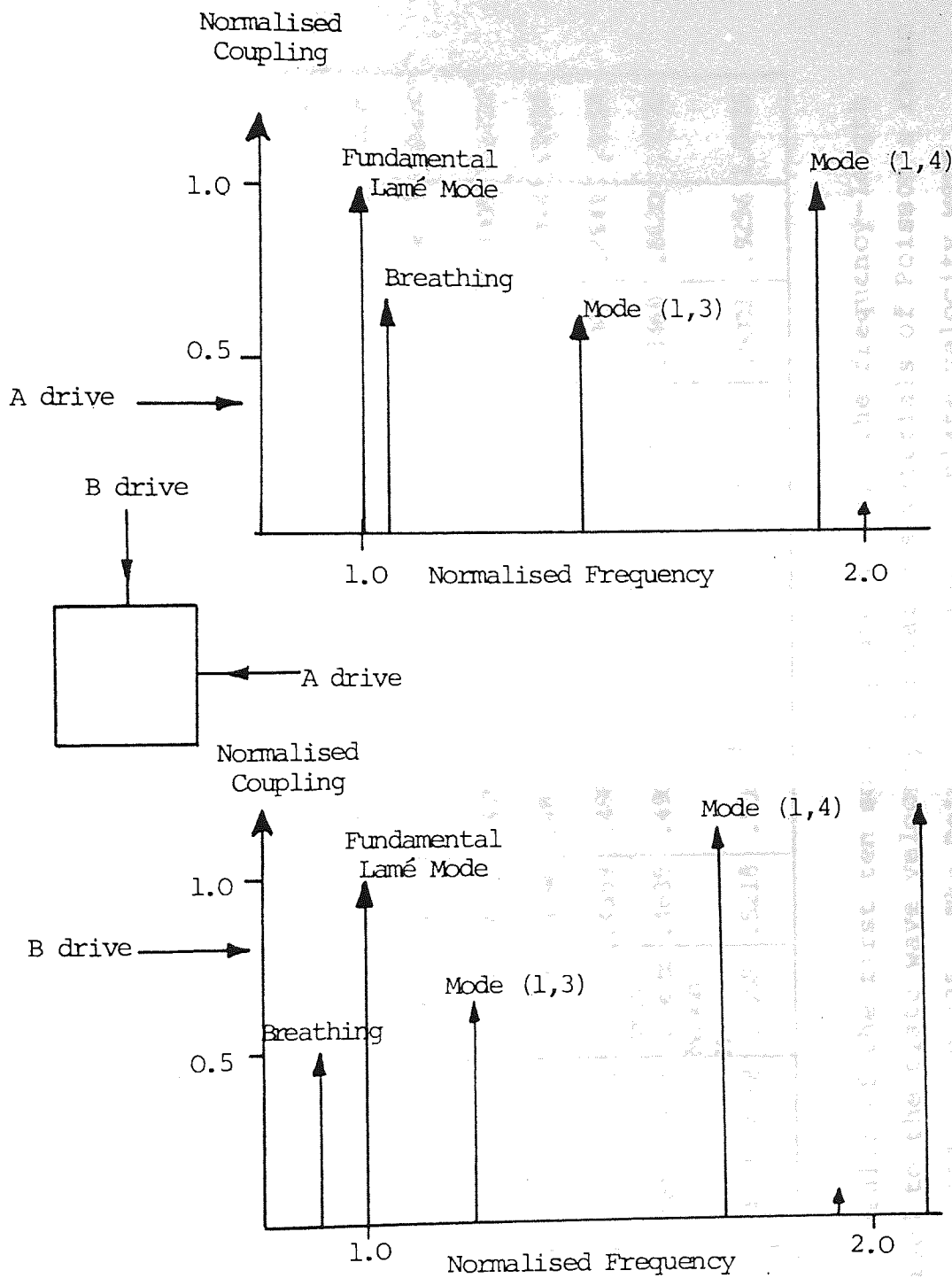
Fig. 3.12   Spectrum for Nuclear Graphite showing effect of anisotropy

-48-

TABLE 3.1

Sample	Measured From the Disk Poisson's Ratio σ	C_p	Mason Mode 1	2	Lamé Mode 3	4	Breathing Mode 5	6	7	8	9	Lamé Mode 2 10
							$\ell f / C_p$					
Brass	0.357	3695	.3572	.3846	.4003	.4645	.5556	.5698	.6740	.7682	.7812	.8006
Aluminium	0.338	5490	.3591	.3862	.4058	.4660	.5536	.5799	.6768	.7731	.7886	.8116
Copper	0.328	3917	.3605	.3880	.4072	.4666	.5528	.5800	.6778	.7771	.7893	.8142
Black Plastic	0.313	2840	-	.3898	.4138	.4705	.5525	.5902	-	-	.8035	.8276
Steel	0.285	5395	.3719	.3918	.4215	.4739	.5460	.5963	.6959	.7966	.8073	.8430
Mica	0.223	7880	.3840	.4022	.4363	.4790	.5359	.6174	.7063	.8157	.8305	.8726
Glass	0.220	5568	.3861	.4039	.4396	.4828	.5379	.6181	.7069	.8169	.8318	.8792
Silica	0.165	5860	.4010	.4076	.4559	.4880	.5284	.6367	.7166	.8387	.8541	.9118
Silicon	0.140	2885	.4071	very close to Mason Mode	.4635	.4905	.5229	.6471	.7322	.8469	.8620	.9270
Pyrolytic Graphite	-0.075	3428	.4688	.4358	.5218	.5052	.4829	.7190	.7828	.9001	.9256	1.0436

The experimental results of the first ten square plate modes. The frequency-length products normalised to the plate wave velocity for various materials of Poisson's ratio values range from 0.357 to -0.075. The Poisson's ratios and plate velocity were measured from the disk resonant frequency. The accuracy is better than 0.1%.

TABLE 3.2

Sample	Poisson's Ratio σ	Plate Length mm.	Lamé mode Frequency KHz	Breathing Mode Frequency KHz	$\frac{f_{Breathing}}{f_{Lamé}}$
Brass	0.357	36.0	41.088	57.030	1.3880
Aluminium	0.338	48.0	46.414	63.309	1.3640
Copper	0.328	27.0	59.080	80.275	1.3588
Black Plastic	0.313	36.0	32.642	43.590	1.3354
Steel	0.285	35.0	65.040	84.335	1.2970
Mica	0.223	25.4	166.25	135.38	1.2280
Glass	0.220	77.6	38.593	31.543	1.2235
Silica	0.165	44.4	60.181	69.721	1.1585
Silicon	0.140	50.0	26.760	30.163	1.1272
Pyrolytic Graphite	−0.075	25.0	71.550	66.215	0.9254

This shows the measured values of the Lamé and the breathing modes and the variations of their ratios with the Poisson's ratio.

TABLE 3.3

Sample	σ	C_s msec^{-1}	Length mm	Lamé Modes Frequency in KHz		
				First	Second	Third
Brass	0.357	2095	36.0	41.088	82.170	123.260
Aluminium	0.338	3159	48.0	46.414	92.825	139.235
Copper	0.328	2271	27.0	59.080	118.152	177.230
Black Plastic	0.313	1664	36.0	32.064	64.125	96.190
Steel	0.285	3226	35.0	65.040	130.02	195.05
Mica	0.223	4912	25.0	135.380	270.65	406.05
Glass	0.220	3477	77.6	31.543	63.05	94.610
Silica	0.165	3786	44.4	60.155	120.150	180.455
Silicon	0.14	1892	50.0	26.710	53.22	79.95
Pyrolytic Graphite	-0.075	2537	25.0	71.550	142.65	213.78

The harmonic relationship of the Lamé modes.   Measurement
carried out for various materials shows the modes are harmonically
related to better than ½%.

TABLE 3.4

Sample	Measured from the Disk		Square Plate				
	σ	C_s m.sec^{-1}	Length mm	Lamé Mode		Mason Mode	
				f KHz	$\dfrac{\sqrt{2}\ell f}{C_s}$	f KHz	$\ell f/C_s$
Brass	0.357	2095	36.0	41.088	0.9985	36.180	0.6217
Aluminium	0.338	3159	48.0	46.414	0.9974	40.956	0.6211
Copper	0.328	2271	27.0	59.08	0.9933	52.292	0.6217
Black Plastic	0.313	1664	36.0	32.064	0.9810	–	–
Steel	0.285	3226	35.0	65.040	0.9979	57.396	0.6250
Mica	0.223	4912	25.4	135.380	0.9900	121.110	0.6263
Glass	0.220	3477	77.6	31.543	0.9956	27.706	0.6183
Silica	0.165	3786	44.4	60.155	0.9977	52.905	0.6204
Silicon	0.14	1892	50.0	26.710	0.9982	23.490	0.6208
Pyrolytic Graphite	–0.075	2537	25.0	71.550	0.9971	64.281	0.6334

The experimental results for Lamé and Mason modes.
The precise values of the frequency are obtained for
various materials. The frequency-length product is
normalised to the shear velocity (C_s) which was measured
from the disk.

TABLE 3.5

Sample	Measured From the Disk		Mode (4) Square Plate			
	σ	C_o m.sec^{-1}	Length (ℓ) in mm	Freq KHz	$2\ell f$ m.sec^{-1}	$\frac{2\ell f}{C_o}$
Brass	0.357	3452	36.0	47.681	3433	0.9944
Aluminium	0.338	5165	48.0	53.292	5116	0.9905
Copper	0.328	3700	27.0	67.680	3655	0.9878
Black Plastic	0.313	2697	36.0	37.115	2672	0.9907
Steel	0.285	5171	35.0	73.043	5113	0.9888
Mica	0.223	7682	25.4	148.60	7549	0.9827
Glass	0.220	5432	77.6	34.69	5384	0.9911
Silica	0.165	5780	44.4	64.550	5732	0.9918
Pyrolitic Graphite	−0.075	3418	25.0	67.985	3399	0.9945

The experimental results for mode (4), one of the square plate resonant modes. The frequency-length product is very close to the rod velocity (C_o) which was measured from the disk for different materials. The best drive is at 45 degrees of the line with the plate corner.

FREQUENCY SPECTRUM OF RECTANGULAR PLATES

4.1 INTRODUCTION

Thin rectangular plates vibrating in contour modes have been an object of an extensive degree of theoretical and experimental study. The frequency spectrum, that is the relationship between the segment frequencies and the length-to-width ratio of the plates, is of special interest in material investigations and engineering applications.

Onoe, M.[78] was the first to study experimentally the fundamental longitudinal mode of a rectangular plate using a piezoelectric vibrator to excite it. He demonstrated the existence of the edge mode and the breathing modes (defined earlier) experimentally and analytically. Subsequently, evaluations were obtained by tracing these two modes progressively down to a narrow strip. The accuracy was, however, rather limited.

In further investigations, Onoe and Pao[81] traced other extensional modes. Coupled modes were resolved by considering their characterisation in terms of the vibrational displacements around the plate.

Further experimental work by M. Medick and Y. Pao[60]

revealed the existence of the Lamé mode in rectangular plates of integral sides ratio.

The frequency spectrum of a rectangular plate was examined further by P. Lloyd and M. Redwood[48,49]. In their experimental investigations, the existence of the first two beam type flexural modes were reported. This was done by using appropriate electrode configuration system on the surface of the piezoelectric plate in order to excite them.

The Lamé and the Mason modes of a square plate were followed to their geometrical limits. They become, as Redwood indicated, longitudinal and flexural modes respectively of a long bar. The change of the character of the Mason mode as a diagonal shear type mode, to a second harmonic order flexural mode was illustrated.

The other Lamé modes in a rectangular plate were identified in conditions where the side lengths have integral ratios, but their prediction was uncertain.

Further investigations of the frequency spectrum of the longitudinal and the flexural modes have been reported[21,46,59,79]. These analyses have been of major assistance in this experimental work.

More recent experimental and analytical studies by R. Holland[31] have shown the frequency variation for

different modes of a rectangular plate and their vibrational patterns were illustrated, using the same method as Lloyd and Redwood to excite and measure their spectra. But, as mentioned earlier, the coupled modes remained unresolved. His work has been a great help in identifying some unresolved modes in this work, as their predicted vibration patterns indicated the most suitable displacement points for the plate to be driven.

4.2 PRESENTATION OF THE OBSERVATIONS

To understand the frequency spectrum of the rectangular plate modes, it is vital to represent the observations in a unique and clear form to be satisfactory in both experimental and analytical aspects.

It was realised at an early stage that for certain modes it was immaterial which side of the plate was regarded as the "length". In others, the character changed completely. The method of presenting the observations is demonstrated in Fig. 4.1 . The sketches are illustrating the way that the mode has been driven and measured.

Fig. 4.2 shows an empirical representation of the modal spectrum of different Aluminium plate modes. The Aluminium plate was chosen because of its particular compatibility with wire driving system.

Here the axes are the frequency-length and the

frequency-width products. Straight lines through the origin represent constant length-to-width ratios, the 45 degrees lines from the axes being that of the square plate. A rectangular plate of sides length ratio 4-to-1, for example, can be represented in each of the two segments below and above the 45 degrees line. This depends on which side of the plate is being considered as the length and the width of the plate.

Therefore the results could all be placed on a 45 degrees segment, but where the frequencies are not the same for a 90 degrees rotation of the modal pattern, the other segment is used to enable the continuity of the mode to be followed.

4.3 ASPECTS OF THE IN-PLANE RECTANGULAR PLATE MODES

In the past chapter, a large number of square plate modes and their vibrational patterns have been identified and described. Modes with symmetrical and non-symmetrical nodal patterns and their dependence on the material properties have been demonstrated.

Fig. 4.2 , shows that there exists two low order types of modes in the narrow rectangular plate. These are the longitudinal modes dominated mainly by the length of the plate and the Young's modulus when the width is much less than the length. These are excited by the axial

drive at the remote end point of the plate, and have an asymptotic value approaching the rod velocity.

The other type of mode was already shown by P. Lloyd, et al., to be the in-plane flexural vibration along the length of the plate. These are similar to that of "free-free bar" flexural vibrations. The length and the width are the controlling dimensions and an asymptotic value is expected to approach zero frequency but a constant value of $f\ell^2/w$ for each mode.

The fundamental of these two modes is shown in Fig. 4.3 . The axial length drive excites the longitudinal, while the mid-length drive coupled strongly to the flexural.

These types of modes have been studied extensively by several authors [31,46,48,53,66,96]. Their results have been of great assistance in the comprehensive work described here.

Two other modes in narrow plates where the width is the controlling dimension exist in addition. These are the end resonances, which are characterised by a large displacement at the corners near the driving point but this diminishes rapidly along the major length of the plate. The vibrations are in fact 'trapped' at the end. The other mode, which can be called the plate resonance, is characterised as ℓf product has a constant value

approaches to half of the plate wave velocity, i.e. the plate width is half the plate wave length.

All the modal vibrations of the square plate are expected to approach one of these modes when the plate length is much greater than the width.

4.4 SOME SPECTRAL CHARACTERISTICS

In a series of experimental investigations, a carefully machined Aluminium plate was driven to investigate the different modes of vibrations. The resonant frequency for each individual mode was measured as the ratio of the length-to-width was altered. Knowing the square plate resonant modes, it is in principle a matter of tracing them down to the narrow strip. To achieve a clear picture of the mode spectrum, it is essential to examine the vibrational pattern of the displacements and the nodal configurations of the vibrational plate. This variation with the geometry of the plate, and in particular the driving conditions for each mode, were observed by using the probe method described already in Chapter Two. This is especially useful for identifying and resolving two or more close modes and for tracing the degenerated modes - which occur at certain plate geometries- to the narrow rectangular strip. The position and orientation of the drive could be selected to give maximum displacement for a particular mode and to discriminate against adjacent ones.

Typically the longitudinal modes are best excited by a
central axial drive.

A close inspection of the graph (4.2), shows that
there are certain modes where the spectrum along the width
is the same as that along the length. The term'image'was
proposed to describe the modes with an identical spectrum
as they are 'imaged' in the 45 degree square plate line.

The lowest of these modes which exhibit the
characteristics of image symmetry are the two fundamental
square plate modes. These have symmetrical nodal lines
parallel to the sides of the square plate in the lowest
mode (Mason Mode), and form the diagonals in the Lamé mode
as was described in the previous chapter. These two modes
are analogous to mode (1,2) of the disk resonance. The
mode has been split into two different modes as a result
of the change of the plate geometry from circular to square.

These two important modes were followed as the plate
geometry was changed, and the frequency spectrum had been
investigated and a full description follows.

On the other hand, the Fig. 4.2 shows certain modes
with no symmetry of the spectrum image along both sides of
the 45 degrees line segment. In other words, the mode
losses its degeneracy as its geometry moves away from the
square plate. An example of these modes are modes (2)
and (6). The typical vibrational patterns of some modes and

their variations with the drive position for both the
symmetrical and non-symmetrical modes are shown in Fig.
4.4. The nodal lines are altered for the non-symmetrical
one according to the driving position, while the
symmetrical modes have no variation in their nodal patterns
form with the position of the drive.

The mode can be excited only when the driving line
is at the antinode, but the two modes can be excited when
the drive is at a proper position.

It is essential to point out at this stage that the
modes with a symmetry image of the spectrum are intersecting
the square plate axis of Fig. (4.2) at a right angle. The
spectrum image is a continuation from the first segment,
and it is analogous to the reflection of an image from a
mirror, while the non-symmetrical ones are intersecting
the square plate axis at an angle less than 90 degrees.
But for this proposal there is an exception, this is
represented by the spectrum of mode$^{(7)}$ Fig. 4.2 . The
spectrum of this peculiar mode will be discussed in detail
later.

4.4.1   The Lamé Modes

These have the unique characteristic of having no
displacements at the corners of the plate, and this allowed
an analytical solution to be obtained by Lamé. In a
square plate this accounts for the precise harmonic

frequency relationship which was found for all the isotropic materials studied. Similarly, rectangular plates with sides whose length are in integral ratios, modes with this particular specification are expected[48]. These are confirmed as several observations were obtained by reducing the size of the plate in steps. The results are illustrated in Table 4.1 . A series of measurements of the Lamé modes were obtained by reducing the size of the Aluminium plate so that its sides ratio are integrally related.

The progress of each of these modes was followed to the narrow rectangular strip geometry. The fundamental Lamé mode of the square plate was found to be approached by the first longitudinal mode of the long strip. The rectangular plate of sides whose length is twice the width has a Lamé mode associated with it, this is formed as a combination of two square plate Lamé mode patterns with the resonant frequency, given in Table 4.1 . This will eventually end as the second longitudinal mode of the narrow strip. Consequently, the third longitudinal mode of the strip is expected to originate from the Lamé mode of a rectangular plate whose length-to-width ratio is three.

In general, the rectangular plate possessing sides whose length-to-width ratio is an integral proportion, will have, among its modes, the Lamé mode associated with it.

The asymptotic frequency spectrum of that mode has to
approach the longitudinal mode of an order equivalent to
the sides ratio of the plate.

Fig. 4.5 shows the nodal configuration pattern of
the fundamental Lamé mode and its variation with the plate
geometry. This will finally become the fundamental
longitudinal mode as the plate gets narrower. The spectrum
has image symmetry along both sides of the plate. The
axial length drive strongly coupled to the longitudinal,
while the width drive progressively gets weaker, and
eventually when the plate is a long narrow strip, the
transfer displacement is so small that it is univerally
taken to be a nodal line at the mid-length of the plate.

The second longitudinal mode is anti-symmetric, that
is, the frequency spectrum along the plate length is not
the same as along its width. Consequently, the third and
the fourth longituindal modes have symmetrical and
anti-symmetrical spectrum image, respectively, along both
the length and width of the plate. This is illustrated
in Fig. 4.6 , the odd longitudinal modes have symmetric
spectrum; e.g. modes of harmonic order 1,3,5,...etc., and
the even ones have anti-symmetric spectrum, that is the
mode order 2,4,6,...etc., of a long rectangular strip.

In other words, in terms of square and rectangular
Lamé modes, it can be said that they are symmetric or

not according to their plate sides ratio, the odd ones are symmetric and the even are not.

The progress of the rectangular plate Lamé modes have thus been followed to their perfect square plate origin. Table 4.2 gives experimental results for some square plate modes all of which become simply longitudinal resonances. This is plotted in a graphical form and is shown in Fig. 4.7 for the first and the third longitudinal modes as the symmetrical modes. The frequency-length product approach to a constant value of the wave velocity in a long rod when the plate is very narrow.

4.4.2 The Mason Mode

This mode was described as the fundamental diagonal shear mode of the square plate resonant, originally developed by W. P. Mason[54] as a low temperature coefficient quartz resonator. Lloyd et al.,[48], were the first to trace its frequency spectrum progress to the narrow rectangular strip. It has been found that this mode is predominantly flexural of the second harmonic order. The change of the character of this mode, from diagonal shear to the flexural mode of a long bar, was demonstrated. This change is accompanied by the radical alteration in the form of the resonant spectrum curve shown in Fig. 4.2. It was realised at an early stage that for certain modes (such as Mason's), it was immaterial which side was regarded

as the 'length'. In others - the plate for example - the character changed completely. It is convenient to say that the former are frequency symmetry (or mirror symmetrical), and the others anti-symmetrical.

Fig. 4.8 , shows sketches for the resonant patterns of the Mason Mode. The radical alteration in the nodal pattern as the plate geometry changes is shown. Two more nodal lines besides the former two are generated as the mode character changes from a diagonal shear to the flexural mode. The axial length and width of the plate is a node, the best driving position is at the far end near the edges. The asymptotic value of $f\ell^2/wC_o$ of this mode might be expected to approach the constant given by Morse[71] as (2.8334). Rotational energy, not considered by Morse, results in a considerable discrepancy.

The experimental results of this mode for various plate geometry is given in Table 4.3. Aluminium plate was used in this measurement with Poisson's ratio $(\sigma=.34)$ and $C_o = 5170$.

Holland has classified all the modes which are ending as flexural modes of an even harmonic order in a group call it 'the diagonal shear modes'. Some of these modes have no displacements in the diagonal direction.

.4.4.3   The Breathing Mode

This is one of the most identifiable square plate vibrational modes, since the phase of the motion for this mode, like the radial mode of the disk resonance(1,R) is constant over the whole plate periphery. The mode is more dependent, unlike the others, on the Young's modulus, because of the change in the area of the plate. The mode is strongly coupled to the driving line at the corners in the diagonal direction. This enables it to be readily distinguished from the other modes. This is strongly assessed to resolve the mode from the others by considering its individual driving position.

The displacements pattern configuration for this mode and its frequency variation with the material characterisations was discussed and elaborated in the previous chapter.

An attempt to trace the mode progress to the narrow rectangular strip has been done by several authors[21,31,60,69,78]. However, their analysis was unsatisfactory in several aspects, mainly because this mode couples with the other modes to form some sort of a degenerate mode at certain plate sides ratio. The drive orientation overcomes this and the mode was followed over the full range of side ratios. It has been erroneously classified as a longitudinal mode of the third harmonic order[48] but

in fact, when it is narrow it is controlled by the plate modulus.

Holland's results of tracing this mode[31] is identical to that of Medick and Poa[60], even though Onoe and Pao[81] had sorted out the edge mode by considering its signficant vibrational displacements at the corners of the plate.

The complication associated with tracing the spectrum of some modes, including the breating mode, when two or more modes degenerate at certain plate sides ratio. This has been resolved by considering the vibrational pattern for each individual mode, and selecting the correct driving position with the line. It is unlikely that two different modes have the similar displacement pattern of vibration at the same frequency. The graphical representation of the progress of the breathing mode with the plate geometry change, is shown in Fig. 4.9 . The driving position of the mode and its coupling with the line is the key to resolve the mode from the others.

A close look to Fig. 4.2 shows that the mode has a constant frequency over the wide range of the length. The frequency width product has a constant value, this approaches half the plate wave velocity when the plate length exceeds twice its width. The experimental results for aluminium, quartz and pyrolytic graphite are given

in Table 4.4. The corresponding graph is Fig. 4.10 .

The mode frequency is precisely measured for different

materials with various width-to-length ratio. The plates

were chosen to be isotropic or near isotropic.and the

rod wave velocity is measured and shown in Table 4.4. The

results of the Fused Quartz is more close to the standard

figure of the plate wave velocity, while that of the

Aluminium are about 5% below that of the standard results.

This is due to the material anisotropy of the Aluminium plate

which was in rolled sheet form. The Pyrolytic graphite

has a negative inplane Poisson's ratio which was already

available from the disk resonant frequency measurements.

The Breathing mode is expected to have a symmetry

of the spectrum (mirror image) along both sides of the

plate as it is shown in Fig. 4.2 . This is clearly

obvious from the diagonal drive of the plate which is

coupled strongly to the driving line.

4.4.4 THE END RESONANCE

In the end resonance, the energy of vibration is

confined to a region near the boundary at the end of the

structure[11]. Onoe[79,81] demonstrated the existence of

this mode experimentally. Further experimental studies

[2,27,60,93] revealed the existence of this mode, and an

attempt to trace its progress has been carried out.

It was found experimentally and theoretically[38] that the strips have only one end resonance where the frequency being characterised by the frequency-width product. The mode has two symmetrical nodal points on the end of the strip.

This resonance could be completely resolved theoretically only by considering waves on the strip having real, complex and imaginary propagation constant[11,38]. These waves in combination at one specific frequency with selected amplitude ratios gives zero stresses at the free end where the resonance occurs. An important aspect of the solution is their considerable dependence on the Poisson's ratio.

The end resonance was investigated experimentally for materials ranging from brass with Poisson's ratio of (0.37) to Pyrolytic graphite with an in-plane value of (-0.10). In an Aluminium plate of the Poisson's ratio (0.34), the end resonance occurs close to the Lamé mode. This was verified by the measurements on a rectangular plate of sides whose lengths ratio have an integral relation. Fig. 4.11 shows the variations of both the end resonance and the Lamé mode with the Poisson's ratio.

In this investigation, the resonant spectrum was again followed by varying the geometry of the plate. This can be identified easily by its characteristic of large displacements at the corners near the driving point. This

diminished rapidly along the major length.

Two different modes, strongly coupled at the corners, have been identified as the plate geometry is approaching the square. These two modes have vibrational patterns so that the end resonance occurs as a result of the degeneracy of these two modes when the plate length exceeds twice its width. The experimental results are shown in Table 4.5 as the plate geometry was changed step by step.

These two modes have most significant displacements at the corners . The phase of the motion is same at the corners near the drive for the two modes, and in reverse phase at the far remote corners,as it is illustrated in Fig. 4.12 . The combination of these two modes will result in strong displacements at the corners where the phases of motion are the same, and a cancellation in the displacements when the phases of the motion are in reverse order.

4.5   NON-IMAGING SPECTRUM MODE

It has been demonstrated before,the existence of two types of modes in the narrow rectangular strip, and these are clearly illustrated in Fig. 4.2 . The spectra are shown in the segments below and above the 45 degrees line which represents the square plate. Some of these modes have symmetry of the image spectrum along the two sides

of the plate, while others have not. The former modes
(the symmetric) have already been described , the lowest
of these were recognised as the Mason and the Lamé modes
where each has two nodal lines - in Mason's case parallel
to the sides and in Lamé's case the two diagonals. The
centre of the plate is a perfect node. These are analogous
to the single mode (1,2) in the disk resonance.

It will be observed that the lowest of the modes with
no imaging of the spectrum along both sides of the plate
are modes (2) and (6) on the square line axis of Fig. 4.2 .
The first of those is strongly coupled at the corners
near the drive vector used for exciting the end resonance
as described in the previous section.

Driving the plate at the mid-length will couple to
the fundamental in-plane flexural mode. This is similar
to the "free-free bar" flexural vibration with an
asymptotic value of $f(\ell^2/w)/C_o$ will approach the
constant given by Morse[71]:-

$$\frac{f(\frac{\ell^2}{w})}{C_o} = \frac{\pi}{4\sqrt{3}} \beta_n^2 = 0.453 \beta_n^2 \tag{4.1}$$

where (n) is the mode number and $\beta_1 = 1.5056$, $\beta_2 = 2.4990$
and β_n for $n \geqslant 3 = (n + \frac{1}{2})$

The fundamental flexural mode will approach a
constant value of (1.0279) for an absolutely thin bar

where the width is very small comparing to the length, this is shown graphically in Fig. 4.13 . The experimental values of $f(\ell^2/w)/C_0$ is plotted for different plate geometries, then the estimated asymptotic value is expected to match with the constant given by Morse. Different materials were used and identical results have been observed (Fig. 4.13).

The sketches of the vibrational displacements patterns for this mode of various plate geometry is shown in Fig. 4.14 . The plate is driven at the mid-length or at a point where the maximum displacements in occur. It can be seen that the axial length drive does not excite this mode, since this point is a node.

Accurate results of the experimental measurements for an Aluminium plate is given in Table 4.6 .

The next mode which has no imaging of the spectrum is mode (6) in Fig. 4.2 . The square plate nodal pattern shows that it has three nodal lines crossing each other at the centre of the plate to form an axial node. This was confirmed by clamping the plate at its axial centre and observing that there was no increase in damping. The mode is analogous to mode (1,3) of the disk resonance, and this is used as an identification of the mode.

The vibrational spectrum of this mode has been examined by driving the plate at two different positions,

and two different modes have been recognised. The first
is the longitudinal mode when the plate is driven at the
remote end. This mode is of the second harmonic order
as it is two Lamé patterns when the plate side ratio is
exactly two. The frequency-length product approaches a
constant value of the rod wave velocity when the plate
width is small comparing to the length. The second mode
is excited by driving the plate at the mid-length, this
is the flexural mode of the third harmonic order, and it
will approach a constant value of $f(\ell^2/w)/C_o$ given by
equation (4,1), which is equal to (5.5548).

Fig. 4.15 is a graphical representation for the two
modes and their splitting as the plate geometry change
away from the square plate. The frequency-length is
normalised to the rod wave velocity which was measured
using a long strip plate machined out from the same plate.
It is essential to mention here that some of the flexural
results have been measured using a small plate because
of the difficulties associated with the low frequency
measurements using the line system. The precise
experimental results are given in Table 4.7, the
normalised frequency for different plate geometries of
an inplane isotropic Aluminium plate for the two modes
are represented.

The considerable change of the vibrational patterns
of this mode and the corresponding nodal configuration is

of great interest. Because of this the mode spectrum was very carefully followed down as the plate geometry changed. Knowing the nodal pattern of the displacements for both the second harmonic longitudinal and the third harmonic flexural modes, the change of the pattern configuration with the geometry of the plate can be predicted. The pattern alteration from the Lamé mode to the longitudinal mode has been described already. The variation of the longitudinal and the transverse displacements was shown in detail, and this can be used to describe the pattern variation as the second Lamé mode changes to the second longitudinal mode. This is acompanied by a radical alteration in the transverse displacement, the plate getting narrower and the longitudinal displacements dominated the mode. The transverse movement is so weak it appears as a node and is normally regarded as such.

Proceeding further, the third order flexural mode has four nodal lines parallel to each other with the fifth one crossing them at half the width. The complete picture of the pattern variation with the geometry of the plate is shown in Fig. 4.16 , and sketches of pattern displacments are illustrated by the arrows which indicate the direction of the movement.

4.6 THE OTHER MODES

The frequency spectrum of some other higher order square plate vibrational modes were carefully investigated these are including the other Lamé modes which were already reported and their harmonic frequency relations were identified in the previous chapter. Some of these modes have been reported and their vibrational spectrum have been investigated by several authors[31,32,48], but only for limited plate side ratios.

The spectra of odd harmonic longitudinal modes always have symmetry of image along the length and the width of the plate, but not the even order modes. They become inherently flexural of odd harmonic orders. For excitation they are best driven at the mid-length.

Fig. 4.2 clearly illustrates the above discussion. The image spectrum is a continuation of the original one, and this is crossing the 45 degrees line at a right angle. While the non-imaging spectrum seems to cross this line at an acute angle. There are exceptions to this proposal as can be seen in the case of the specrum of mode (7). The mode is strongly coupled at the edges at 45 degrees angle with the driving line when the plate is a perfect square, and it progressively approaches the flexural bar mode of the fourth harmonic number when the plate sides ratio is small. In spite of its intersection with the

square plate line at an acute angle, there was no
evidence of the continuation of the spectrum in the other
segments. For this reason the mode assumed to have a
symmetry of the spectrum image along the two sides of the
plate, but this mode continues to be somewhat of an
enigma.

The spectrum of the even harmonic order flexural is
typified by the Mason mode, which has an imaging along
the both sides of the plate as it was shown before. It
is proposed that all the flexural modes of even harmonic
order have the same spectral characteristics.

4.7   MODE DEGENERACY OF THE RECTANGULAR PLATES

Some square plate modes are degenerate in that two
modes have the same frequency and nodal pattern. These
lose their degeneracy if the plate geometry moves away
from the perfect square. It can also be removed when the
plate material ceases to be isotropic.

In a rectangular plate, degenerate modes commonly
occur. This is well illustrated in Fig. 4.2, where two
spectra intersect each other at certain plate length-to-
width ratios. For instance, the two fundamental square
plate modes - those of Lamé and the Mason - approach the
first longitudinal and the second flexural modes
respectively,as the plate geometry changes. It can be

seen in Fig. 4.2 that the two mode spectra are degenerate at the two successive plate sides ratios (83/50) and (25.4/7). It was found that the plate side ratio for these conditions modes are virtually the same for all isotropic materials[35].

4.8 GENERAL COMMENTS

The frequency spectra of a large number of rectangular plate modes have been identified and discussed. The materials used in this measurement chosen to be isotropic, although some show a small anisotropic effect.

Modes with certain well-defined vibrational patterns were easy to identify and their resonant frequencies were followed over a wide range of geometries. Modes of special interest were examined. Of these are the end resonance and the plate resonance. The end resonance is well defined when the length is more than twice the width. It will be seen in Fig. 4.2 that two modes which are completely separate in the square plate come together to form the end resonance. The plate resonance was found to be the breathing mode when the geometry becomes that of the square plate. This has a special interest in material characterisation as it shows the effect of the Poisson's ratio on the resonant frequency. By using two different modes of the plate, some materials moduli and other engineering constants can be calculated and identified. This is comprehensively treated in the early chapters.

The complexity of the vibrational patterns for some higher order modes set a limit to the procedure for following the spectra. The recurrence of the Lamé mode pattern at certain plate geometries gives a valuable clue to their identity. The Lamé mode always tends to approach the longitudinal mode when the plate width becomes small compared to its length. The nodal pattern symmetry and the phase of the motion at different points on the plate periphery is valuable in the process of recognising the mode spectrum and predicting their asymptotic behaviour. Certain nodal vibrational patterns can be simple at certain sides ratios, while the alteration of their geometry tend to change them to an extremely complicated form. Some of these vibrational patterns have complex nodal structures, but using the probe technique, and clamping the plate at certain points provide valuable additional evidence. As an example for the pattern complexity as the plate geometry change is mode (2,2) shown in Fig. 4.17. The nodal lines at certain plate sides ratio have a curved form but are lines of zero stress. This can be interpreted as a result of generation of some other nodes and antinodes on the pattern. The Lamé resonant mode will be identified when the plate sides ratio will have a value of (3:1). This mode approaches the longitudinal mode of the third harmonic order, when the plate length is much greater than the width as has been shown earlier. This mode has

an image of spectrum along both sides of the square

plate line of Fig. 4.2.
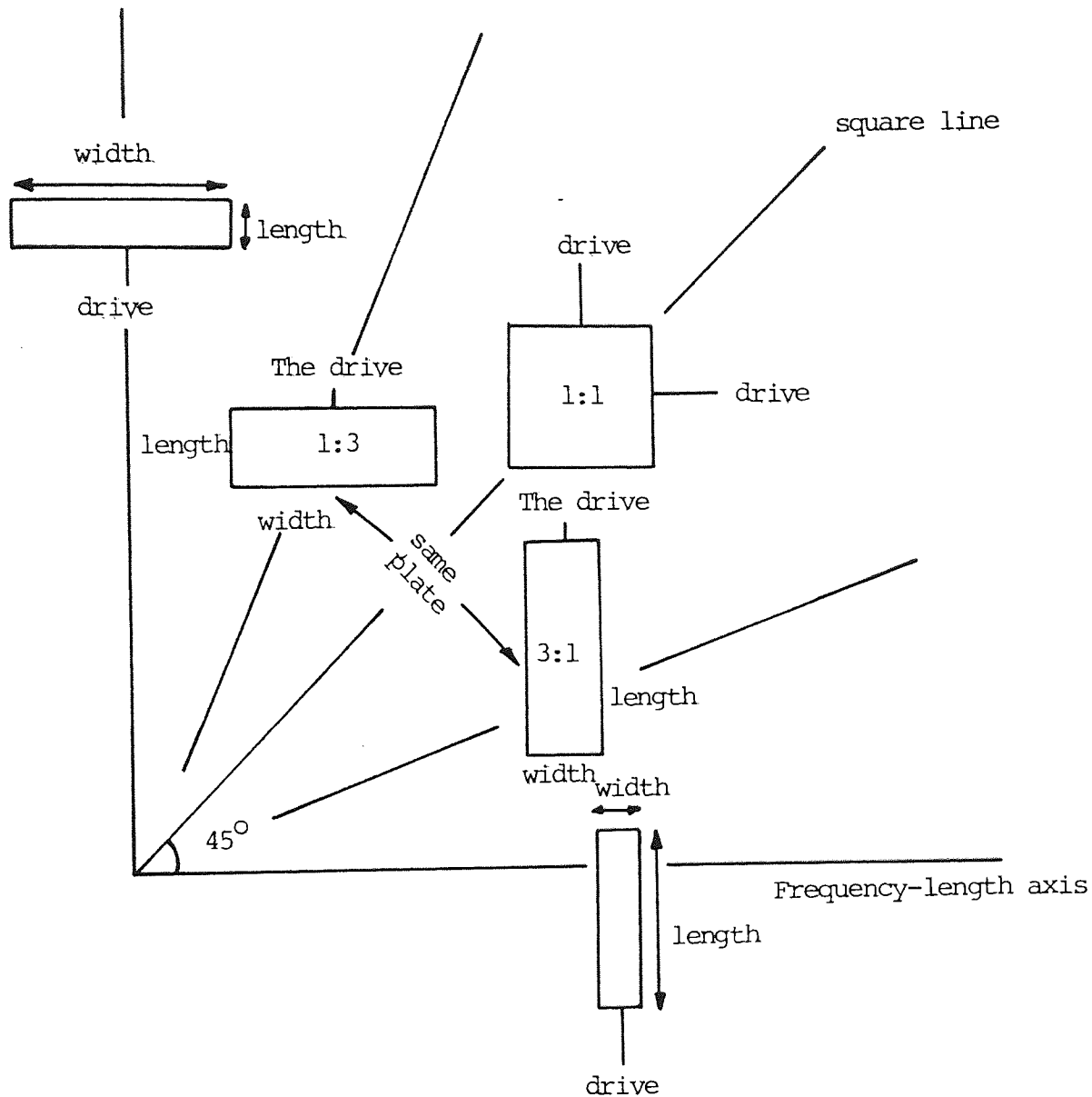
Fig. 4.1 The presentation of the frequency spectrum according to the plate drive. The angle is proportional to the length-to-width atio. An angle of 45 degrees represents a perfect square plate.

Fig. 4.2   An empirical presentation of the observations

for Aluminium rectangular plate, $(C_o=5170 \text{ m.sec}^{-1}$

and Poisson's ratio $\sigma = 0.34)$. Here the modes

spectra are presented by the width and the length

of the plate considering the frequency has a

fixed value of 100 KHz. The two segments below

and above the square plate line (45 degrees line)

are presenting conditions of the mode when they

are driven at an axial length and width

respectively. Anti-symmetric modes are showing

completely different spectra at each segment,

while the symmetric modes have mirror image of

the spectra.

Figure. Plot of frequency–width product (vertical axis, 5 to 70) versus frequency–length product (horizontal axis, 0 to 100) and $2\ell f/c_0$ (0.5 to 3.5), showing modes: Square plate line, The Plate Resonance, The End Resonance, Mode (2,2), Mode (1,3), Breathing Mode, Lamé Mode, Mason Mode, Flexural 1, Flexural 2, Flexural 3, Flexural 4, The plate resonance, Square Plate Line, Longitudinal 1, Longitudinal 2, Longitudinal 3, with numbered points 1–9.

Axial
length
drive

mid-length drive is the best to couple the flexural

Fig. 4.3   Sketches for the resonant vibrational patterns for
the fundamental longitudinal and in-plane flexural modes
of a narrow rectangular plate.

The longitudinal modes are best excited by a central axial
drive at the remote end; while the flexural modes need
different driving conditions, normally at the position
where the vibrational displacements have maximum amplitude.

NODE   NODE   NODE

NODE

NODE
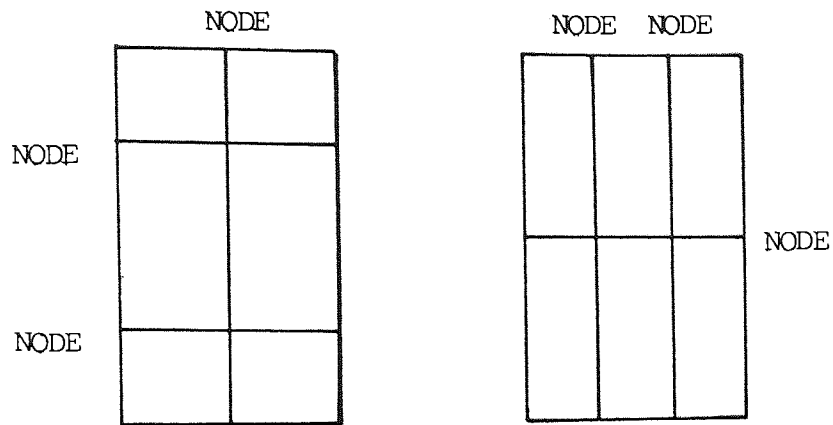
(A)

Frequency is not equal (no image)

NODE   NODE

NODE   NODE
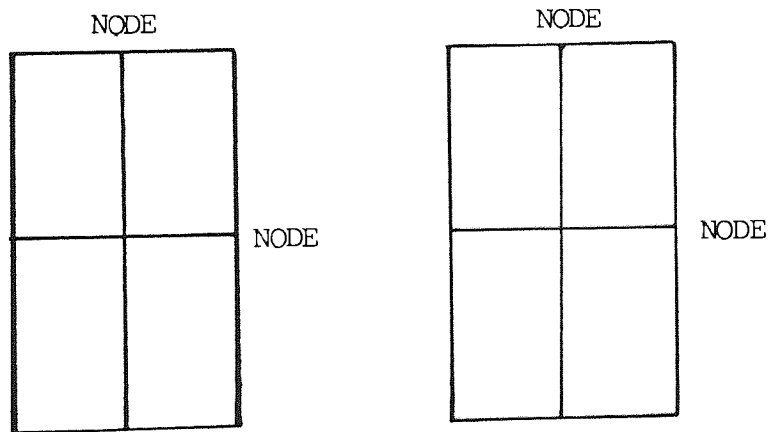
(B)

Frequency equal (equal image display)

Fig. 4.4 This diagram shows sketches for the nodal patterns of
         the non-symmetrical and symmetrical modes of the
         rectangular plate.
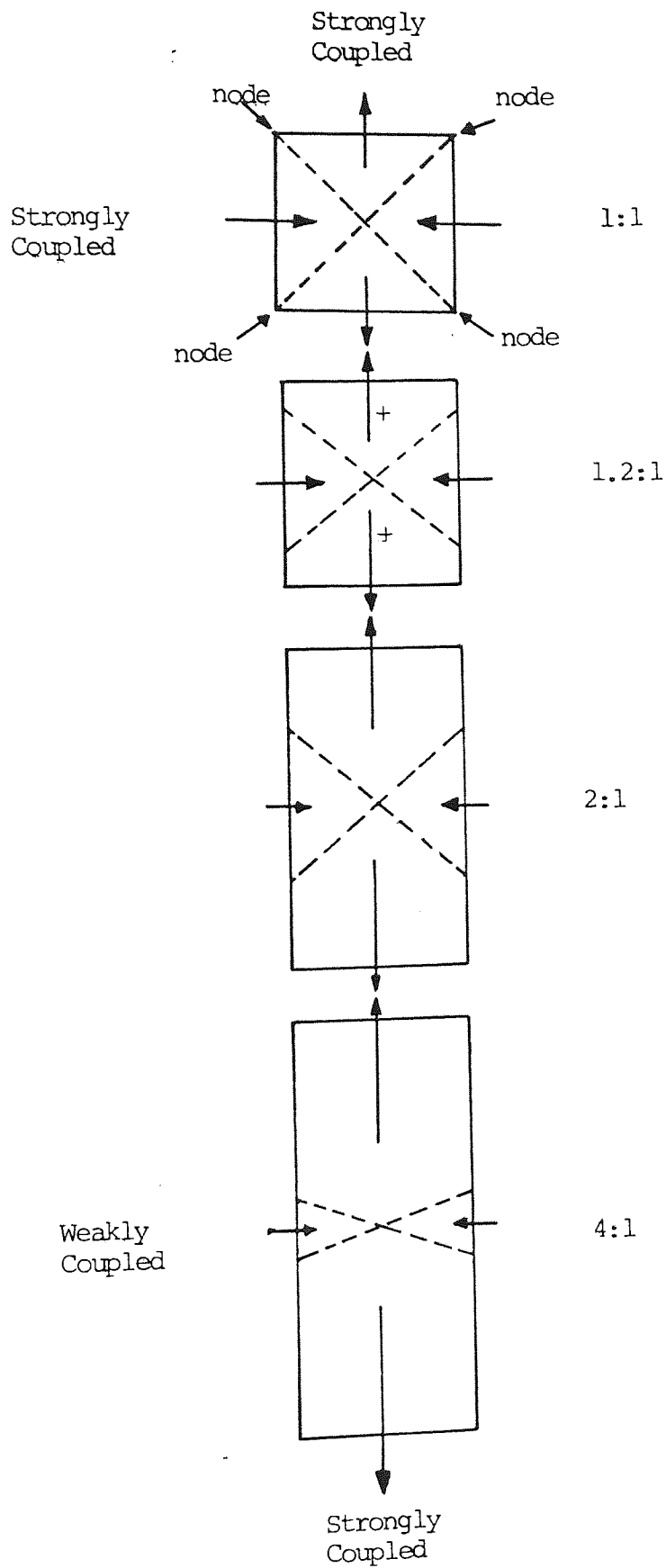
Fig. 4.5 The variation of the nodal pattern configuration of the Lamé mode with the width-to-length ratio of the plate.

-84-

SYMMETRIC MODE

$\lambda/4$ $\lambda/4$

1st Order Mode

ANTISYMMETRIC MODE

$\lambda/4$ $\lambda/2$ $\lambda/4$

2nd Order Mode

$\lambda/4$ $\lambda/2$ $\lambda/2$ $\lambda/4$

3rd Order Mode

$\lambda/4$ $\lambda/2$ $\lambda/2$ $\lambda/2$ $\lambda/4$

4th Order Mode

$\lambda/4$ $\lambda/2$ $\lambda/2$ $\lambda/2$ $\lambda/2$ $\lambda/4$

5th Order Mode

$\lambda/4$ $\lambda/2$ $\lambda/2$ $\lambda/2$ $\lambda/2$ $\lambda/2$ $\lambda/4$

4th Order Mode
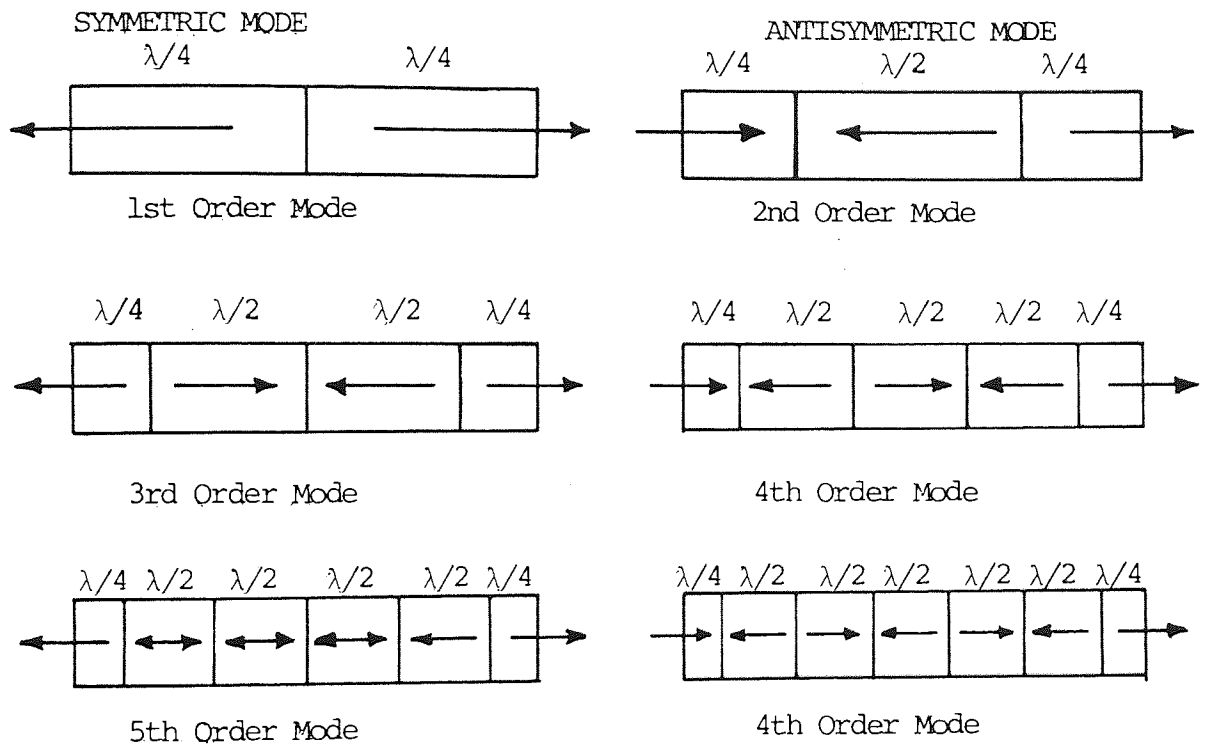
Fig. 4.6   The longitudinal Rectangular plate modes and their
           nodal pattern configurations. The symmetric modes
           have nodes at the mid-length of the plate with an odd
           harmonic mode orders, while the antisymmetric modes have
           antinode at mid-length of the plate with an even
           harmonic mode orders.

The Frequency Spectrum of the First and the Third
Longitudinal Modes of an Aluminium Isotropic Plate.

$2\ell f = 3C_O$

7000

$(C_O = 5170 \text{ m.sec}^{-1}$
Poisson's ratio = 0.34)

Lamé
Mode

Square Plate

ℓf

5000

Drive

Drive

ℓ

w

Drive

ℓ

w

3000

Third Longitudinal

$2\ell f = C_O$

Lamé Mode

First Longitudinal

1000

O   0.5   1.0   1.5   2.0   2.5

w/ℓ
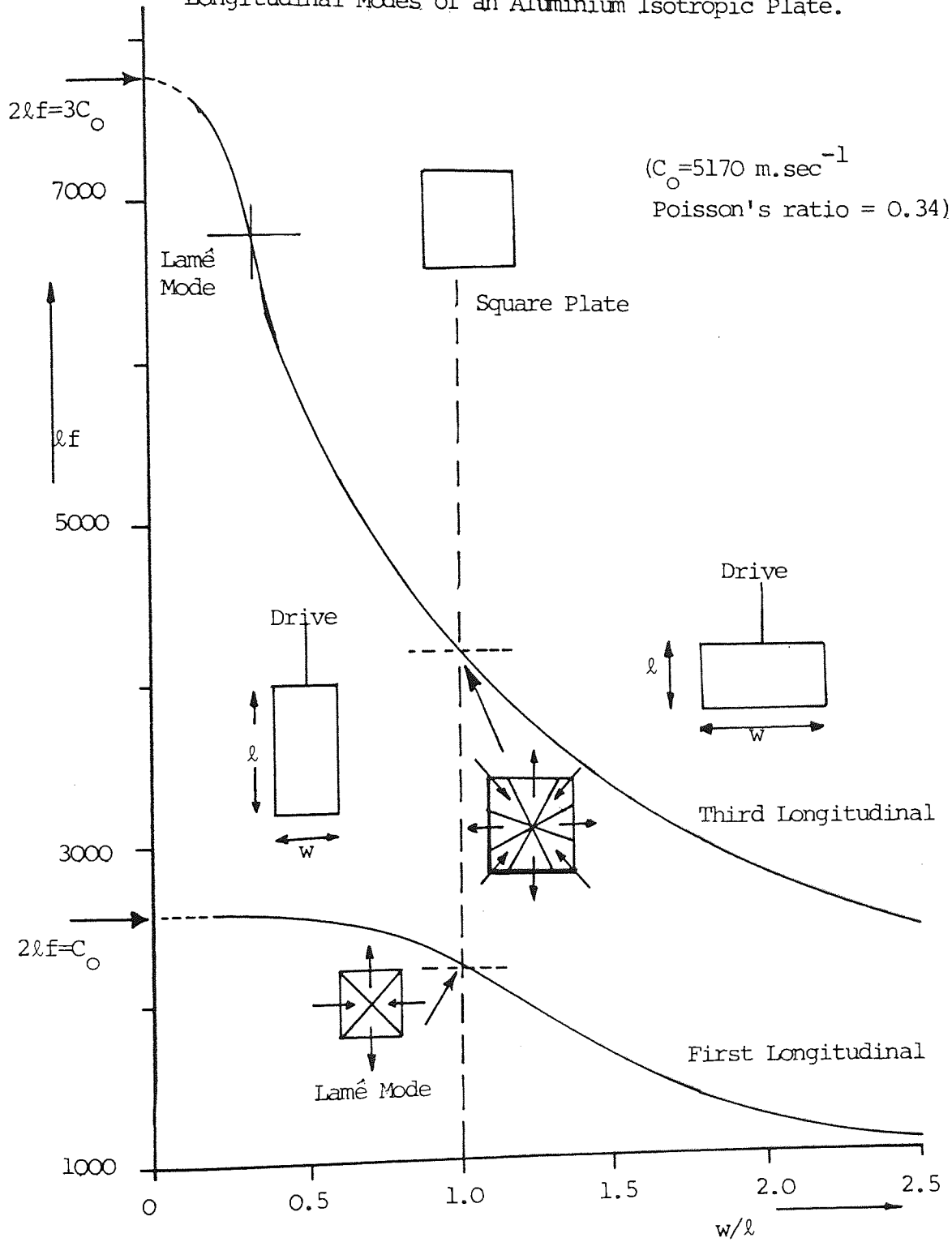
Fig. 4.7 This is a direct graph of the experimental data given
in Table 4.2

Square.
Plate
Geometry
(1:1)
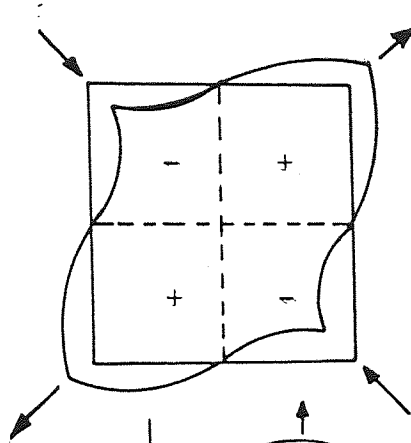
Diagonal
Shear
Mode

Rectangular
Plate
(1.2:1)
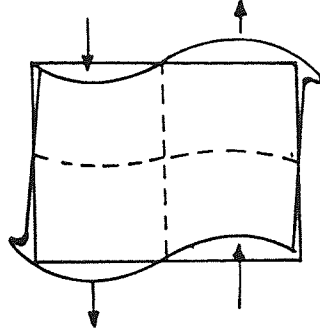
Rectangular
Plate
(2:1)
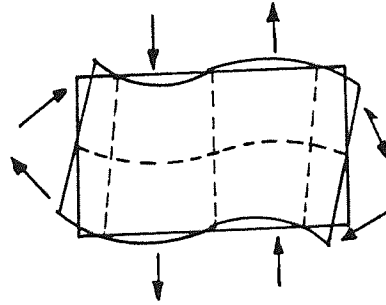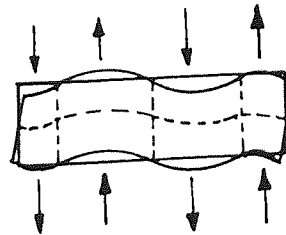
Second order
Flexural
Mode

Long Strip

Fig. 4.8   The change of the modal pattern configuration of Mason
Mode to flexural bar mode of the second harmonic order
as the plate geometry changes.
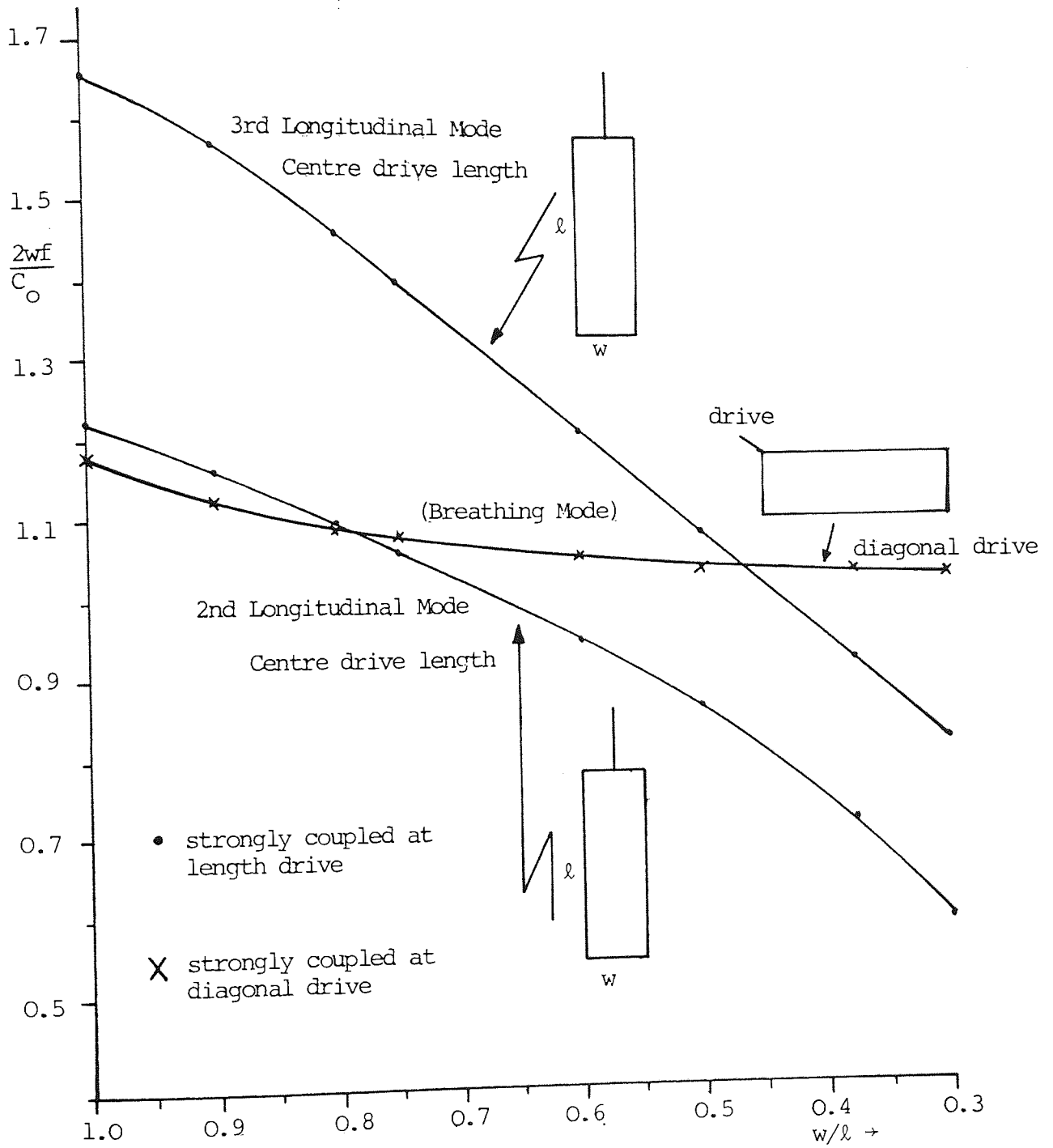
Fig. 4.9 Graphical plot of the progress of the breathing mode through the variation of the plate sides ratio. (Aluminium plate $C_O = 5160 \text{ m.sec}^{-1}$ and $\sigma = 0.34$).
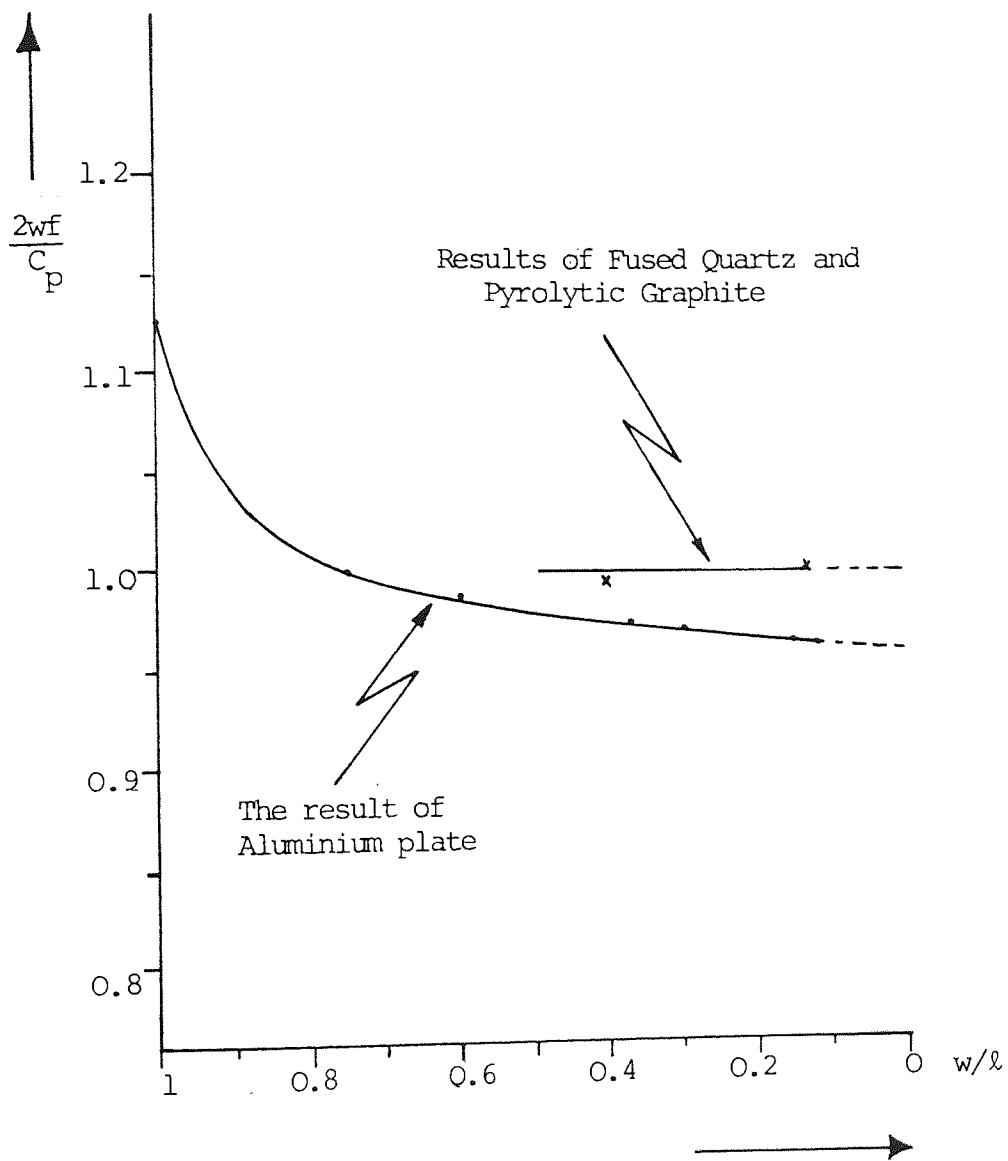
Fig. 4.10   The graphical representation of the breathing mode
            variation with the plate geometry. The result plotted
            from Table 4.4.

Lamé Mode and the End Resonance
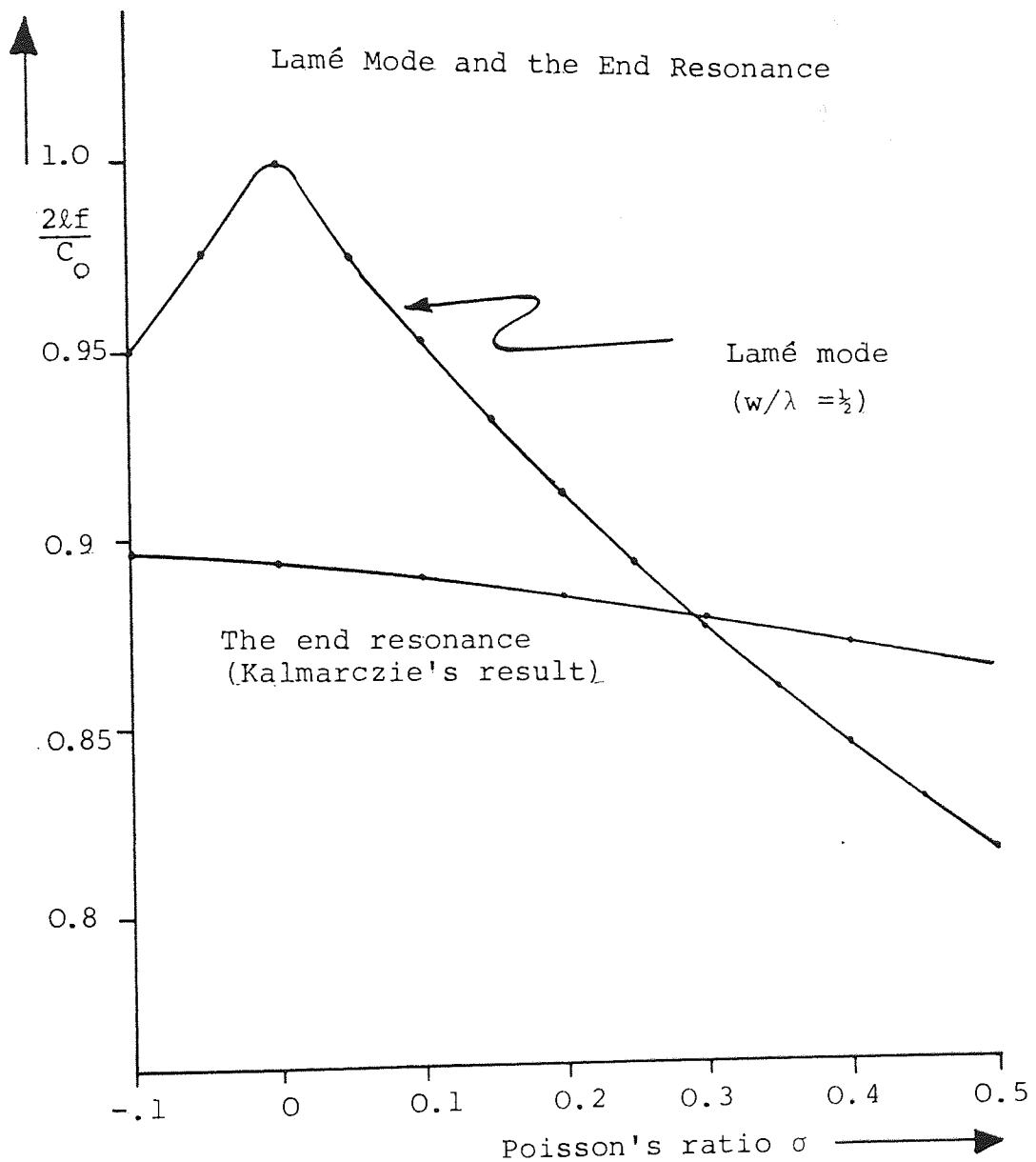
Fig. 4.11 Graphical plot for the variations of Lamé mode and the
end resonance as a function of Poisson's ratio. The
values of the normalised frequency for the end resonance
obtained from Kalmarczie's thesis (Reference 38). Values
of the Lamé mode obtained from the table in Appendix A.

Square
Plate

1:1

Frequency not equal

Rectangular
Plate

2:1

Frequency is equal
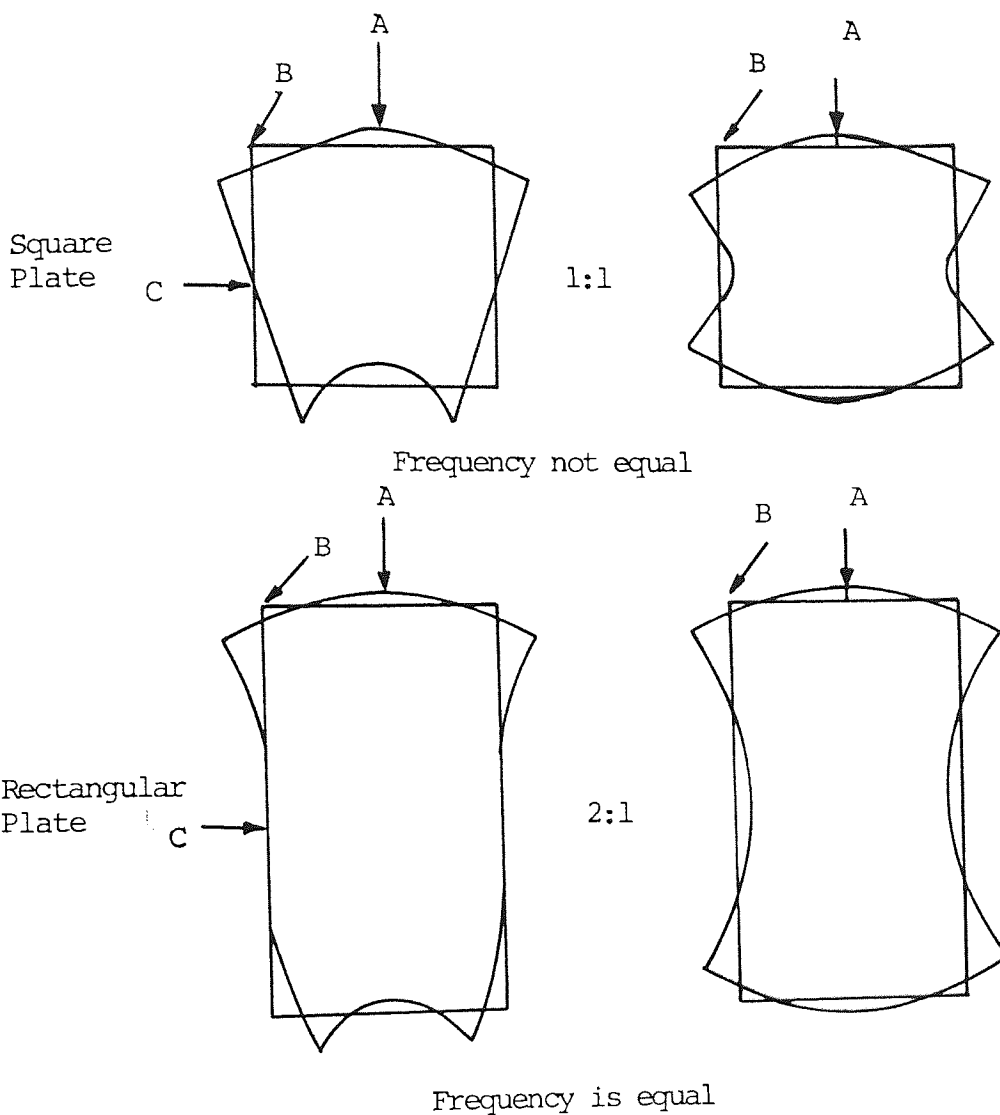
A = Fairly coupled   B = Strongly coupled   C = Node

Fig. 4.12   Sketches for the pattern displacements of the two modes
which their frequencies degenerate to form the end
resonance when the plate length exceeds twice its width.
As the plate increase, the displacements near the drive
add together and at the remote end cancel out.
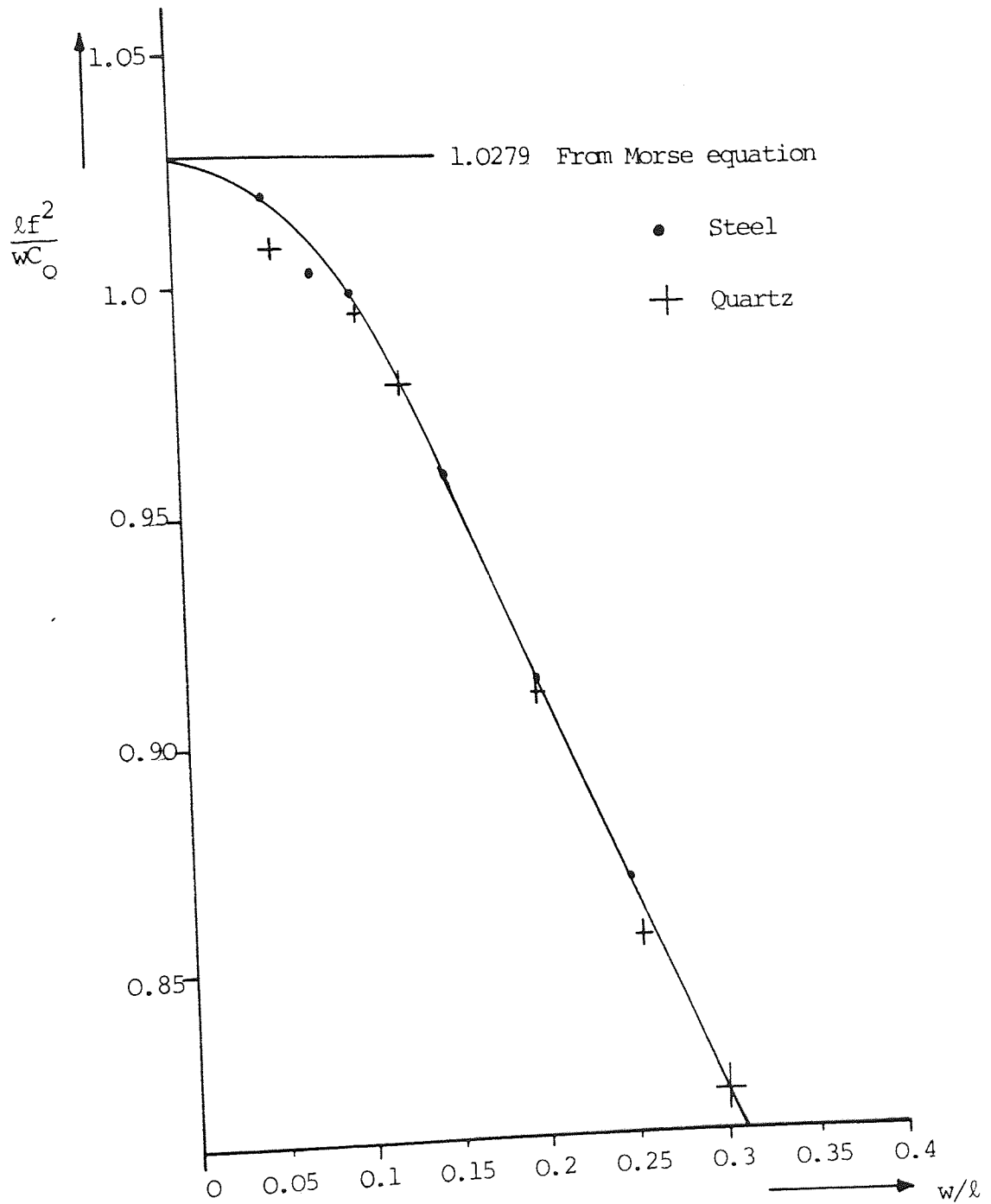
Fig. 4.13 Graphical plot for the variation of the fundamental flexural mode of a rectangular plate with the plate sides ratio. The asymptotic value is obtained from equation (4.1).
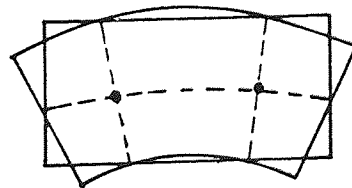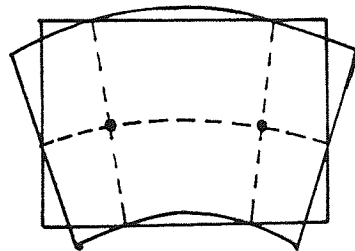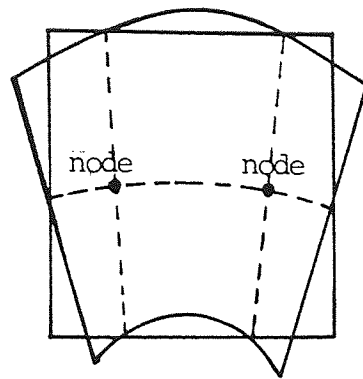
Fig. 4.14 This diagram shows the variations of the vibrational displacement pattern configurations of the fundamental flexural mode as the plate geometry change. The mode will approach the fundamental 'free-free bar' flexural vibration.
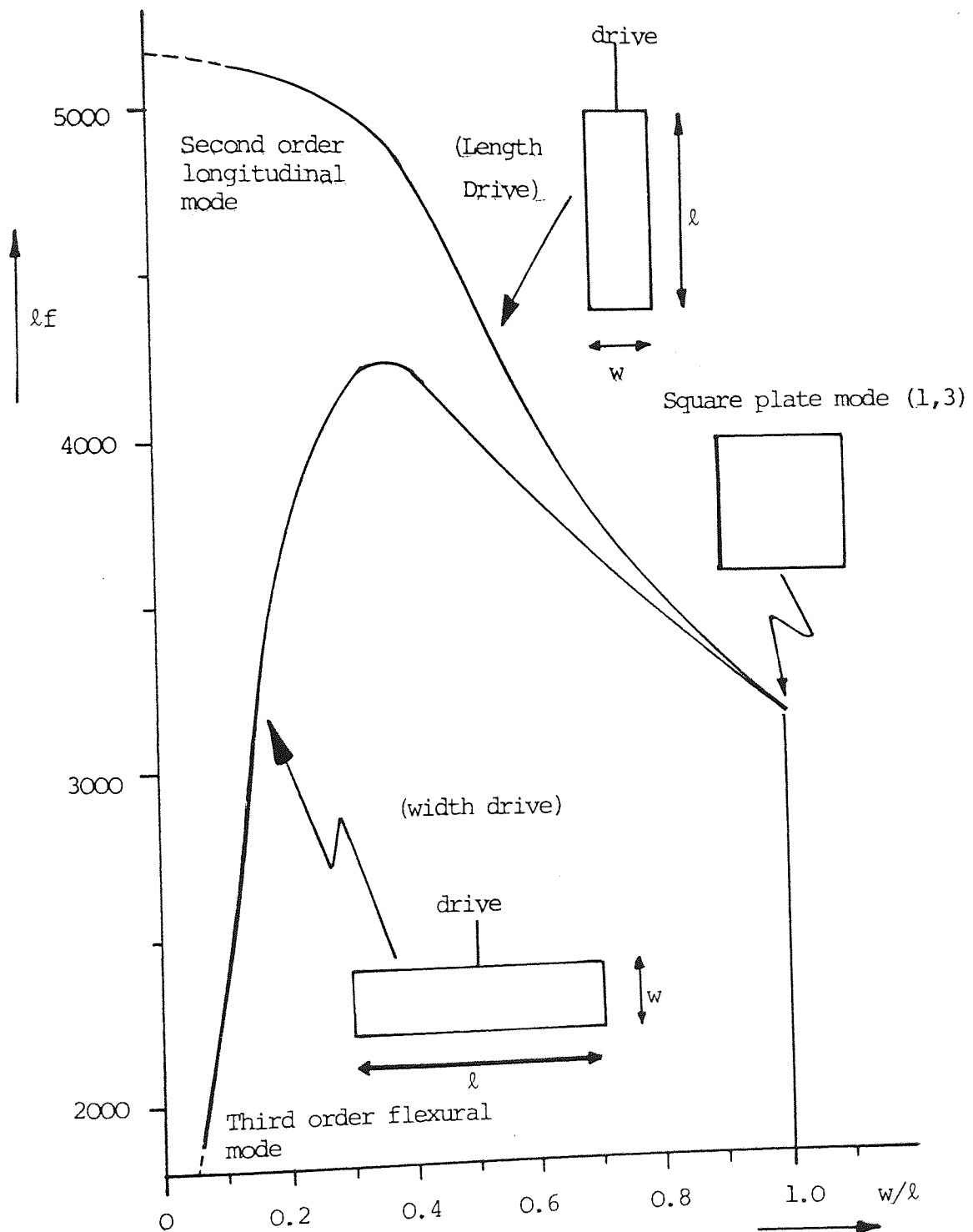
Fig. 4.15 Graphical plot for the frequency spectrum of the square plate mode (1,3) (Mode (6) in Fig. 3.1) as the plate geometry change. The mode split into two separate modes at different driving position. Longitudinal mode when the plate driven at the remote far end, and flexural mode excited by an axial width drive (Aluminium plate, $C_o = 5170$ m.sec^{-1} and $\sigma = 0.34$).

Square
Plate

1.2:1

2:1

3:1

Fig. 4.16

5:1

10:1

STRIP

2nd Mode Longitudinal

3rd Mode

Bar Flexural
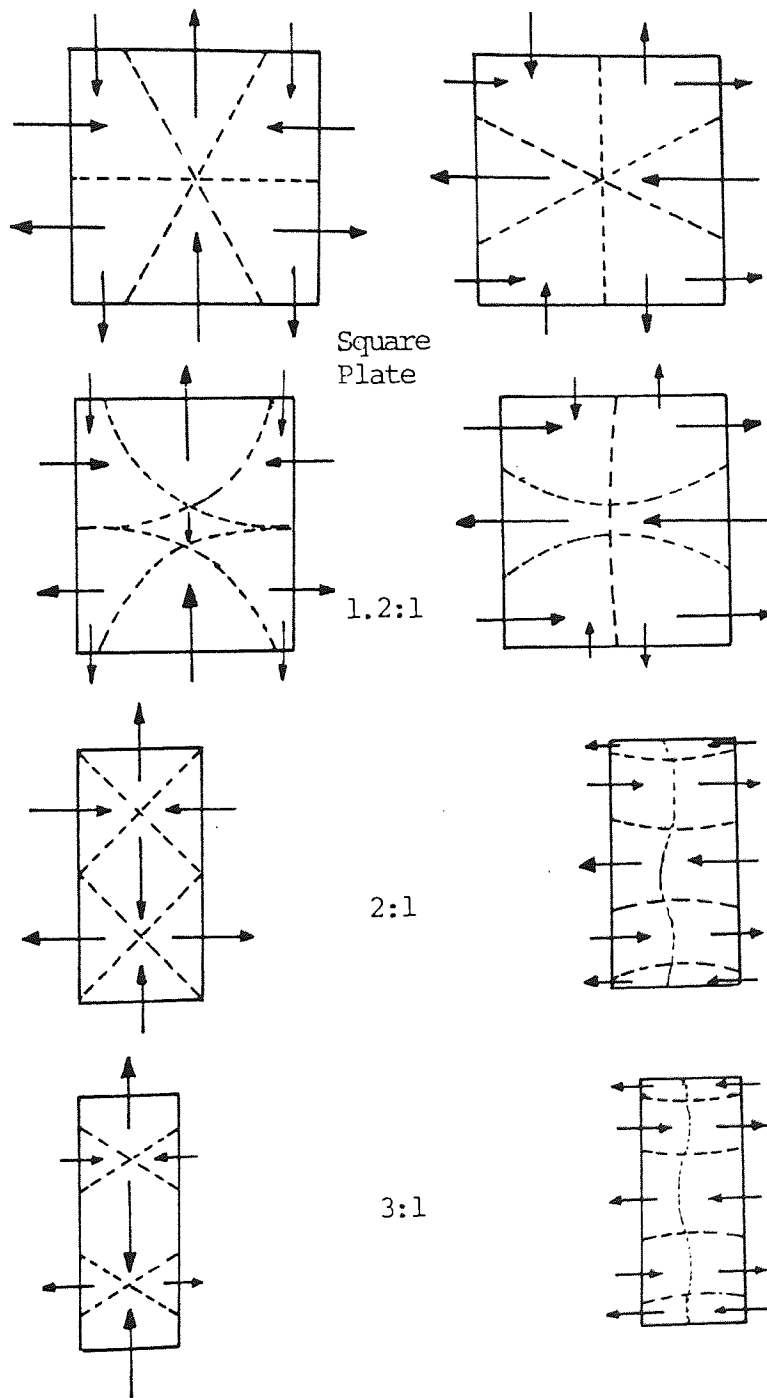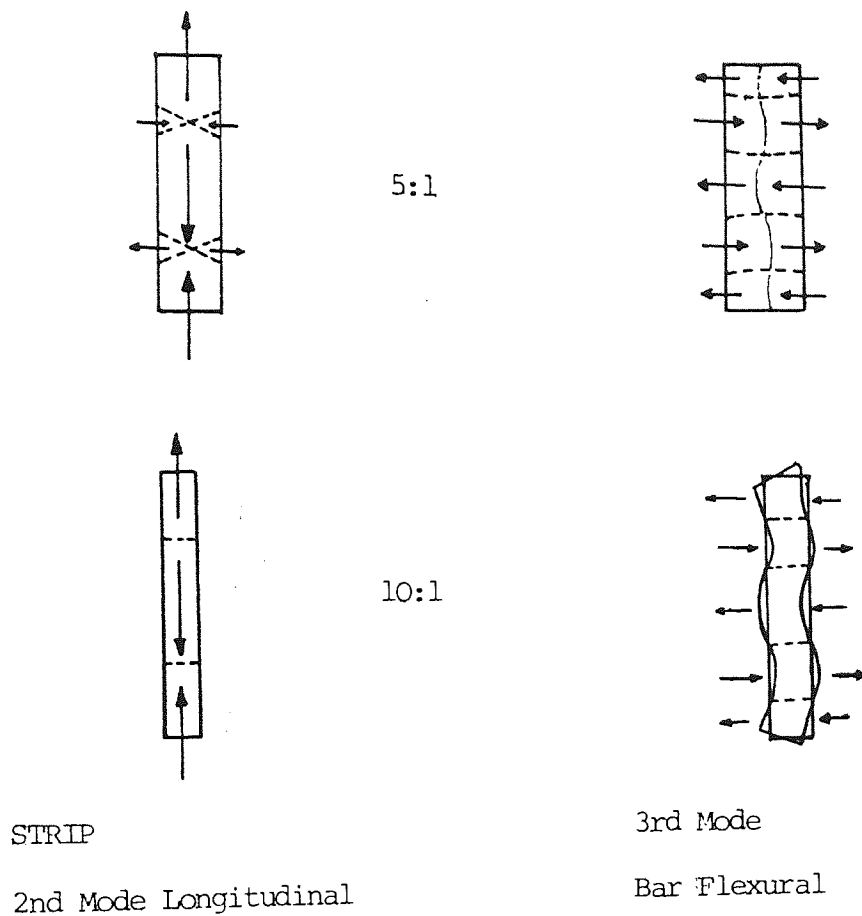
Fig. 4.16   This is showing the radical variation of square plate
mode (1,3) as the plate sides ratio change. The mode
split into two different modes as the plate changes to
a narrow strip. These two modes are the second
longitudinal and the third in plate flexural of a long
narrow strip.

Rectangular Plate

Square Plate
Mode (2,2)

2:1

1.5:1

1:1

Centre is node
straight nodals line
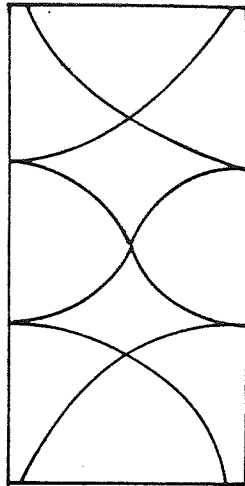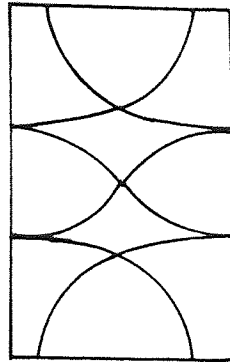
Nodal pattern having curved shape.

The third
harmonic order
Lamé mode
(Corners are
nodes)
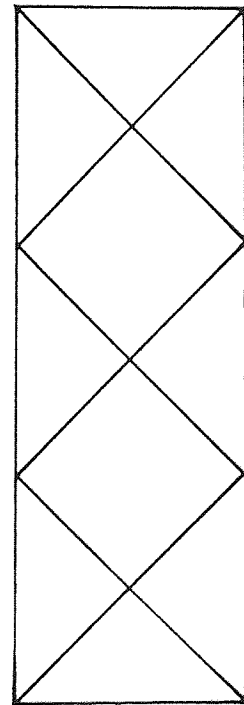
3:1
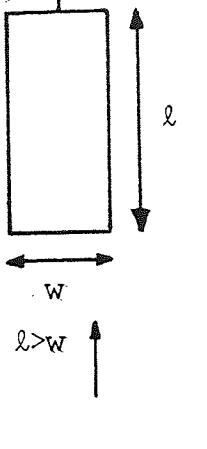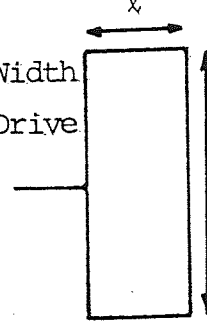
Fig. 4.17 This is showing the pattern variation of the square plate
mode (2,2) to rectangular Lamé mode when the plate length
is exactly three times the width. This radical alteration
is accompanied by a change in the nodal pattern
configurations.

TABLE 4.1

The Length mm	Length:Width	Frequency KHz	$f\ell$ m.sec^{-1}	fw m.sec^{-1}	$\dfrac{fw}{C_s}$
35	1:1	64.082	2242.86	2242.86	0.7102
70	2:1	63.989	4479.23	2239.62	0.7092
105	3:1	63.860	6705.31	2235.10	0.7078
140	4:1	63.877	8942.78	2235.70	0.7079
175	5:1	63.926	11187.0	2237.40	0.7085

Experimental results for the Lamé modes of Aluminium plate having harmonic side ratios. (C_o = 5170 m.sec^{-1}, C_s = 3158 m.sec^{-1} and σ= 0.34).

TABLE 4.2

	w/ℓ	ℓf_1	$\dfrac{\ell f_1}{C_o}$	ℓf_3	$\dfrac{\ell f_3}{C_o}$
Length Drive	0.20	2577.0	0.4985	7562.9	1.4628
	0.24	2578.8	0.4988	7433.8	1.4379
	0.30	2574.4	0.4988	6287.1	1.3625
	0.375	2550.3	0.4933	6287.1	1.2161
ℓ	0.417	2547.0	0.4926	5914.5	1.1440
	0.500	2528.4	0.4891	5658.0	1.0944
	0.625	2496.9	0.4830	5125.3	0.9914
w	0.708	2466.5	0.4771	4927.8	0.9532
$\ell > w$	0.750	2443.7	0.4727	4832.9	0.9348
	0.834	2385.1	0.4613	4651.7	0.8997
	0.917	2314.2	0.4476	4493.7	0.8692
$\ell = w$	1.00	2222.7	0.4299	4311.9	0.8340
	1.044	2175.2	0.4207	4217.1	0.8157
	1.143	2054.6	0.3974	4007.4	0.7751
	1.263	1910.0	0.3694	3754.9	0.7263
	1.412	1747.1	0.3379	3490.5	0.6751
	1.449	1656.1	0.3203	3349.9	0.6479
	1.600	1560.6	0.3019	3203.3	0.6196
$\ell < w$	1.712	1464.7	0.2833	3066.7	0.5932
ℓ	1.845	1363.4	0.2637	2935.8	0.5679
	2.000	1264.2	0.2445	2829.0	0.5472
Width Drive	2.398	1061.5	0.2053	2464.4	0.4767
	2.667	956.4	0.1850	2357.7	0.4560
w	3.334	772.3	0.1494	2113.3	0.4088
	4.167	618.9	0.1197	1784.1	0.3451
	5.000	515.4	0.0997	1512.6	0.2926

Experimental results for the first and the third longitudinal modes and their variations with the plate sides ratio. Aluminium plate was used with $C_o = 5170$ msec^{-1} and Poisson's ratio = 0.34.

TABLE 4.3

$\ell \times w$ mm$\times$mm	w/ℓ	Frequency in KHz	ℓf	$\dfrac{\ell f}{C_o}$
30×30	1.00	64.262	1927.9	0.3729
40×30	0.750	56.271	2250.8	0.4354
70×50	0.714	32.910	2303.7	0.4456
80×50	0.625	31.080	2486.4	0.4809
50×30	0.600	50.588	2529.4	0.4892
90×50	0.556	29.251	2632.6	0.5092
100×50	0.500	27.305	2730.5	0.5281
34×15	0.441	82.277	2797.4	0.5411
50×20	0.400	56.558	2827.9	0.5470
40×15	0.375	69.373	2774.9	0.5367
120×40	0.334	22.740	2728.8	0.5278
50×15	0.300	52.719	2636.0	0.5099
70×20	0.286	37.212	2604.8	0.5038
80×20	0.250	30.806	2464.5	0.4767
35×8	0.229	67.020	2345.7	0.4537
75×15	0.200	28.904	2167.8	0.4193
96×15	0.156	19.395	1861.9	0.3601
80×8	0.100	16.23	1298.4	0.2511

Experimental results of the variation of the Mason mode with the plate geometry. The mode will be ended as a second order "free-free-bar" flexural vibration. (Results for Aluminium plate $\sigma = 0.34$).

TABLE 4.4(a)

Plate velocity (C_p)=5487 m.sec^{-1} and $\sigma = 0.34$

Length mm.	Width mm.	w/ℓ	Frequency KHz	$2wf$ m.sec^{-1}	$\dfrac{2wf}{C_p}$
30	30	1.00	101.012	6060.7	1.1046
40	30	0.75	93.227	5593.6	1.0194
50	30	0.60	90.780	5446.8	0.9927
60	30	0.50	88.355	5385.6	0.9815
80	30	0.375	89.095	5345.7	0.9742
100	30	0.300	88.790	5327.4	0.9709
125	30	0.24	87.836	5328.6	0.9711
150	30	0.20	87.363	5241.8	0.9553
175	30	0.175	87.310	5238.6	0.9547
200	30	0.150	88.903	5334.2	0.9722

TABLE 4.4(b)

FUZED QUARTZ
$\sigma=0.165$ $C_o=5736.3$ $C_p = 5816.0$

ℓ	w	w/ℓ	f	$2wf$	$2wf/C_p$
31.67	12.7	0.401	227.542	5780.0	0.9938
37.236	12.7	0.341	228.765	5811.0	0.9991
63.35	12.7	0.20	228.250	5780.0	0.9938
101.6	12.7	0.125	229.710	5835.0	1.0033

TABLE 4.4 (c)

Pyrolytic Graphite					
$\sigma = -0.075$		$C_o = 3715$			$C_p = 3725.5$
ℓ	w	w/ℓ	f	2wf	$2wf/C_p$
31.75	12.7	0.40	145.42	3693.7	0.9915
63.35	12.7	0.20	148.47	3771.1	1.0122

The variation of the Breathing mode with the plate geometry.

The value of 2wf is approaching C_p for long strip.

TABLE 4.5

Aluminium plate (σ=0.34)					
Plate Width mm	w/ℓ	First Mode		Second Mode	
		Frequency KHz	w×f	Frequency KHz	w×f
30	1.0	70.613	2118.4	86.182	2586.5
30	0.75	74.330	2230.0	77.27	2318.1
30	0.60	74.763	2242.9	76.180	2285.4
30	0.50	76.635	2299.1	76.635	2299.1
30	0.376	75.630	2268.9	75.430	2262.9
30	0.30	75.434	2263.0	75.434	2263.0
20	0.2	113.150	2263.0	113.150	2263.0

Experimental result for the frequency spectrum of the end resonance is a result of combining two modes, one symmetric and the other antisymmetric. These are separated at different frequencies when the plate is nearly square.

TABLE 4.6

$\ell \times w$ mm$\times$mm	w/ℓ	Frequency KHz	ℓf	$\dfrac{\ell^2 f}{wC_o}$
30$\times$30	1.000	70.613	2118.4	0.4101
30$\times$25	0.834	66.725	2001.8	0.4651
30$\times$19	0.634	60.696	1820.9	0.5566
40$\times$20	0.500	41.478	1661.1	0.6424
34$\times$15	0.441	45.463	1545.7	0.6784
48$\times$20	0.417	31.730	1523.0	0.7077
50$\times$20	0.400	29.489	1474.5	0.7137
50$\times$15	0.300	25.080	1254.0	0.8093
60$\times$15	0.250	18.412	1104.7	0.8555
75$\times$15	0.200	12.400	930.0	0.9003
92$\times$15	0.163	8.580	789.4	0.9373
96$\times$15	0.156	8.050	772.8	0.9576
60$\times$8	0.113	11.200	672.0	0.9758

The experimental results for the fundamental in plane flexural mode of rectangular plates. This table shows the variations of the value of $\ell^2 f/wC_o$ as a function of the plate geometry.
(C_o for Aluminium = 5165 m.sec^{-1} and σ=0.34)

TABLE 4.7

ℓ×w mm×mm	w/ℓ	Axial Length Drive		Mid-Length Drive	
		Frequency KHz	ℓf m.sec^{-1}	Frequency KHz	ℓf m.sec^{-1}
48 48	1.00	65.864	3161.5	65.870	3161.5
48 46	0.958	67.299	3230.4	67.153	3223.3
48 44	0.917	68.951	3309.7	68.557	3290.7
48 42	0.875	70.361	3377.3	69.877	3354.1
48 40	0.834	71.984	3455.2	71.117	3413.6
48 38	0.792	73.645	3535.0	72.721	3490.6
48 36	0.750	75.653	3631.3	75.260	3612.5
48 34	0.708	77.752	3732.1	75.758	3636.4
48 32	0.667	80.163	3847.8	77.575	3723.6
48 30	0.625	82.626	3966.1	79.101	3796.9
48 28	0.584	85.658	4111.6	80.858	3881.2
48 26	0.542	89.073	4275.5	82.590	3964.3
48 24	0.500	92.453	4437.7	84.634	4062.4
48 22	0.458	96.154	4615.4	86.187	4137.0
48 20	0.417	99.640	4782.7	87.558	4202.8
48 18	0.375	102.068	4899.3	88.245	4235.8
48 16	0.334	103.737	4979.4	88.935	4268.9
		2nd Longitudinal		3rd Flexural	

The experimental results of mode (1,3) square plate and its frequency variation with the plate geometry. Two modes are recognised at two different driving positions: The longitudinal mode of the second harmonic order and the flexural mode of the third harmonic order. (The measured results are from Aluminium plate, C_o = 5165 msec^{-1} and Poisson's ratio = 0.34).

CHAPTER FIVE

WAVES AND VIBRATIONS ON ISOTROPIC RECTANGULAR

PLATES AND STRIPS

5.1 INTRODUCTION

In the previous chapter the experiments showed that
the frequency of the longitudinal modes of thin
rectangular plates increases as the width decreases. For
a narrow strip the frequency-length product for a given
mode will have a constant value due to standing waves
produced at the rod velocity.

In this chapter, some theoretical aspects will be
represented and discussed which describe and analyse
the different modes of vibration of the plate and strip,
and compare it to the experimental results. This can be
fulfilled mainly by considering the theory behind the
wave motion and the vibration of the plate, where the
body exhibit a resonance as a result of wave reflecting
back and forth between two impedance discontinuities.

The method of the general theory of elasticity can
be applied only for certain problems of elastic vibrations.
Lamé [45] has described simple modes of vibration of
isotropic rectangular plates. The modes are exact solutions
of the equation of motion as it satisfies the conditions

-106-

of having no stresses at the corners of the plate.

Morse (1950)[73] has described some modes of the wave propagation which satisfy the boundary conditions for the free vibrations of long isotropic bars of rectangular cross section based on the general elastic equation of motion.

An empirical study by Graff[26] shows an extensive analysis for the modes of the wave motions and vibrations of isotropic plates and rods.

5.2 THE BASIC THEORY

The frequency equation for the waves propagating in a homogeneous isotropic elastic plate have been developed by Rayleigh (1889)[89] and Lamb[43,44] independently. The solution of this theory has been presented by several authors [24,62,63,65,66,67,68], and the complete frequency spectrum have been extensively reported[62,26], resulting in an almost complete understanding of the behaviour of their dispersion curves.

Waves propagated in an isotropic elastic body exhibit two types of velocities; these are the dilational and the shear wave velocities. In an infinite plate, the dilational velocity is the bulk velocity and in a strip it is the plate velocity (C_p).

The relations between the plate and the shear velocities in the strip can be expressed as:-

$$\left(\frac{C_s}{C_p}\right)^2 = \left(\frac{1-\sigma}{2}\right) = \theta$$

or

$$C_s = C_p \ \theta^{\frac{1}{2}} \tag{5.1}$$

Consider an isotropic elastic plate of an infinite length and width with a thickness (2b) as shown in Fig. 5.1. The frequency equation which describes the symmetric and anti-symmetric waves propagated in the plate was originally given by Rayleigh and Lamb, and was conveniently given by Graff as:-

$$\frac{\tan \beta b}{\tan \alpha b} + \left[\frac{4\alpha\beta\gamma^2}{(\beta^2-\alpha^2)^2}\right]^{\pm 1} = 0 \begin{cases} +1 & \text{Symmetric} \\ -1 & \text{Anti-symmetric} \end{cases} \tag{5.2}$$

where

$$\left. \begin{aligned} \alpha &= \gamma(\phi^2\theta-1)^{\frac{1}{2}} \\ \beta &= \gamma(\phi^2-1)^{\frac{1}{2}} \\ \gamma &= \frac{2\pi}{\lambda} \end{aligned} \right\} \tag{5.3}$$

In recent years, much work has been done in calculating the roots of Rayleigh-Lamb's transcendental frequency equation in order to determine the various modes of the wave propagated in an infinite plate, and the dispersion relations for various waves.

-108-

Equation (5.2) may be readily solved for a given relation between the wavelength term (γb) and the phase velocity normalised to the shear (ϕ). This solution is also valid in the case of a thin long strip by considering its width (w) is equal to (2b) and the constant θ has a value given in equation (5.1), i.e. the plate velocity now replaces the bulk velocity in all the equations.

This equation can be solved using a numerical approach to find the roots of the equation for both the symmetric and non-symmetric modes. Where possible this formula has been put into a form which is more workable numerically and in which the variables have more direct physical meaning. Table 5.1 gives some considerations to be taken to fulfil the requirements for solving this equation easily.

Some general features of the symmetric solution are immediately evident:-

(a)   When (ϕ^2-2) = 0, the solution is independent on Poisson's ratio, and requires:-

$$\gamma b = \frac{\pi}{2}$$

or

$$\pi \frac{w}{\lambda} = \frac{\pi}{2}$$

(5.4)

The values of $\phi = \sqrt{2}$ define the solution which was already given by Lamé for some modes of certain conditions, that is when the wave length is twice the plate width.

-109-

These are modes with nodes at the corners of the plate, and are universally known as Lamé modes. In the previous chapter, extensive experimental measurements for various materials with a wide range of Poisson's ratio show a good agreement with these theoretical results indicating that the Lamé modes are shear type modes since the frequency normalised to the shear are independnet of Poisson's ratio.

(b) For small values of γb, the relation is linear and we have:-

$$\phi = 2(1-\theta)^{\frac{1}{2}}$$

or

$$C_\phi = C_s \{2(1+\sigma)\}^{\frac{1}{2}} \qquad\qquad (5.5)$$

This is the wave velocity in a thin rod (C_o). The small value of γb means the value of (w/λ) is small, or the wave length is greater than the width, and then the velocity will get closer to the rod velocity C_o.

(c) For large values of γb, the formula will be:-

$$(\phi^2-2)^2 = 4(1-\phi^2\theta)^{\frac{1}{2}}(1-\phi^2)^{\frac{1}{2}} \qquad\qquad (5.6)$$

This equation is defining the Rayleigh surface wave, and ϕ approaches a constant value - which is dependent on the Poisson's ratio - as γb becomes higher.

(d) For small values of γb, the solution for the first anti-symmetric mode can be approximated to:-

-110-

$$\gamma b = \left[\frac{3}{4(1-\theta)}\right]^{\frac{1}{2}} \phi$$

or

$$\frac{f\ell^2}{wC_s(1-\theta)^{\frac{1}{2}}} = \frac{2\pi}{\sqrt{3}} \tag{5.7}$$

Equation (5.7) is similar to the Morse result[71] for the 'free-free bar' flexural vibration, see equation (4.1).

The solutions for the wave equation according to the table above will determine the different modes of propagation in an isotropic plate. These modes have been studied extensively by several authors[59,60,62,63,65,68,73,74,74,80] comprehensive treatment was published by Graff[26]. The solution for the first symmetric mode requires ϕ to have a value greater than one, but $\phi\theta^{\frac{1}{2}}$ less than one. While the solution for the first anti-symmetric mode requires ϕ to be less than one. All the other modes - symmetric or anti-symmetric - require ϕ to be greater than one.

The phase velocity normalised to the shear wave velocity as a function of (w/λ) for the first three modes is given in Table 5.2 and shown graphically in Fig. 5.2. The first anti-symmetric mode is indicated by the curve a_1. For long wavelengths $(w/\lambda=0)$ a_1 approaches zero, and for short wavelengths it approaches the Rayleigh wave velocity. The first and the second symmetric modes are

represented by the curves s_1 and s_2 respectively. For long wavelengths s_1 approaches the "rod" velocity (C_o), and for the short wavelengths it approaches the Rayleigh wave velocity. The normalised frequency-length product of the second mode s_2 has an asymptotic value of one for short wavelengths, and shows a cut-off phenomenon where the curve approaches infinity for longer wavelengths.

These three modes are extremely important experimentally as they represent the different groups of the square and the rectangular plate vibrational modes. In particular is the curve s_1 since it represents the variation of the phase velocity of the longitudinal vibrational modes of a rectangular strip with the width-to-wavelengths ratio.

The Lamé mode is one well known solution of the Rayleigh-Lamb equation where the sides of the plates are integers at $\lambda/2$, The experimental results are completely consistent with this.

The next solution for the symmetric mode is representing by the curve s_2 in Fig. 5.2. This mode does not exhibit a cut-off frequency and is determine primarily by the width dimension. The solution for the square plate geometry is obtainable by proposing that the wavelength is twice the width, i.e. $w/\lambda=1/2$. This is the ideal condition to be considered for the wave to exhibit a resonance

in the plate. Such a solution is present in the breathing
vibrational mode of the square plate. Since the Young's
modulus has a major contribution in this mode, the
variation of Poisson's ratio modulus must have an influence
on the phase velocity normalised to the shear. This can
be computed and a comparison with the experimental results,
which have already been given in Chapter Three, can be
made.

The computed results of the breathing mode for a range
of the Poisson's ratio is given in Table 5.3. The
corresponding frequency ratio of this mode to the
fundamental Lamé mode is plotted for both experimental
results and the computed results for different Poisson's
ratio, and it is shown in Fig. 5.3.

The two results are close to each other for the lower
value of the Poisson's ratio, and both have a slight
curvature at this range. But for the higher value of
Poisson's ratio a slight disagreement is shown. This
could be due to the thickness of the plate which will be
most significant for the high Poisson's ratio materials.

Additional information on the resonant modes of the
various plate geometries can be determined by considering
the frequency spectrum of Rayleigh-Lamb modes. The
resulting frequency spectrum for the first five modes as a
function of (w/λ) for the case of Poisson's ratio $(\sigma)=0.33$

is shown in Fig. 5.4 where;-

$$\Omega = \phi \frac{2\gamma b}{\pi} = \phi \frac{2w}{\lambda} = \frac{2wf}{C_s} \qquad (5.8)$$

The experimental measurements already carried out for the different square plate modes is expected to have - for some of them - comparison results. For instance, the Lamé mode gives a perfect matching with the figure in the graph. That is the first symmetry mode when $(w/\lambda) = 1/2$.

The Mason mode is expecting to have the same value as the anti-symmetric mode. But this gives a higher value of (w/λ); this is equal to (0.75) instead of the (0.5) assumed. This result is rather interesting and a similar feature for (w/λ) for the other modes can be determined.

Figure 5.5 shows some vibrational patterns of the square plate modes and their defining values of the width-to-wavelength ratios. The harmonic relationship of the Lamé modes is clearly shown since each of them is represented by a certain mode of the wave propagation. The other square plate modes which are described as the flexural modes, are determined from the first anti-symmetric modes. These will have higher values for (w/λ) from that obtained from the Mason mode according to their resonant frequencies.

Table (5.4) gives the computed frequency spectrum of the breathing mode, assuming it is the second symmetric mode.

The frequency is controlled by the plate width dimension.
The frequency-width product approaches a constant value
when (w/λ) becomes smaller. The frequency equation was
solved for Poisson's ratio (0.33) and the plate geometries
were found by assuming $(\lambda=2\ell)$. The asymptotic value of
$(2wf)$ is close to the plate wave velocity (C_p). The
experimental measurements have already shown the
dependence of the breathing mode on the width dimension
of the plate.

5.3 THE LONGITUDINAL RESONANCE

In the longitudinal resonance, most of the wave
motion is directed along the length of the plate. One
can now think of the longitudinal resonance as the result
of waves reflecting back and forth between two impedance
discontinuities. For example, consider a thin bar or a
strip free on both ends, the wave will be in resonance
when the wave reflecting from either end will undergo
a phase reversal.

The velocity of the wave moving along the length of
the plate is then called the phase velocity. If a very
narrow plate is considered (i.e. $w \ll \lambda$) the phase velocity
will approach the rod velocity (C_o)

The vibrations of various modes are shown in Fig. 5.6.
For the fundamental the ends are going in and out together

(reverse phase). In the second mode they vibrate in phase, and so on. i.e. odd orders are in the reverse phase and even orders are in phase. For all cases the system is dynamically balanced. The wavelength will be given by $2\ell/n$ where ℓ is the length and n the mode order.

It was mentioned earlier that for an indefinitely narrow strip there is no dispersion and the phase velocity is equal to the wave velocity in the rod (C_O), otherwise a correction must be applied to the phase velocity due to the width of the plate which has a considerable effect on the lateral contraction.

The formula for the correction is that which was described by Rayleigh-Lamb frequency equation mentioned earlier. The solution for the first symmetric mode is represented by the variation of the phase velocity corresponding to the shear with the width-to-wavelength ratio. This has a considerable dependence on the Poisson's ratio. The graphical plot of R, the phase velocity normalised to the rod velocity (C_O) versus (w/λ) is shown in Fig. 5.7 for different Poisson's ratios.

A complete tabulation of values of R for a wide range of Poisson's ratios, from $(\sigma=0.5)$ to $(\sigma=-0.1)$ step (0.01) is given in the appendix A.

5.4 THE EXPERIMENTAL MEASUREMENTS

The materials used in this investigation cover the range from Aluminium with Poisson's ratio ($\sigma=0.34$) to Pyrolytic Graphite ($\sigma=-0.10$). They have been prepared by machining them to thin narrow strip geometries and chosen to be homogeneous and in-plane isotropic or orthotropic materials. The longitudinal resonant modes have been excited by coupling the driving line to the plate at its remote end toward the axial direction. The resonant frequencies for different longitudinal modes were precisely measured, and the harmonic relations for these resonant modes were soon identified.

Aluminium was first investigated in detail. It has been machined from a disk prepared as a thin plate sliced from a cylindrical rod. The plate made in this manner was isotropic in its in-plane direction where the vibrational displacements are taking place, but not in its thickness where the grains are elongated and no movement is expected to occur.

The results of the experimental measurement are given in Table 5.5, the frequencies were measured for each mode, and the phase velocities were calculated from the frequency-wavelength product. The wavelength is simply related to the length of the plate from the relation $\lambda= 2\ell/n$ where n is the harmonic mode order, and

the formula for the phase velocity will then be:-

$$C_\phi = 2\ell \frac{f}{n} \qquad (5.9)$$

The width-to-wavelength ratio is related through the following formula:-

$$\frac{w}{\lambda} = n \frac{w}{2\ell} \qquad (5.10)$$

This indicates that the ratio of (w/λ) is linearly proportion to the mode order (n).

The variation of the phase velocity $C\phi$ for the Aluminium rectangular strip with (w/λ) through the harmonic mode order (n) is shown in Fig. 5.8. This is similar to the curves, shown in Fig. 5.7, which were for the Rayleigh-Lamb longitudinal frequency equation, where the curvature of the phase velocity versus (w/λ) is controlled by the Poisson's ratio of the material measured. The phase velocity has a cut-off value when (w/λ) or (n) is zero. This gives the correct value of the phase velocity when the wavelength is infinitely greater than the width of the plate. This value is the true rod velocity (C_o). It can be found by extrapolating the curve in the above figure.

A comparison between this result and the theoretical results shown earlier indicates that the correction can be made for the phase velocity using the tables given in the

Appendix A.

This correction is often called the Rayleigh-Lamb phase velocity correction, and the rod velocity (C_o) can be found as soon as the correct value of the Poisson's ratio has been chosen.

It is important to mention at this stage that the smooth curvature of the phase velocity versus (w/λ) is limited to a certain mode harmonic order. This depends on the plate geometry or plate sides ratio. In other words, it depends on the value of (w/λ). The experimental results shows that when the value of (w/λ) exceeds $(1/2)$, the mode will no longer be related in a harmonic order.

Problems accompanied by using the tables of the Rayleigh-Lamb phase velocity correction, are usually related to the values of (w/λ) being used. These must be matched with the experimental values obtained. The method to obtain such similar values of (w/λ) to that in the table is by smoothing the curve of Fig. 5.8 (mathematically or graphically) and extrapolating the deserved values of (w/λ) to match those given in the table.

The final results of the Aluminium plate modes phase velocities correction for different Poisson's ratios is given in Table 5.6. R is the Rayleigh-Lamb normalised phase velocity to the rod velocity $(R=2\ell f/C_o)$.

The graphical variation of this correction is shown in Fig. 5.9. The deviation of the curves depend on the value of the Poisson's ratio chosen from the table. The value inferred from the graph is 0.33 with an uncertainty of about ±0.01.

Materials like silica and glass are expected to be isotropic in their properties. These are considered to be the most homogeneous materials in this investigation. They provide reference standard of measurements for verifying experimentally the analytical approaches shown earlier. The longitudinal modes of the silica have been measured and the values of the phase velocities and the width-to-wavelength ratio have been determined by following the procedure described earlier.

Table 5.7 gives the measured results, and the graphical plot for the phase velocity as a function of (w/λ) is shown in Fig. 5.10.

The procedure of determining the correction of the phase velocities corresponding to the different values of Poisson's ratio made use of the table in Appendix A. Table 5.8 demonstrates the calculated values, and these are shown graphically in Fig. 5.11. The values of the Poisson's ratio were chosen from the table to show a comprehensive variation for the corrected phase velocity curves.

The above figure shows an acceptable result of the Poisson's ratio for the material used. The value is close to that obtained from the same material by using the disk resonator.

The experimental results from the glass strip is given in Table 5.9. The values of the phase velocity for the different modes and the corresponding values of (w/λ) is shown graphically in Fig. 5.12. The corresponding correction for the phase velocity according to the table in the Appendix A for different Poisson's ratio is given in Table 5.10. These values are graphically represented in Fig. 5.13. The result obtained for the glass Poisson's ratio is fairly close to that obtained from the disk resonator. Although the disk resonator gives the result directly and more precisely due to the tabulated eigen values available, there are certain problems accompanied with both procedures which effects or alters the accuracy of the measurements. These problems are related to the geometry of the plate (disk), and the thickness of the plate which have a vital influence in the measurements and the final results.

Even though the results from this method give a guide to determine the mechanical properties of the material with a precise figure. This might be an alternative method for evaluating and measuring the rod velocity for isotropic and orthotropic materials and their Poisson's ratios. This

is very important in the field of the material studies and in determining the mechanical characteristics and the properties of the metals. This has a wide range of applications especially in the field of the non-destructive testing and evaluations of the materials.

The grains orientation in the material will have a significant influence on the values of the rod velocity and the Poisson's ratio. This is demonstrated clearly in the case of Aluminium plates machined from a rolled sheet metal. Further studies and investigations for the case of anisotropic materials will follow later.

The solution of the Rayleigh-Lamb frequency equation is also obtained for the negative values of Poisson's ratio. These will give virtually identical solutions to the positive values as the energy balance is unchanged. The resultant ambiguity in the sign of Poisson's ratio can usually be resolved. This is shown in the table in Appendix A. The solution is symmetric to that of positive Poisson's ratio for only the lower value of (w/λ). This means the solution can only be used for narrow strips. When the value of (w/λ) is close to the (0.5) or above it, the disagreement is shown for the two Poisson's ratio (the negative and the positive).

Pyrolytic graphite is a polycrystalline form of graphite grown from the vapour phase by the thermal decomposition

of a carbon-bearing gas a refractory mandril[84].

Pyrolytic graphite is a material which has negative Poisson's ratio. This was prepared in a narrow thin strip geometry. The longitudinal resonant frequencies were measured and the phase velocity as a function of the modes order has been determined and given in Table 5.11. The variation of the phase velocity with the value of (w/λ) is shown graphically in Fig. 5.14.

The phase velocity was corrected for specific values of (w/λ), using the eigen values for negative Poisson's ratio. In fact, by using either eigen values of positive or negative Poisson's ratio it should not effect the result. The complete results for the range of Poisson's ratios is given in Table 5.12.

Figure 5.15 shows the final plots of the curves for different Poissons ratio. The curve with less curvature indicates the closest value of the Poisson's ratio for the material measured.

5.5 THE LONGITUDINAL RESONANT MODES RELATIONS

The relations between the longitudinal resonant frequency and the modes order (n) for a narrow thin strip have been demonstrated previously. This was given by the Rayleigh-Lamb frequency equation which has been

-123-

explored earlier. The experimental results supported this relation for a limited value of width-to-wavelength ratios (w/λ), where this is linearly proportional to the mode number (n). The values of the Young's modulus and the Poisson's ratio modulus can be obtainable by applying the required correction for the phase velocity as described above. This method is applicable only for isotropic or orthotropic materials.

It has been shown experimentally that this relation is no longer valid when the value of (w/λ) exceeds (0.5), and the modes order will no longer be in a harmonic relationship.

The following is an attempt to find a simple, direct method of determining the longitudinal elastic modulus for the materials in long strips geometry, by obtaining a relationship between the resonant frequency and the mode order (n).

The measurements carried out for the silica material of a long strip geometry revealed that the longitudinal resonant modes have a clear frequency dispersion. This was presented in Fig. 5.10. To obtain the true rod elasticity the curve must be extrapolated back to zero value of (w/λ). A simple parabolic mathematical formula was found to fit the values of the resonant frequencies to a smooth curve for low (w/λ). This enabled a precise value

of C_O to be obtained and to attach a probable error to it. Although the formula was given by Rayleigh-Lamb has been well demonstrated, it requires tabulated eigen values for different Poisson's ratios to make full use of it.

The crutial point about the resonant frequency curve is its radical variation when the value of (w/λ) is close to or above the (0.5).

The Table 5.13 gives the measured longitudinal phase velocity for silica and the calculated value of (w/λ) which is obtainable from the relation $(5,10)$. This is linear proportion to the mode order (n). The table also shows the quadratic and the cubic values of (n). The variation of the phase velocity with each of these three values of n, n^2 and n^3 is shown graphically in Fig. 5.16.

A close inspection of these three curves shows that the curve has been flattened as the index of the mode order increases from 1 to 3. In fact the lower segment of the curve for n^3 retains a slight curvature which can be easily taken into account.

This relation is extremely useful for determining the Young's modulus and the Poisson's ratios modulus precisely for the materials of having rectangular strip geometries. It is obtained directly from the experimental results by fitting them in a quadratic curve using a least squares fit method.

It should be noticed that this is only applicable in a case of the lower longitudinal modes order where the ratio of (w/λ) is low and does not exceed the (0.5) value. The modes relations for an Aluminium plate is also presented here. The resonant frequencies of the longitudinal modes were measured for the mode order, and the phase velocity as a function of (w/λ) has been determined. This is given in Table 5.14 where the values of n^2 and n^3 are also presented.

The variations of the phase velocity as a function of the modes order (n) is shown graphically in Fig. 5.17. This is clearly shown in the quadratic variation of the curve for the phase velocity with the n^3.

This method is more convenient and accurate than the graphical method to obtain the rod velocity (C_o), which does not yield good results in practice.

It is of interest that in rods where the corresponding correction (Bancrofts)[4] is used, the very simple relationship $\frac{2f\ell}{n} = k(w/\lambda)^2$ is valid.

5.6   FINAL COMMENTS

The difference between the wave motion and the vibration is that the latter arose from standing waves while the former consists of waves propagated in the medium. The nature of the reflection from the boundary

to form standing waves has yet to be fully resolved.

The Rayleigh-Lamb equation is concerned with the waves travelling in a solid media and the dispersion relationships with the wave number. This dispersion is dependent on the ratio of the plate width side to the wavelength. It was found to be valid in the case of the longitudinal resonant modes in a narrow strip but only for limited values of (w/λ). This dependence on the value of Poisson's ratio for the materials; i.e. materials with high Poisson's ratio will have more dispersion, while the one with zero Poisson's ratio will have no dispersion at all, since there will be no lateral movement.

For materials with negative Poisson's ratios, the Rayleigh-Lamb equation predict the same results as the positive Poisson's ratio. This was verified experimentally and a precise result was observed.
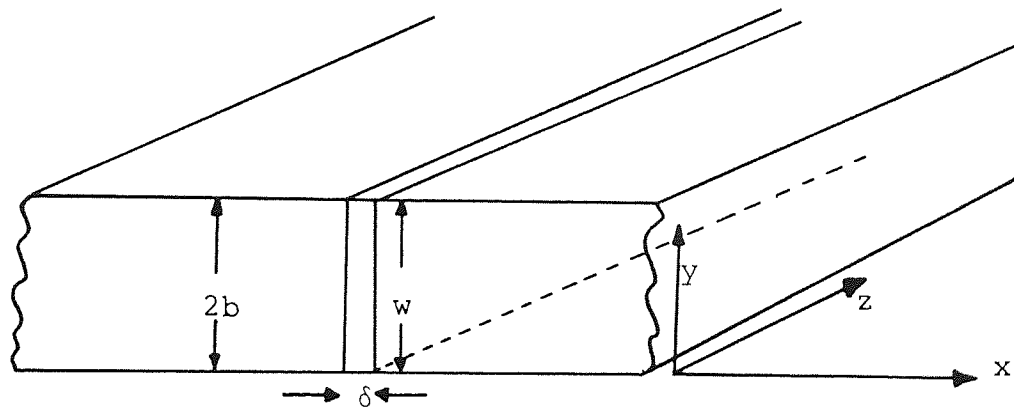
Fig. 5.1   The coordinate system of an isotropic elastic plate of infinite length and width of thickness (2b), and the corresponding thin strip of width (w).
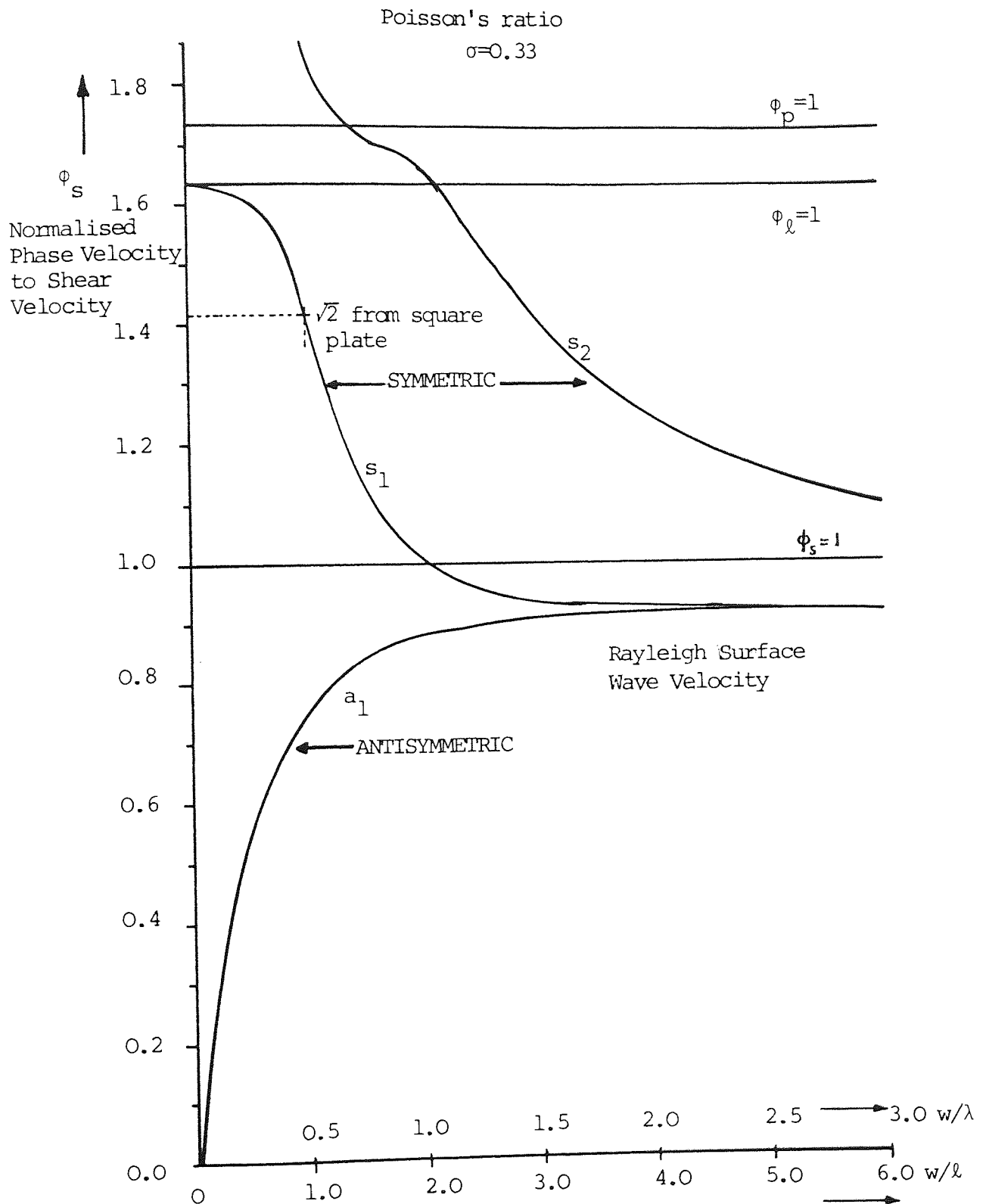
Fig. 5.2 The variations of the normalised phase velocity to the shear with the plate geometry assuming $\lambda = 2\ell$ and $\gamma b = \pi w/\lambda$ and for Poisson's ratio 0.33
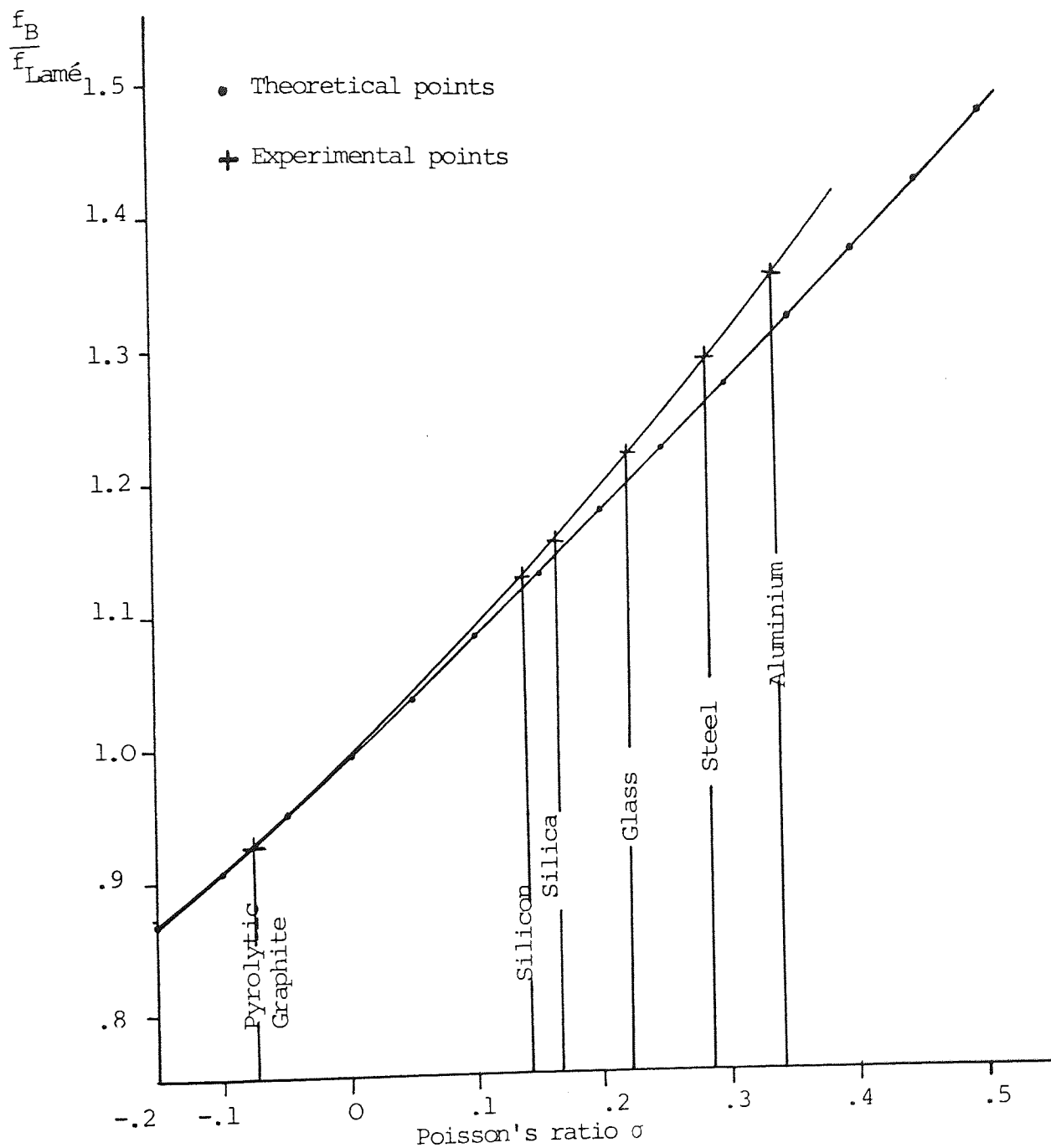
Fig. 5.3 The graphical representation for the variation of the breathing to the Lamé modes ratio as a function of Poisson's ratio. The experimental and the theoretical results are close at the lower range.

Fig. 5.4   The frequency spectrum for the lowest symmetric

and antisymmetric modes of Rayleigh-Lamb frequency

equation as a function of (w/λ).

This clearly shows some solutions of the

vibrational square plate modes.   The Lamé modes

are exact solutions which are obviously

harmonically related.
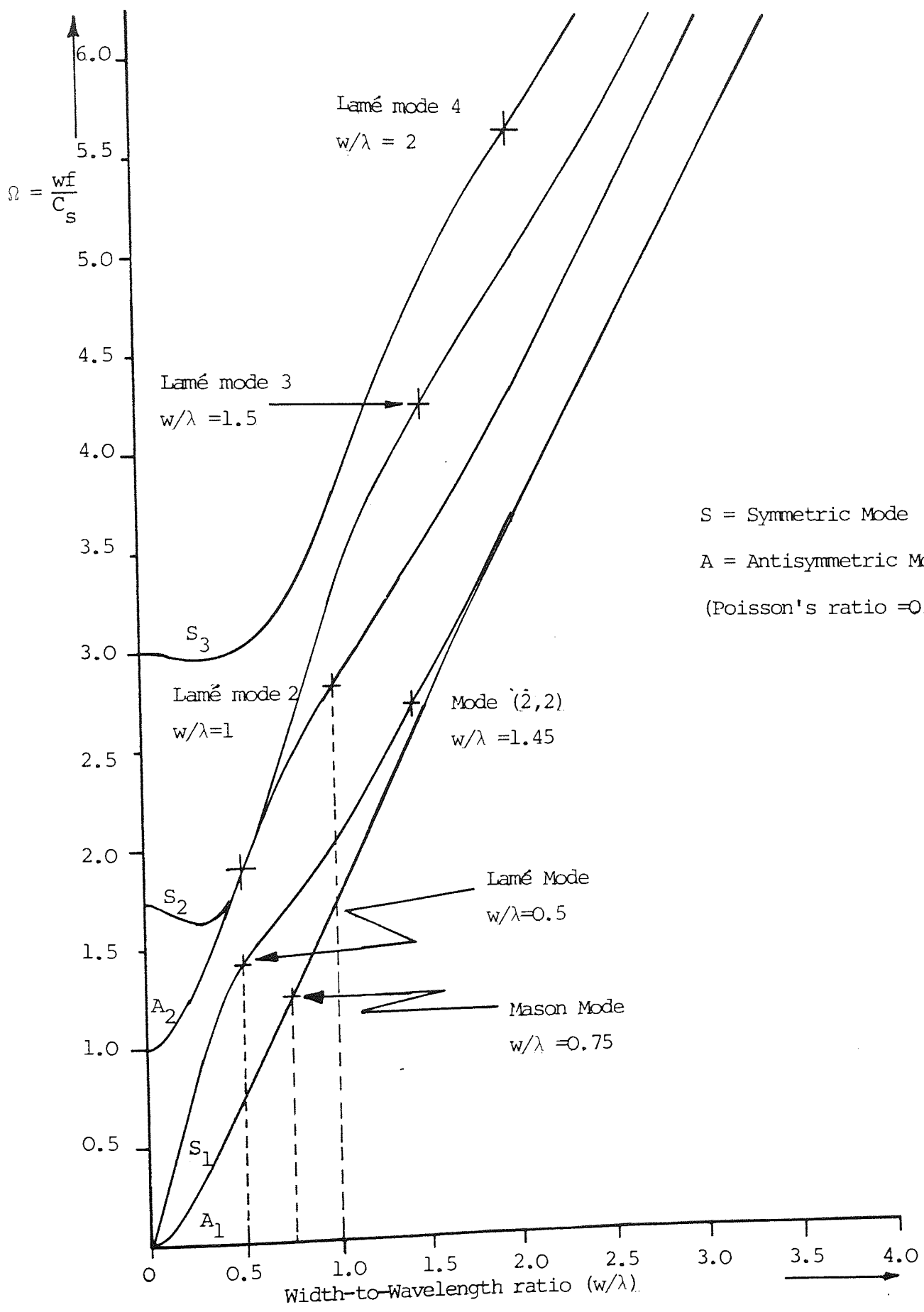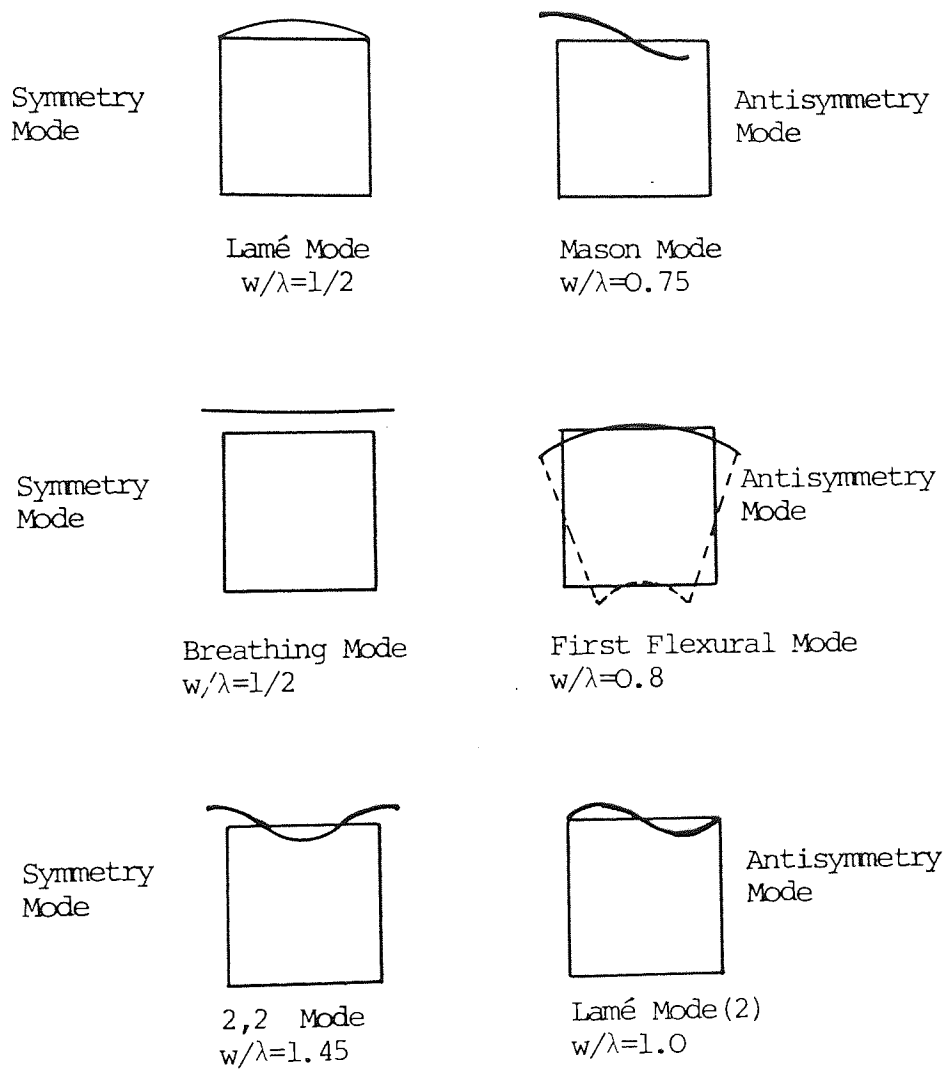
Fig. 5.5 Sketches for the lowest square plate nodal patterns and their width-to-wavelength ratio as they have been determined from the solution of the Rayleigh-Lamb frequency equation for the symmetric and antisymmetric modes.

The Fundamental Mode

$\lambda/4$ $\lambda/4$

W

$\ell=\lambda/2$

The Second Mode

$\lambda/4$ $\lambda/2$ $\lambda/4$

$\ell=\lambda$

The Third Mode

$\lambda/4$ $\lambda/2$ $\lambda/2$ $\lambda/4$

$\ell=\dfrac{3\lambda}{2}$
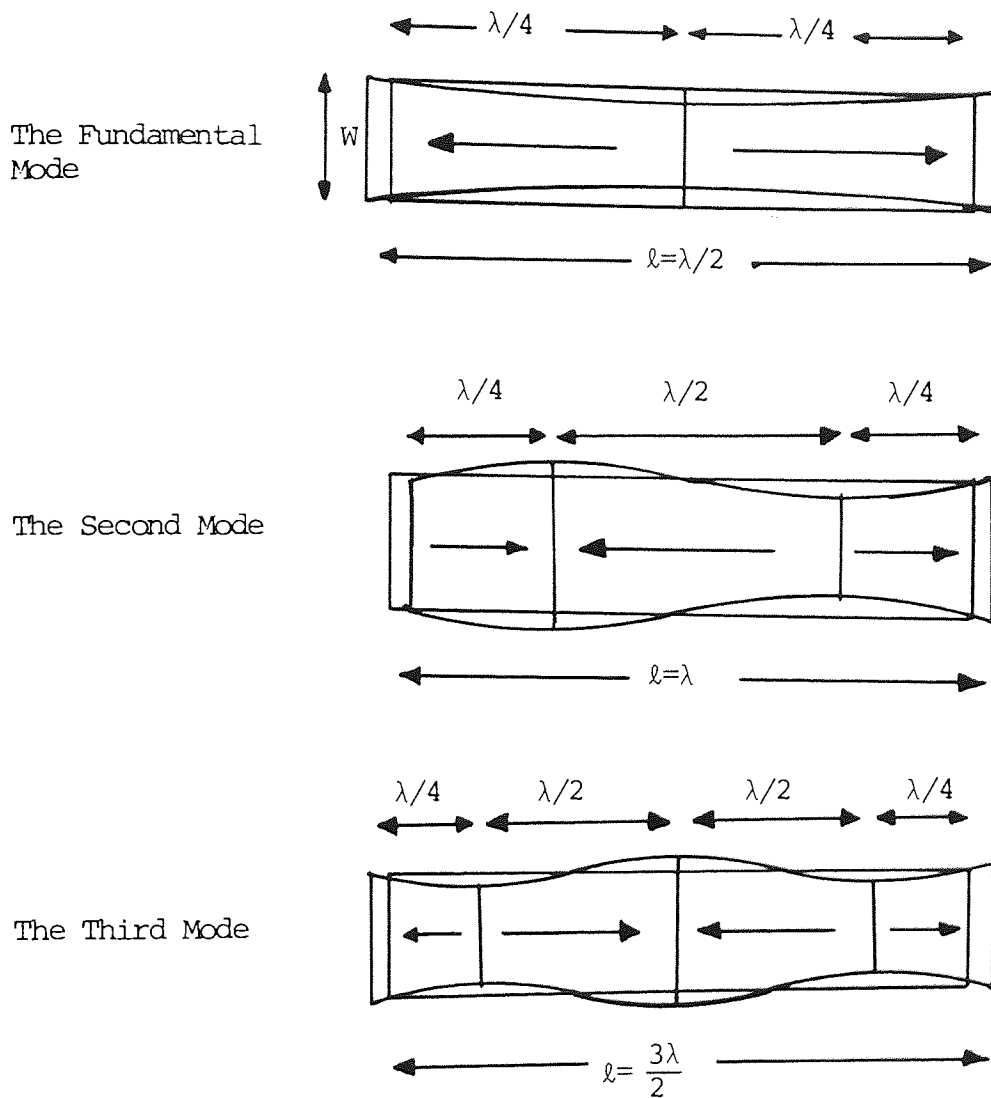
Fig. 5.6   The longitudinal resonant modes of a rectangular strip.
Sketches for the first three modes.

$$R = \frac{C_\phi}{C_o} = \phi \left(2\left(1+\sigma\right)\right)^{-\frac{1}{2}}$$

$$\text{where } \phi = \frac{C_\phi}{C_s}$$

$$C_\phi = \lambda f$$
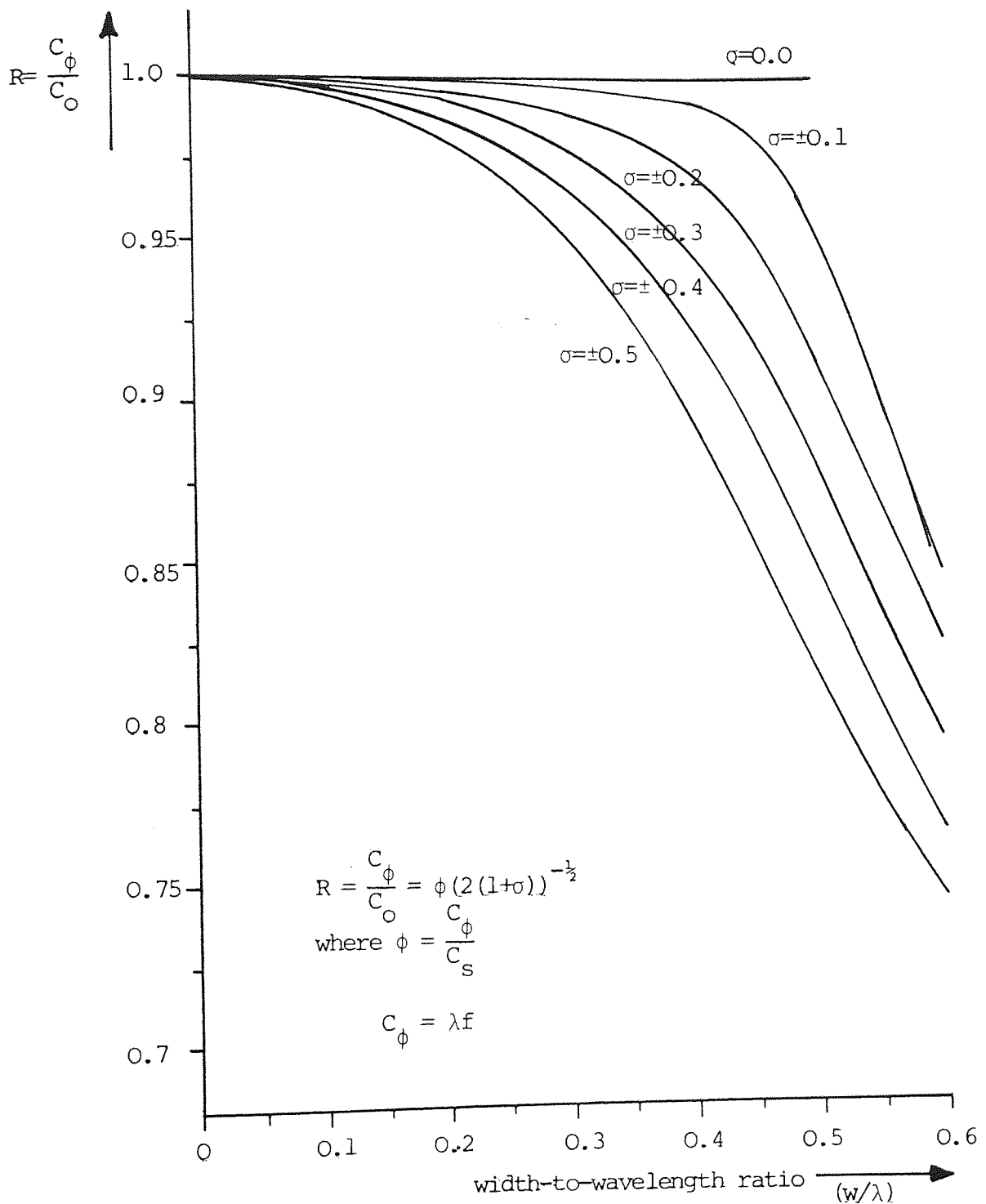
Fig. 5.7   Graphical plot shows the variations of the longitudinal resonance normalised to the rod velocity as a function of (w/λ) for different Poisson's ratio values. R obtained from the solution of Rayleigh-Lamb frequency equation.

-134-
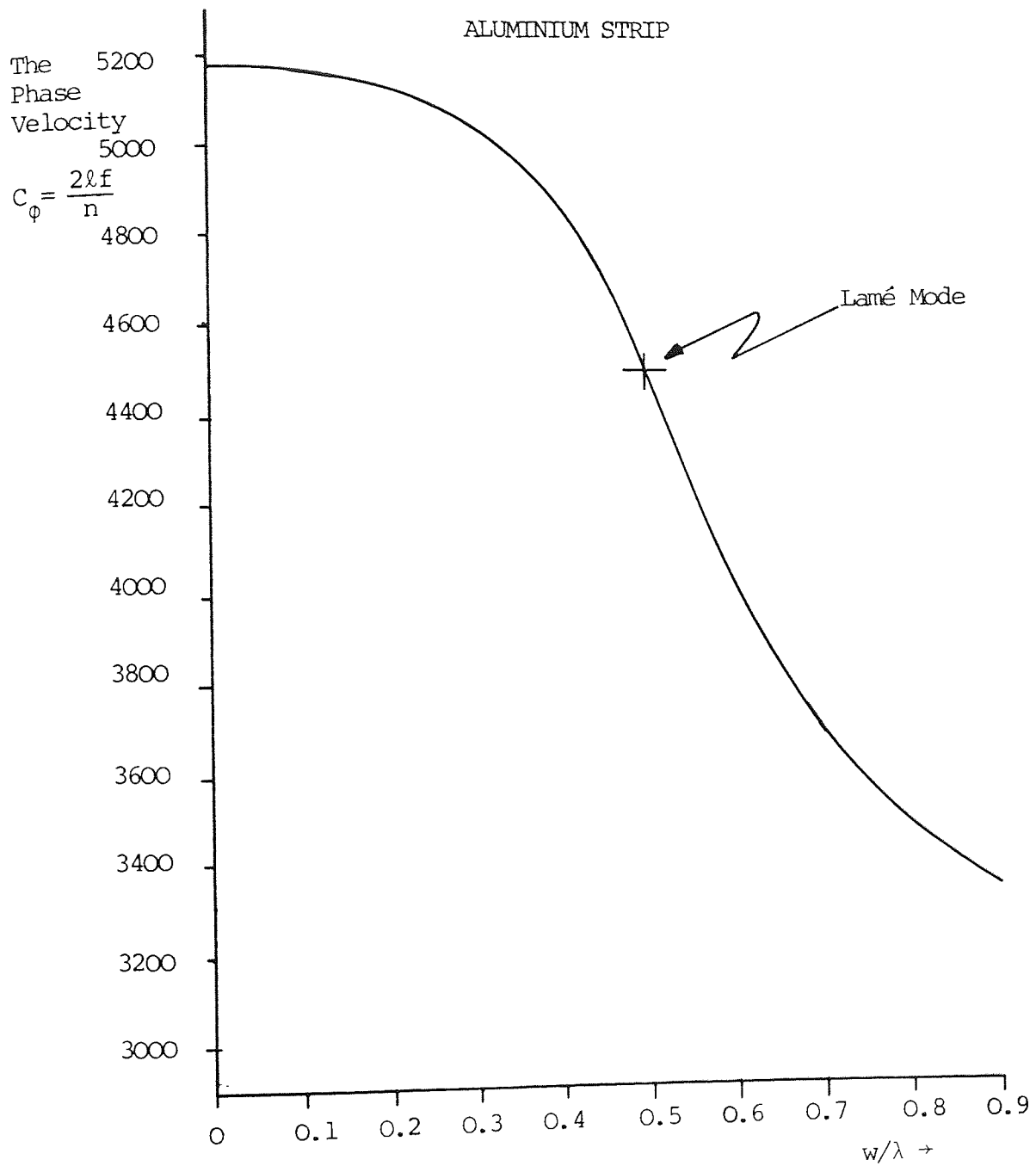
Fig. 5.8 The variation of the phase velocity for Aluminium plate with (w/λ). The value of the rod wave velocity can be found by extrapolating the curve.
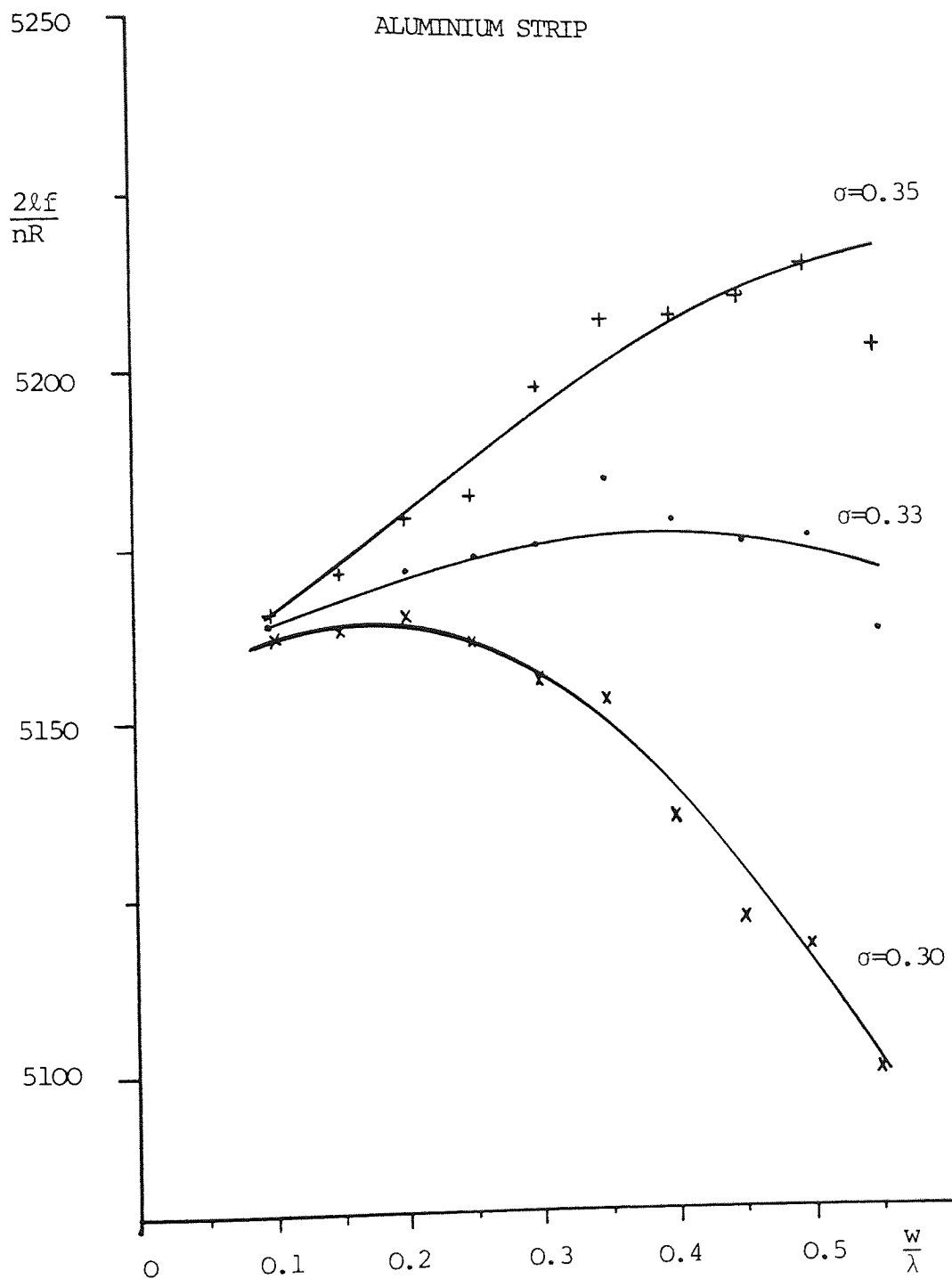
Fig. 5.9 The graphical plots show the variations of $(2\ell f/nB)$ with (w/λ) for Aluminium plate using three different Poisson's ratio values. It is apparent that $\sigma=0.33$ is the better postulated value for Aluminium. R is obtained from the table in Appendix A.

-136-
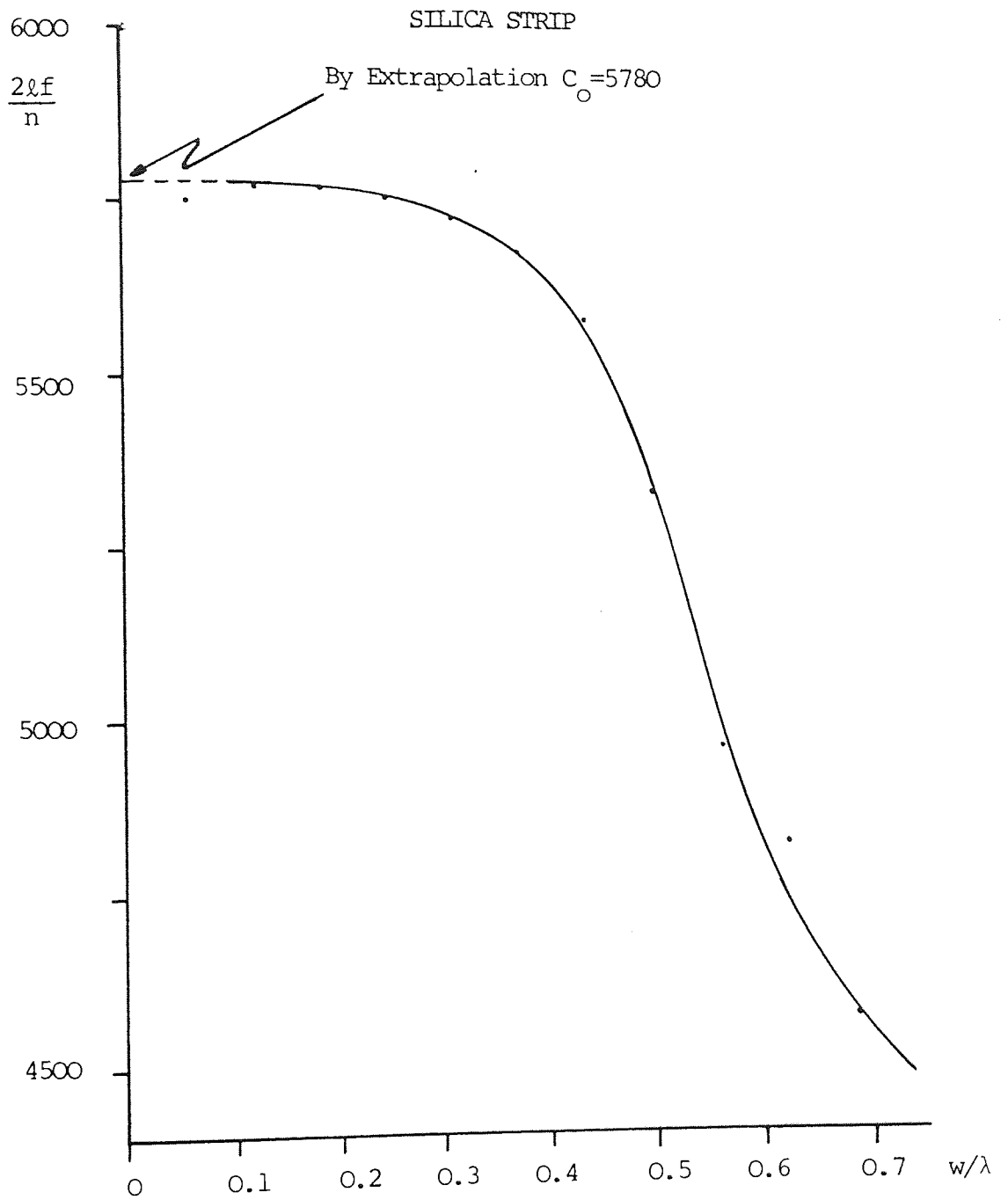
Fig. 5.10 The phase velocity spectrum of the longitudinal silica strip modes as a function of w/λ which is directly related with the modes order (n).
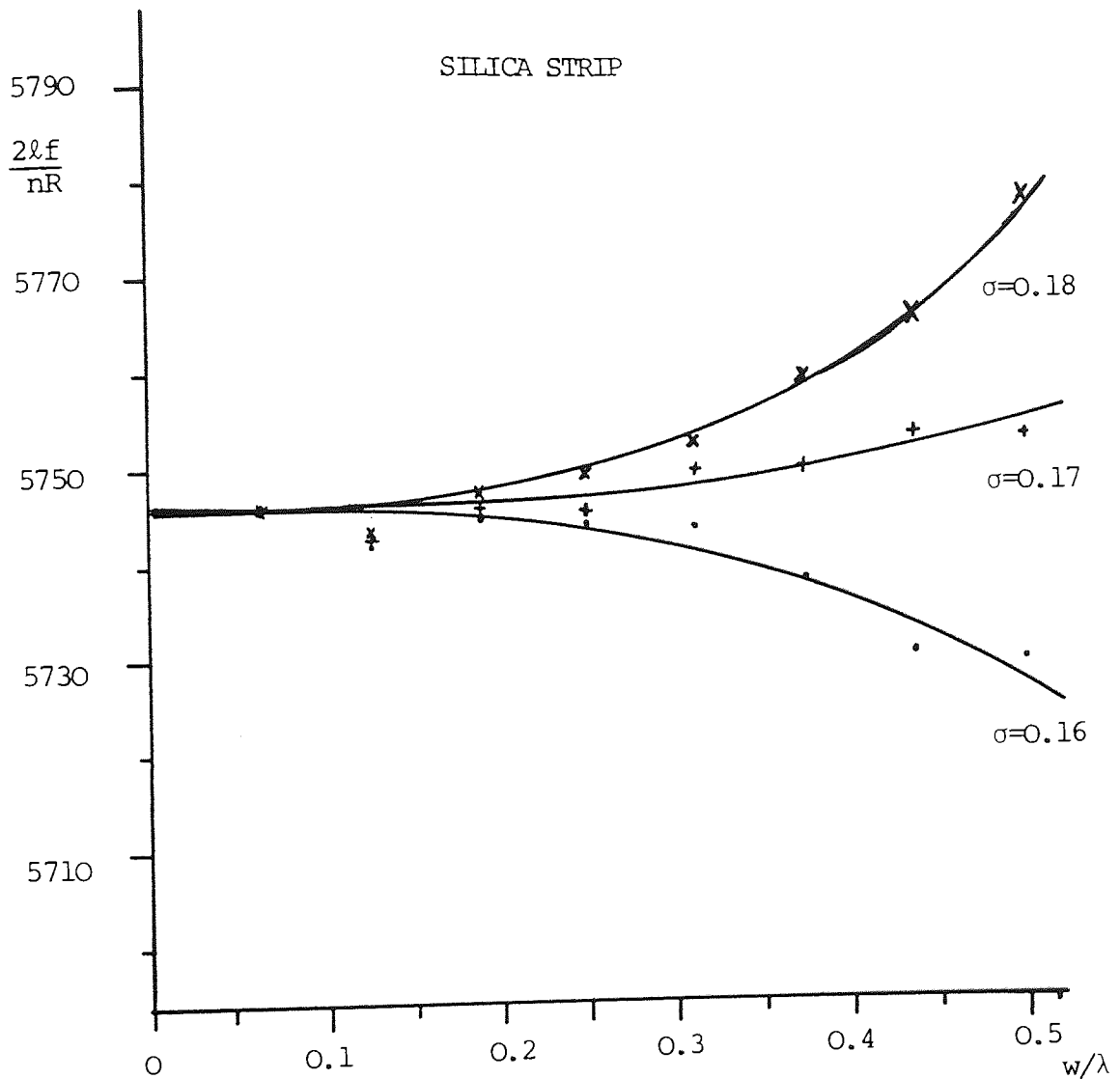
Fig. 5.11 The graphical plots for the phase velocity corrected
using the eigen value (R) from the table in Appendix A
for different Poisson's ratio. It is evident that the
closest value of Poisson's ratio for silica is (0.17).
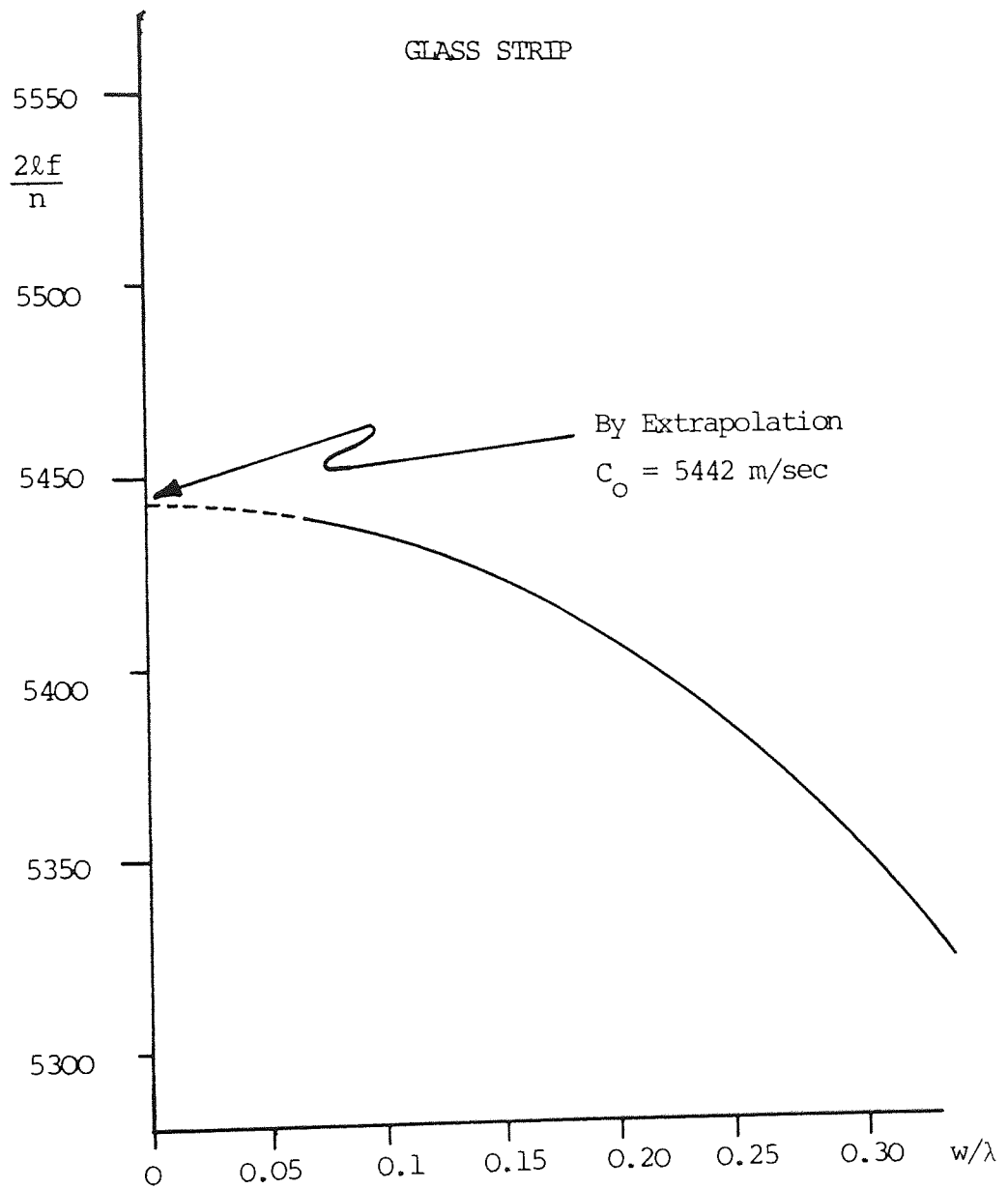
Fig. 5.12   The frequency spectrum as a function of the plate width-to-wavelength ratio for Glass having strip geometry. (ℓ=77.76 and w=9.7 mm).

GLASS STRIP

77.67×9.7
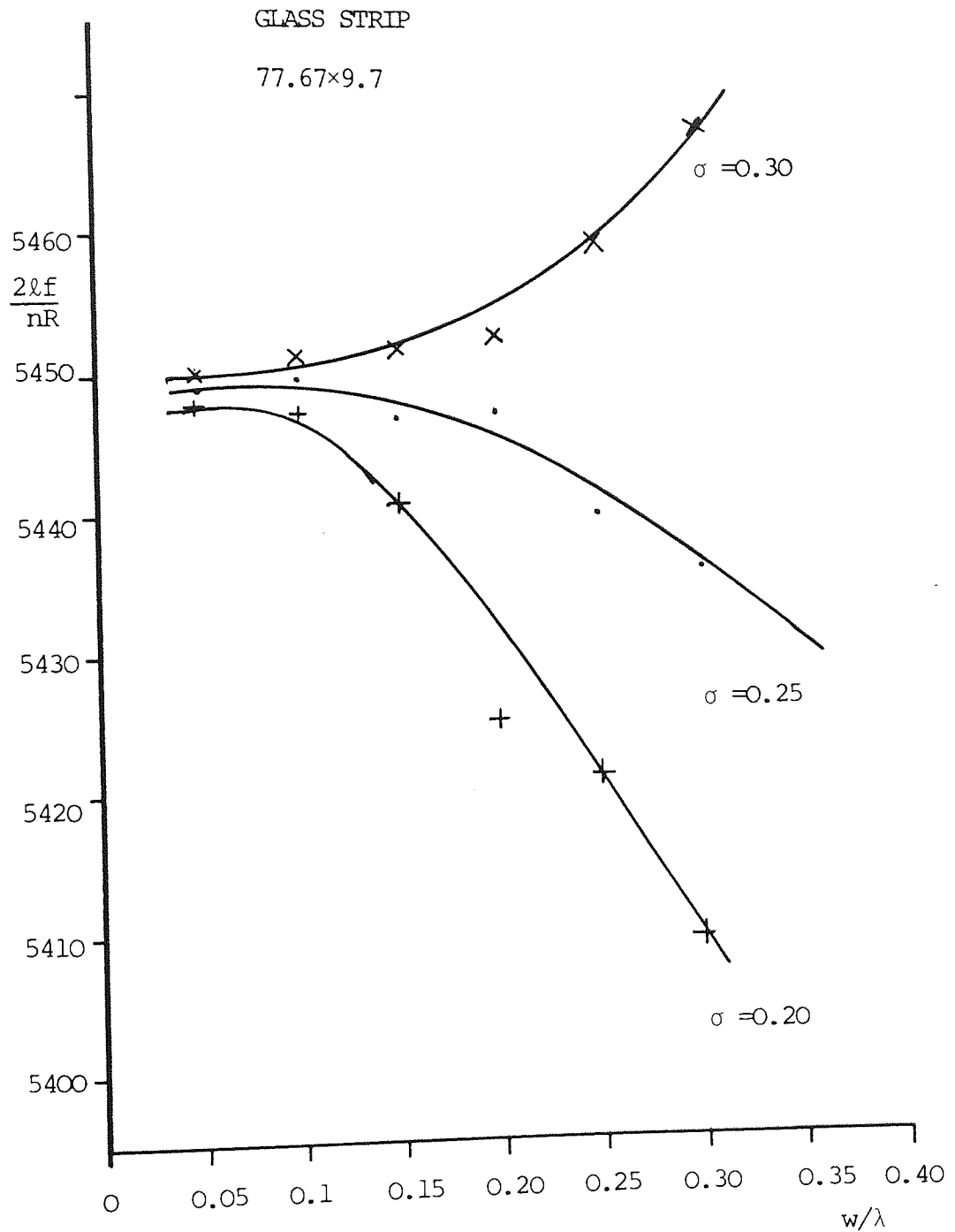
Fig. 5.13   The graphical plot for the value of $(2\ell f/nR)$, where R from the table in Appendix A, as a function of the plate width-to-wavelength ratio. Three different Poisson's ratio values were used in this figure.
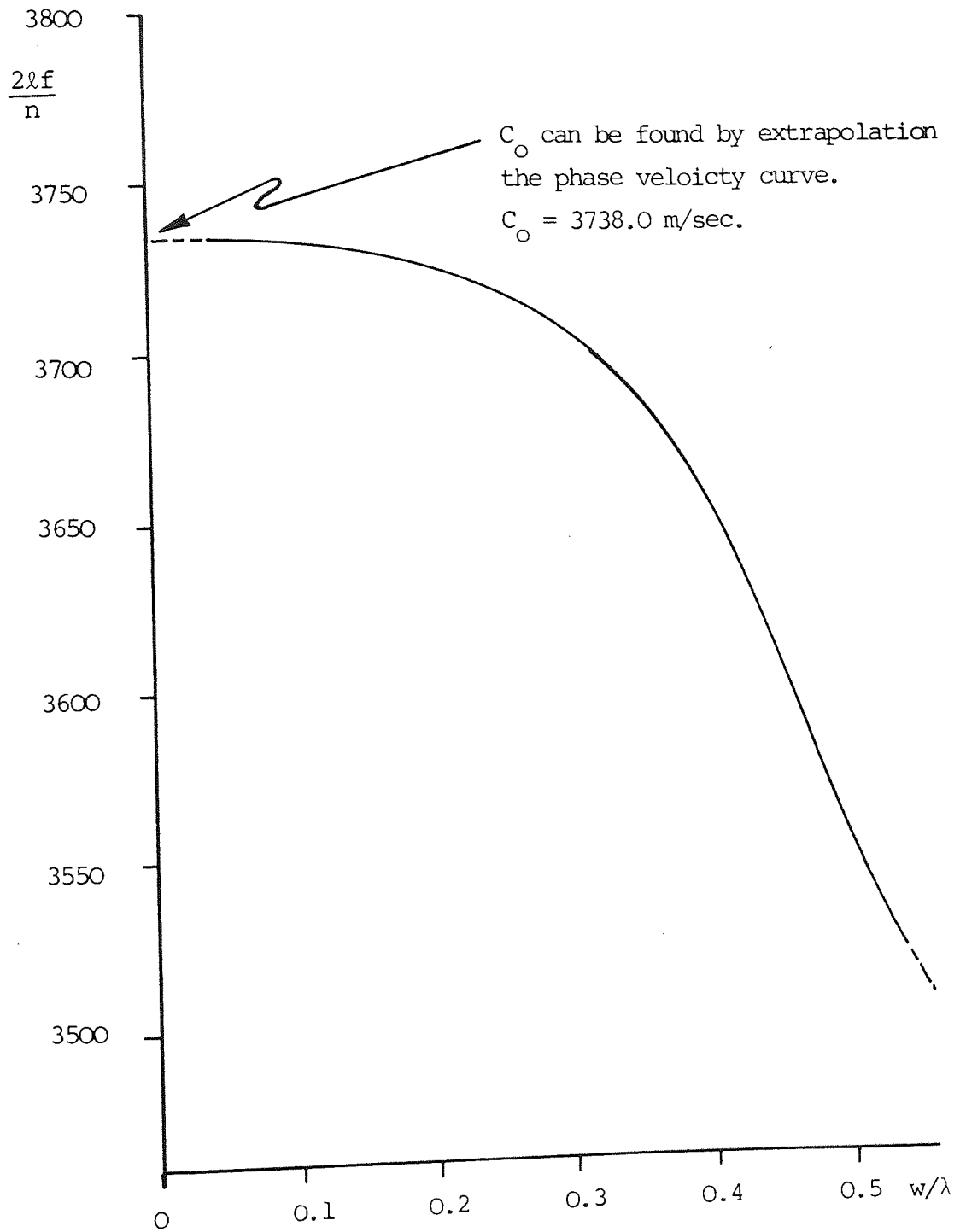
Fig. 5.14 Pyrolytic Graphite phase velocity spectrum as a function of (w/λ).
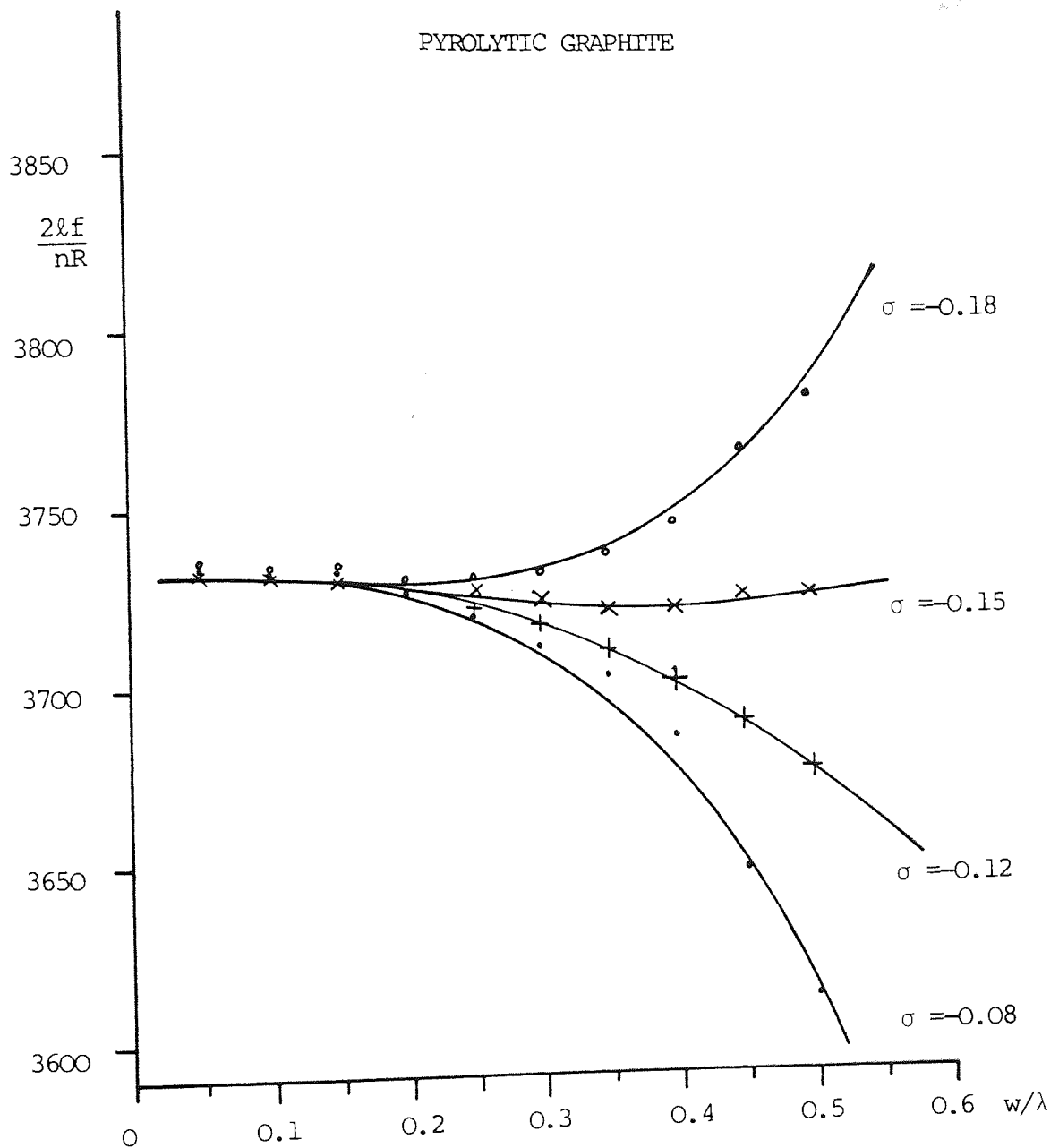
FIG. 5.15   Graphical plot of the corrected phase velocity values
as a function of (w/λ). Four different Poisson's ratio
values used, and it is apparent that $(\sigma=-0.15)$ is the
nearest Poisson's ratio value for Pyrolytic Graphite.
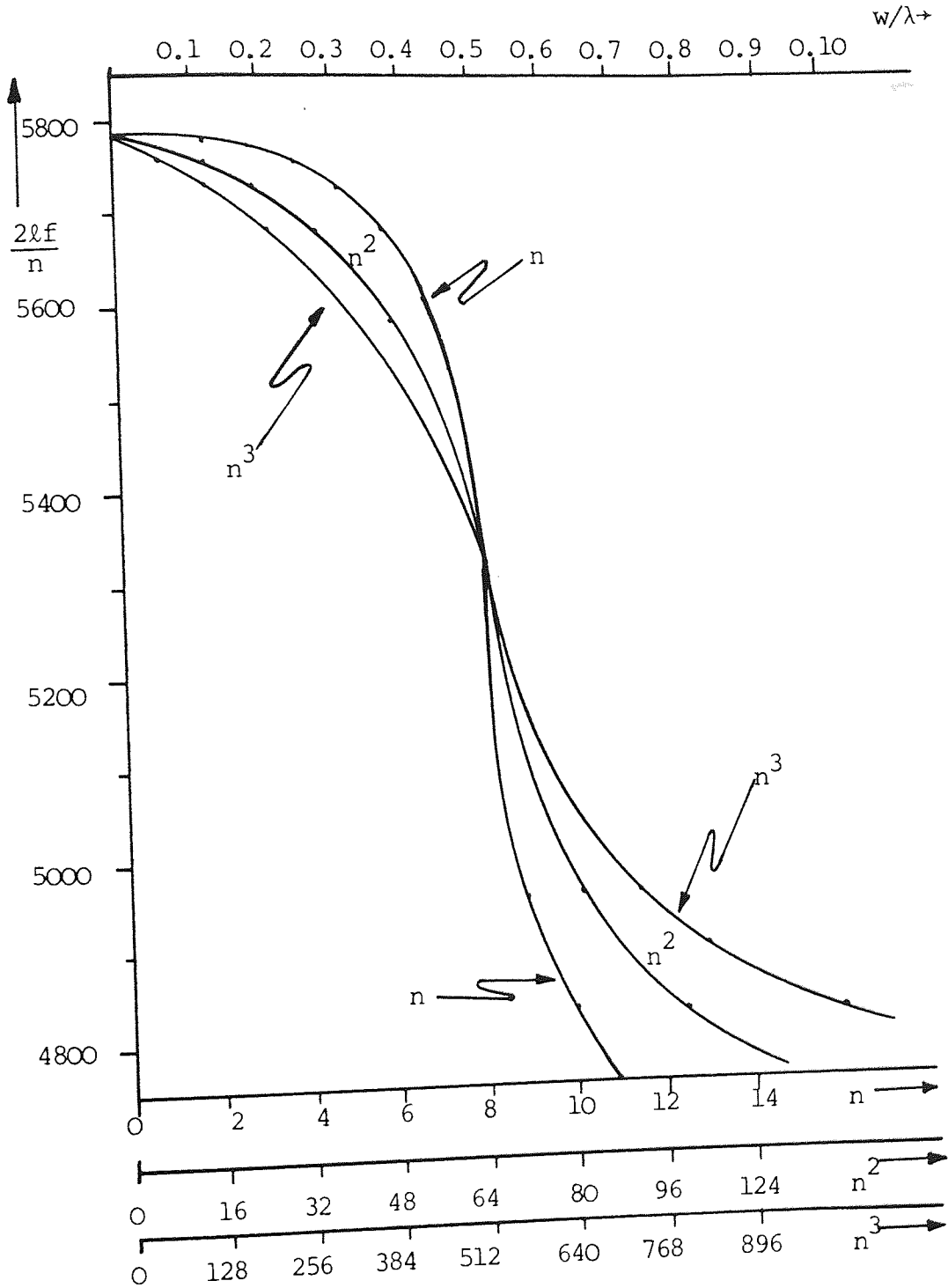
SILICA

FIG. 5.16 The variations of the longitudinal phase velocity with n, n^2 and n^3 in silica rectangular strip, where n is the mode orders.

ALUMINIUM PLATE
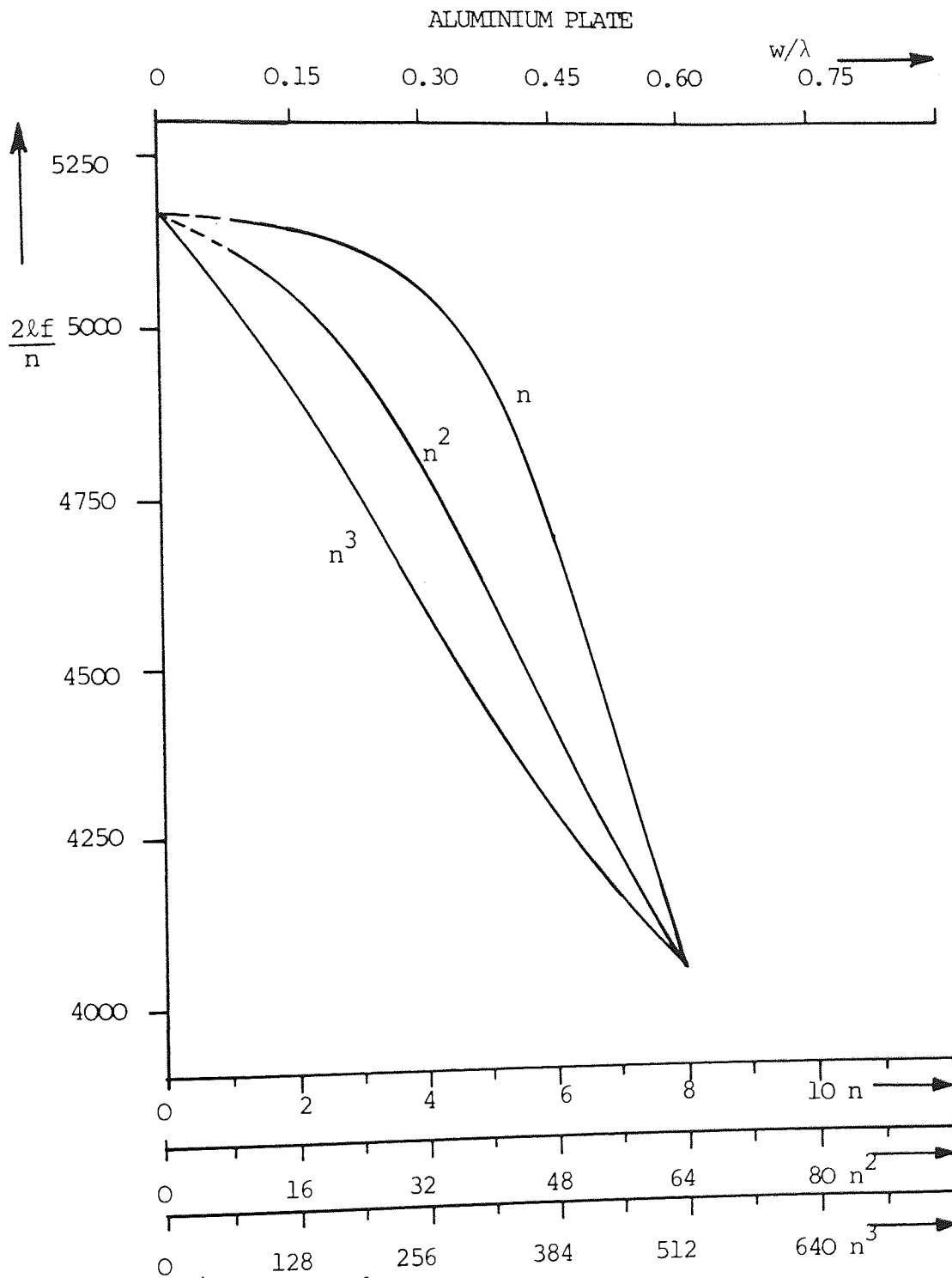
Fig. 5.17   Shows the variations of the longitudinal phase velocity
with n, n^2 and n^3 in Aluminium, rectangular strips,
where n is the mode order.

TABLE 5.1

	SYMMETRY	NON-SYMMETRY
$\phi<1$	$\dfrac{\tan\gamma b(1-\phi^2)^{\frac{1}{2}}}{\tanh\gamma b(1-\phi^2\theta)^{\frac{1}{2}}}=\dfrac{4(1-\phi^2\theta)^{\frac{1}{2}}(1-\phi^2)^{\frac{1}{2}}}{(\phi^2-2)^2}$	$\dfrac{\tanh\gamma b(1-\phi^2)^{\frac{1}{2}}}{\tanh\gamma b(1-\phi^2\theta)^{\frac{1}{2}}}=\dfrac{(\phi^2-2)^2}{4(1-\phi^2)^{\frac{1}{2}}(1-\phi^2\theta)^{\frac{1}{2}}}$
$\phi>1$ and $\phi\theta^{\frac{1}{2}}<1$	$\dfrac{\tan\gamma b(\phi^2-1)^{\frac{1}{2}}}{\tanh\gamma b(1-\phi^2\theta)^{\frac{1}{2}}}=\dfrac{4(\phi^2-1)^{\frac{1}{2}}(1-\phi^2\theta)^{\frac{1}{2}}}{(\phi^2-2)^2}$	$\dfrac{\tan\gamma b(\phi^2-1)^{\frac{1}{2}}}{\tanh\gamma b(1-\phi^2\theta)^{\frac{1}{2}}}=-\dfrac{(\phi^2-2)^2}{4(\phi^2-1)^{\frac{1}{2}}(1-\phi^2\theta)^{\frac{1}{2}}}$
ϕ and $\phi\theta^{\frac{1}{2}}>1$	$\dfrac{\tan\gamma b(\phi^2-1)^{\frac{1}{2}}}{\tanh\gamma b(\phi^2\theta-1)^{\frac{1}{2}}}=-\dfrac{4(\phi^2-1)^{\frac{1}{2}}(\phi^2\theta-1)^{\frac{1}{2}}}{(\phi^2-2)^2}$	$\dfrac{\tan\gamma b(\phi^2-1)^{\frac{1}{2}}}{\tanh\gamma b(\phi^2\theta-1)^{\frac{1}{2}}}=-\dfrac{(\phi^2-2)^2}{4(\phi^2-1)^{\frac{1}{2}}(\phi^2\theta-1)^{\frac{1}{2}}}$
$(\phi^2-1)=\delta$ Very small	$\dfrac{\tanh\gamma b(1-\theta)^{\frac{1}{2}}}{\gamma b}=\dfrac{1}{4(1-\theta)^{\frac{1}{2}}\delta}$	$\dfrac{\tanh\gamma b(1-\theta)^{\frac{1}{2}}}{\gamma b}=-4(1-\theta)^{\frac{1}{2}}\delta$
$(\phi^2-2)=\delta$ Very small	$\dfrac{\tan\gamma b}{\tanh\gamma b(1-2\theta)^{\frac{1}{2}}}=\dfrac{4(1-2\theta)^{\frac{1}{2}}}{\delta}$	$\dfrac{\tan\gamma b}{\tanh\gamma b(1-2\theta)^{\frac{1}{2}}}=\dfrac{\delta}{4(1-2\theta)^{\frac{1}{2}}}$
γb Large	$(\phi^2-2)^2=4(1-\phi^2\theta)^{\frac{1}{2}}(1-\phi^2)^{\frac{1}{2}}$	$(\phi^2-2)^2=4(1-\phi^2\theta)^{\frac{1}{2}}(1-\phi^2)^{\frac{1}{2}}$
γb Small $\phi>1$ and $\phi\theta<1$	$\phi=4(1-\theta)^{\frac{1}{2}}$	.....
γb and ϕ Small	.....	$\dfrac{\tanh\gamma b(1-\phi^2)^{\frac{1}{2}}}{\tanh\gamma b(1-\phi^2\theta)^{\frac{1}{2}}}=1+\dfrac{\phi^2}{4(1-\phi^2)^{\frac{1}{2}}}$

The conditions of the Rayleigh-Lamb frequency equation for the wave propagated in the materials to be considered for both the symmetric and antisymmetric modes. $\phi=\lambda f/C_s$ (the phase velocity normalised to the shear) and $\theta=(1-\sigma)/2$.

TABLE 5.2

(Poisson's Ratio $\sigma = 0.33$)

w/λ	ϕ Antisymmetry 1	ϕ Symmetry 1	ϕ Symmetry 2
0.0	0.0	1.63095	∞.
0.05	0.1455	1.63020	17.180
0.10	0.2141	1.6279	8.4804
0.15	0.3912	1.6238	5.5696
0.20	0.4834	1.6173	4.1238
0.25	0.5577	1.6074	3.2720
0.30	0.6172	1.5924	2.7245
0.35	0.6651	1.5692	2.3560
0.40	0.7038	1.5332	2.1085
0.45	0.7355	1.4809	1.9491
0.50	0.7615	1.4142	1.8539
0.60	0.8013	1.2766	1.7664
0.70	0.8296	1.1693	1.7302
0.80	0.8501	1.0943	1.7083
0.90	0.8654	1.0430	1.6886
1.00	0.8770	1.0000	1.6635
1.10	0.8859	0.9831	1.6259
1.20	0.8929	0.9658	1.5749
1.30	0.8983	0.9536	1.5186
1.40	0.9026	0.9447	1.4640
1.50	0.9060	0.9382	1.4142
1.75	0.9117	0.9286	1.3130
2.00	0.9150	0.9240	1.2401
2.25	0.9168	0.9216	1.1875
2.50	0.9178	0.9204	1.1491
2.75	0.9184	0.9198	1.1204
3.00	0.91870	0.9195	1.0988
5.00	0.9191	0.9191	1.0300

The solution of the Rayleigh-Lamb transcidental frequency equation for the first three modes.   -146-

TABLE 5.3

Poisson's ratio σ	ϕ_B For the Breathing Mode	Ratio of $\dfrac{\phi_B}{\phi_{Lam\acute{e}}}$
0.50	2.1058	1.4890
0.45	2.0331	1.4376
0.40	1.9584	1.3848
0.35	1.8836	1.3319
0.30	1.8100	1.2799
0.25	1.7380	1.2290
0.20	1.6686	1.1799
0.15	1.6016	1.1325
0.10	1.5371	1.0869
0.05	1.4746	1.0427
0.00	1.41421	1.0000
-0.05	1.3490	0.9539
-0.10	1.2860	0.9093
-0.15	1.2250	0.8662

The computed values of the breathing to the Lamé frequency ratios for different Poisson's ratio values. It is assumed that the second symmetric mode of the Rayleigh-Lamb frequency equation represents the breathing mode. ϕ for the Lamé mode is equal to $\sqrt{2}$.

TABLE 5.4

(Poisson's ratio $\sigma=0.33$)

Geometry Length:Width	w/λ	w/ℓ Assuming $\lambda=2\ell$	ϕ	$\Omega = \dfrac{2wf}{C_s}$	$\dfrac{2wf}{C_p}$
Square Plate (1:)	0.50	1.00	1.8539	1.8539	1.0730
	0.45	0.90	1.9491	1.7542	1.0153
	0.40	0.80	2.1085	1.6868	0.9763
	0.35	0.70	2.3560	1.6492	0.9545
	0.30	0.60	2.7245	1.6347	0.9462
Rectangular Plate (2:1)	0.25	0.50	3.2720	1.6360	0.9469
	0.20	0.40	4.1238	1.6500	0.9550
	0.15	0.30	5.5696	1.6710	0.9672
	0.10	0.20	8.4804	1.6960	0.9816
Strip (10:1)	0.05	0.10	17.1800	1.7180	0.9944
	.	.	.	.	.
	.	.	.	.	.
	.	.	.	.	.
Asymptotic Value	0.0	0.0	Infinity	Expected to Approach 1.7277	1.0000

The frequency spectrum for the second symmetric mode of the Rayleigh-Lamb frequency equation. The mode is controlled by the plate width, and the frequency times twice the width has a constant value approaches the plate wave velocity (C_o). For this reason, this represents the frequency spectrum of the breathing mode.

TABLE 5.5

ALUMINIUM STRIP

n	f in KHz	f/n	2ℓf/n	w/λ
2	25.725	12.863	5145	0.150
3	38.375	12.792	5117	0.225
4	50.490	12.623	5049	0.300
5	61.555	12.311	4924	0.375
6	70.446	11.741	4696	0.450
7	76.515	10.931	4372	0.525
8	81.120	10.140	4056	0.600

The measuremental results of the longitudinal
Aluminium rectangular plate modes. The phase
velocity was determined from the phase frequency
and the length of the plate. The value of w/λ is
the result of the w/ℓ ratio and the mode orders n
product. The plate dimensions are 200 mm by 30 mm.

TABLE 5.6

ALUMINIUM STRIP

w/λ	2ℓf/n	2ℓf/nR		
		σ=0.30	σ=0.33	σ=0.35
0.10	5155	5163	5165	5166
0.15	5145	5164	5168	5171
0.20	5130	5166	5173	5179
0.25	5100	5162	5175	5184
0.30	5055	5157	5177	5192
0.35	4990	5155	5186	5208
0.40	4870	5136	5180	5209
0.45	4700	5121	5176	5212
0.50	4490	5119	5178	5217
0.55	4250	5104	5161	5198

The longitudinal phase velocity corrections for Aluminium plate as a function of Poisson's ratio. The eigen value (R) is the Rayleigh-Lamb phase velocity correction given in the table in Appendix A.

TABLE 5.7
SILICA

n	w/λ	f in KHz	f/n	2ℓf/n
1	0.0625	28.295	28.295	5749.5
2	0.1250	56.835	28.418	5774.4
3	0.1875	85.265	28.422	5775.3
4	0.2500	113.435	28.359	5762.5
5	0.3125	140.910	28.182	5726.6
6	0.3750	167.815	27.969	5683.3
7	0.4375	192.365	27.481	5584.1
8	0.5000	209.936	26.242	5332.4
9	0.5625	219.745	24.416	4961.4
10	0.6250	237.716	23.772	4830.5
11	0.6875	247.325	22.484	4568.8

The experimental results show the phase velocity of the longitudinal modes of silica (fuzed quartz) strip. The plate geometry is 101.6 mm by 12.7 mm.

TABLE 5.8
SILICA STRIP

n	w/λ	2ℓf/n	2ℓf/nR		
			0.16	0.17	0.18
1	0.0625	5746.5	5746.5	5746.5	5746.5
2	0.1250	5742.0	5742.1	5742.2	4742.3
3	0.1875	5736.0	5743.8	5745.6	5747.2
4	0.2500	5724.8	5744.9	5747.5	5750.3
5	0.3125	5704.4	5744.7	5750.4	5753.4
6	0.375	5664.2	5738.8	5750.6	5759.3
7	0.4375	5565.0	5731.3	5754.6	2766.8
8	0.5000	5320.0	5729.6	5754.2	5779.0

The experimental results of the silica rectangular
strip (101.6 mm × 12.5 mm). The longitudinal phase
velocity has been corrected using the eigen value R
for different Poisson's ratio from the table in
Appendix A. .

-152-

TABLE 5.9

GLASS STRIP

Mode Number (n)	w/λ	f in KHz	f/n	$2\ell f/n$ m.sec^{-1}
1	0.0624	34.953	34.953	5429.6
2	0.1249	69.811	34.906	5422.2
3	0.1873	104.420	34.807	5406.9
4	0.2500	138.637	34.659	5384.0
5	0.3122	172.095	34.419	5346.6

The experimental results of the longitudinal modes for the glass strip. The phase velocity for each mode is determined as a function of the mode orders (n). The strip is of a geometry 77.67 mm by 9.7 mm.

TABLE 5.10
GLASS STRIP

w/λ	2ℓf/n	2ℓf/nR		
		Poisson's Ratio 0.20	Poisson's Ratio 0.25	Poisson's Ratio 0.30
0.05	5438.0	5438.2	5438.3	5440.0
0.10	5434.0	5437.7	5440.0	5442.3
0.15	5422.0	5430.8	5435.0	5441.8
0.20	5403.0	5415.4	5438.0	5440.9
0.25	5384.0	5413.5	5429.9	5449.6
0.30	5350.0	5399.3	5426.2	5458.2

The phase velocity is normalised to the eigen value (R) for three different Poisson's ratio values. The phase velocity (2ℓf/n) has been found from the velocity dispersive curve in Fig. 5.12.

TABLE 5.11

PYROLYTIC GRAPHITE

Mode Order n	w/λ	f in KHz	f/n	$2\ell f/n$
1	0.0464	13.44	13.44	3736.0
2	0.0928	26.873	13.437	3735.0
3	0.1392	40.208	13.403	3726.0
4	0.1856	53.513	13.378	3719.1
5	0.2320	66.767	13.353	3712.2
6	0.2784	80.113	13.352	3711.9
7	0.3248	93.030	13.290	3694.6
8	0.3712	105.766	13.221	3675.4
9	0.4176	117.940	13.105	3643.2
10	0.4640	129.290	12.929	3594.3

The experimental results of Pyrolytic Graphite. The longitudinal modal frequency was measured and the phase velocity calculated for each mode harmonic number (n). (Plate length = 139.0 mm and width = 12.9 mm)

TABLE 5.12

PYROLYTIC GRAPHITE

w/λ	2ℓf/n	2ℓf/nR				
		σ=0.08	σ=0.10	σ=0.12	σ=0.15	σ=0.18
0.05	3736.3	3736.3	3736.3	3736.3	3736.3	3736.3
0.10	3733.5	3733.5	3733.5	3733.5	3736.3	3736.3
0.15	3730.8	3730.8	3733.5	3733.5	3733.5	3736.3
0.20	3725.2	3728.0	3728.0	3730.8	3730.8	3739.1
0.25	3716.9	3719.6	3722.4	3725.2	3728.0	3730.8
0.30	3705.7	3708.5	3714.1	3716.9	3725.2	3733.5
0.35	3689.1	3697.4	3703.0	3711.3	3722.4	3736.3
0.40	3664.0	3689.1	3691.8	3703.0	3722.4	3747.4
0.45	3608.4	3647.4	3666.8	3689.1	3728.0	3766.9
0.50	3475.0	3611.3	3644.6	3677.6	3726.5	3774.8

The calculated values of (2ℓf/nR) show the corrections
applied to the phase velocity for five different
Poisson's ratio values. (R from the table in Appendix A)

TABLE 5.13

SILICA

n	w/λ	$2\ell f/n$	n^2	n^3
1	0.0625	5749.5	1	1
2	0.125	5774.5	4	8
3	0.1875	5775.3	9	27
4	0.25	5762.5	16	64
5	0.3125	5726.6	25	125
6	0.375	5683.3	36	216
7	0.4375	5584.1	49	343
8	0.500	5332.4	64	512
9	0.5625	4961.4	81	729
10	0.625	4830.5	100	1024
11	0.6875	4568.8	121	1331

The variations of the phase velocity with the modes order for the silica (fuzed quartz) strip of length 101.6 mm and width 12.7mm. $\sigma=0.165$ $C_o=5783$ mm.

TABLE 5.14

ALUMINIUM

n	w/λ	$2\ell f/n$	n^2	n^3
2	0.150	5145	4	8
3	0.225	5117	9	27
4	0.300	5049	16	64
5	0.375	4924	25	125
6	0.450	4696	36	216
7	0.525	4372	49	343
8	0.600	4056	64	512

This shows the variations of the longitudinal phase velocity as a function of the modes order (n) for Aluminium having strip geometry; length=200 and width=20mm. (σ=0.34 and C_o=5165 m.sec^{-1})

CHAPTER SIX

THE LONGITUDINAL ELASTICITY

MEASUREMENTS OF ANISOTROPIC MATERIALS

6.1 INTRODUCTION

There is general agreement about the problems
associated with the materials being anisotropic. Although
the theoretical treatments were, to some extent, restricted
only for isotropic materials, there are certain cases when
these are difficult to obtain, or in other cases where
the degree of the anisotropy is required to be measured.
For example, non-metals such as graphite which are
isostatically prepared can be expected to be isotropic.
This is the case where the advanced technical apparatus is
required to be used and better results needed to be
obtained and resolved.

The method of the delay line pulse-echo system is
again used here to observe the spectrum of the various
geometries. The general feature of the apparatus was
fully covered in Chapter Two of this work.

This investigation can be considered as an extension
to the work which was successfully carried out by
Bell et al. [8, 9] using this technique for measuring
the elastic constants and for ultrasonic characterisation

-159-

of refractories at high temperatures.

In this chapter, further investigations related to the angle dependence of the longitudinal elastic modulus of anisotropic materials will be considered in detail. Their industrial applications in the field of the material studies and as a practicle tool in investigations related to non-destructive testing will be also shown.

6.2   GENERAL ASPECTS OF ANISOTROPIC EFFECTS ON THE MODAL
       RESONANCES

Extensive experimental measurements on disks machined from drawn rod revealed that they are isotropic. No significant displacements occur in the axial thickness direction of the disk, and consequently anisotropic effects associated with the longitudinal grains are not present. Meanwhile, the disks cut from the rolled metal sheets show considerable anisotropy. This arises from the nature of the rolling process. In aluminium and steel, the fundamental modes of the vibration which has two nodal diameters was found to be split into two modes. Their frequencies differ by a few percent when excited parallel and perpendicular to the direction of the roll. In square plates, the resonant modes are also effected by grain orientation. The elastic anisotropy removes certain mode degeneracy, and they become double. Fig. 6.1 demonstrates this effect on certain modes of different

resonators. The modes split due to the effect of rolling and they become double.

The effects of the grain direction on the elastic measurements of the materials can be better studied by considering the longitudinal modes of long strips. Here the particle motions have only one direction parallel to the plate length, and the effects due to the grains present are evident. The modes can be simply excited by an axial length drive of the plate with the line. The longitudinal vibration of rectangular plates and strips have been extensively studied in the early stages of this work. An empirical treatment has already covered the spectral harmonic relations, and their dispersion characteristics as a function of the plate width-to-wavelength ratios.

Further investigations concerning the longitudinal modes of anisotropic materials having strip geometries will be discussed and explored in the coming sections.

6.3. SAMPLE PREPARATION

The moderate anisotropy which occurs in rolled metal sheets was found to have a highly sensitive effect on certain modal vibrations of plates. Mode splitting is evident for the lowest mode of disks (two nodal diameters), but is not so evident at the higher modes. Splitting is

observed on higher modes of rectangular plates which are cut with sides parallel to the grain direction making the elastic anisotropy match with the plate geometry.

Different types of anisotropic materials have been employed in this investigation and accurate measurements have been obtained. The materials being investigated have been in the form of rolled metal sheets. They range from shim steel, mild steel and aluminium. The grains due to the rolling process of the metal are elongated with the length dimension of the plate. These are quite observable by polishing and examining the surface of the plate through a conventional microscope.

The materials have been prepared as thin narrow strip geometries machined out of the sheet plate with the grains oriented at an angle with the length axis of the plate. Consequently these will have an angle with the direction of the wave motion in the plate since the latter is directed with the plate length.

Grains elongated parallel to the plate length are considered to have an angle of zero degrees. While perpendicular to the length the angle is "90" degrees. The grains angle is considered in this measurement to be between "0°" and "90°". Symmetry of results about these two angles are expected.

Fig. 6.2 shows photographically the samples prepared

with the grains orientations. Here the grains considered
to be oriented to the north when they are parallel to the
length of the strip. That with grains across the length
(perpendicular to it) are considered to be oriented to
the east. The other three samples have been cut with
grains which are oriented at an angle between the north
and the east direction. The 45 degrees angle is clearly
the north-east direction. The choice of the geographic
direction in indicating the grains orientation is not
essential, but here it is used as an easier and more
convenient method to indicate the angles.

6.4 YOUNG'S MODULUS RELATIONS WITH THE GRAIN ORIENTATION

Shim steel cut in strip geometries as described
above were the first to be investigated. The strips were
driven at an end, after which the longitudinal resonances
were excited and measured. An accurate value of the rod
velocity was then obtained from the plotted values of
the phase velocities as a function of their longitudinal
mode orders. This has been extrapolated as the value of
(w/λ) approaches zero. A great deal of the procedures
and the theoretical treatments for doing this have been
given and explored in the previous chapter.

Knowing the rod velocity, the Young's modulus can
be found through the well known relationship:-

$$E = c_o^2 \rho \qquad (6.1)$$

Where E is the Young's modulus, C_O is the rod velocity and ρ is the density of the material measured.

Full experimental results for shim steel are given in Table 6.1. The rod velocity was measured with respect to the grains elongated at an angle with the length of the strip. The corresponding elasticity was then calculated from the relation (6.1). The variation of the rod velocity with the grain orientation is shown graphically in Fig. 6.3. The angle corresponds to the length axis of the plate.

The primary inspection of the results in the figure above reveals the complex cyclical variations of the rod velocity and, consequently, the Young's modulus of the materials (shim steel) corresponding to the grains direction which is the rolling direction of the metal sheet. Two peaks can be observed in this curve, one at an angle of zero degrees (grains parallel to the length) and one at an angle of 90 degrees (grains across the length). The latter has a higher amplitude. The minimum value of the rod velocity occurs at an angle of about 45 degrees of the grains with the length.

This is an interesting result, since it was initially assumed that the variation might be of a sinusoidal form rather than of a distorted wave form, which obviously needs more complicated mathematical expression to be fit.

However, this result cannot be considered as general and relations of the rod velocity with the grains direction. Further measurements on different rolled metal sheets have shown different variations of the rod wave velocity and, in addition, the elasticity as a function of the grains orientation.

The measurements carried out on two different rolled metal sheets of steel show two different results. In those obtained from the sheet (A), the results were similar to those obtained from the shim steel shown above, while the results obtained from the other sample, sheet (B), show completely reverse values.- the maximum now occurring at 45 degrees.

Fig. 6.4 shows graphically the variation of the Young's modulus as a function of the grains orientation for shim steel and steel (A). This demonstrates very well the identical variations for both of these samples. It is clearly noticeable that the maximum amplitude of the elasticity occurs at an angle of 90 degrees (grains perpendicular to the length of the strip).

If the curve in the figure above is symmetrical about $\theta = 0^{\circ}$ and $\theta = 90^{\circ}$, then this can be mathematically expressed as:-

$$E_{\theta} = E_{o} + E_{1} \cos 2\theta + E_{2} \cos 4\theta \qquad (6.2)$$

-165-

where E_θ is the elasticity at the angle θ in degrees, and E_0, E_1 and E_2 are constants which can be determined for each given sample from the measured values given in the table above. Then by entering the values of θ from zero degrees to 360 degrees a plot of the theoretical variations of the elasticity with the grain angles is obtained. This is shown in the figure above (Fig. 6.4). The two results are quite close, but it can be demonstrated better if more terms are added to the mathematical expression above.

The measurements on steel sheet (B) are fully given in Table 6.2. The variations of the Young's modulus as a function of the grains angle are plotted and shown graphically in Fig. 6.5. Here the curve has a peak of maximum rod velocity at an angle of about 45 degrees, and it has two minima values at zero and 90 degrees angle respectively. The values obtained in this work were confirmed also by exciting the flexural resonant modes of the strips, and the rod velocity was determined by using the formula given by Morse[71] which has already been described and shown in Chapter Four. The results of this method have been found identical to the longitudinal resonance method, which has essentially been employed in this work.

Aluminium metal strips cut from rolled sheets have also been investigated. Accurate measurements of the rod wave velocity for each strip with various grain angles

-166-

have been obtained. The full experimental results are given in Table 6.3. The precise value of the Young's modulus is also determined, and its variation as a function of the grains orientation is shown graphically in Fig. 6.6. The waveform in Fig. 6.6 is close to that of the shim steel, but the curve is less distorted. The amplitude of the two maximum values at "0" and "90" degrees are close to each other.

The three constants E_0, E_1 and E_2 of equation (6.2) can be determined for each sample from the experimental values obtained and they have been given in the tables above. This is shown in Table 6.4. A final comment can be made about these constants which obviously control the wave form of the elasticity variations with grain angles. This concerns the values of E_1 and E_2 and their signs, which determine the maxima and the minima of the curve. This is obviously clear from the Aluminium constant values. Since the two maxima are close to each other, the value of E_1 is close to zero.

These results need further inspection related to the crystallographic structures of the materials, which need to be investigated in detail as far as the metallurgists are concerned. The two different results shown by two types of rolled steel sheets are interesting for further investigation. The similarity between the steel (B) and the weld, which will be shown later, is

obviously important as far as the crystallographic
structures are concerned. The elementary answer to the
problem of the results obtained from steel (A) and (B)
is that the crystallographic difference of the two
types, due to the heat treatment, might be the cause of
the unusual results shown earlier.

6.5   COMPARISON WITH THE THEORETICAL CONCEPT

The results presented in the previous section show
the experimental measurements of the longitudinal elasticity
with the grains orientation in rolled metal sheets. At
this stage, some aspects of the analytical formulae
concerning the theory of elasticity for anisotropic
materials will be considered. Their comparison with the
experimental results will also be discussed.

The elastic constants matrix for the transverse
isotropic body has been given by Mason[52] shows the
Young's modulus corresponding to the co-ordinating axes
of the body. If the lateral dimensions of it are large
compared with the thickness, the state of the stress is
approximately plane, and the problems of elasticity can
be dealt with on a two dimensional basis. The elastic
constants matrix can be reduced to the following
elements; C_{11}, C_{13}, C_{33} and C_{44} where the first three
elements are represented by the longitudinal modulus.
The matrix is symmetrical and the other elements are zero.

-168-

Cady[17] has shown that C_{11} and C_{33} are the Young's modulus when the grains are parallel and perpendicular to the length axis of the plate respectively. He had shown, in an analytical treatment, that the variation of the Young's modulus with orientation is given by equation (6.3).

$$\frac{1}{E_\theta} = \frac{(1+\cos2\theta)^2}{4C_{11}} + \frac{\sin^2 2\theta}{2C_{13}} + \frac{(1-\cos2\theta)^2}{4C_{33}} \qquad (6.3)$$

where $E_\theta = \rho C_\theta^2$ (C_θ is the rod velocity corresponding to the grains angle θ).

θ is the angle of orientation with the length of the plate.

The three elastic constants can be determined using the experimental results obtained earlier for each rolled metal sheet, since:-

$$\frac{1}{E_{\theta=0^o}} = \frac{1}{C_{11}}$$

$$\frac{1}{E_{\theta=90^o}} = \frac{1}{C_{33}} \qquad (6.4)$$

and

$$\frac{1}{E_{\theta=45^o}} = \frac{1}{4C_{11}} + \frac{1}{2C_{13}} + \frac{1}{4C_{33}}$$

Then by entering the values of θ from 0° to 360° in equation (6.3), the theoretical plot for the elasticity of the material corresponding to the grains orientation,

will be obtained. This shows that the curve is symmetry about $\theta = 0°$ and $\theta = 90°$.

Fig. 6.7 shows a plot for the theoretical elastic modulus obtained from equation (6.3) and the experimental results obtained earlier for shim steel. This clearly shows the close agreement between the curve obtained from the three observations and the two extra readings at $22\frac{1}{2}$ and $67\frac{1}{2}$ degrees.

Similar results are expected to be found for the other measured materials, e.g. steel (both types) and Aluminium. The elastic constants C_{11} and C_{33} are identical to the experimental observations of the elasticity parallel and perpendicular to the rolling process of the metal sheets respectively. The value of C_{13} is only required to be found from equation (6.4). The elasticity obtained from the other extra two observations at $22\frac{1}{2}$ degrees and $67\frac{1}{2}$ degrees grains angles can be regarded as checking results with the theory. This has given an excellent spot on results with high accuracy.

6.6 APPLICATION IN WELD INSPECTION

The excellent results obtained earlier, relating the variation of the longitudinal elastic properties of the materials with the grains rotation along the plate axis, has   clearly shown that the method   used is quite

suitable for such investigations.   This has encouraged

to extend the work for further investigations of the

materials similar in elastic symmetry   in certain

types of weld.

Research in welding technology has increasingly

become of major interest in industrial applications.

Austenitic weldments contain long columnar grains with

the major axis along a $\langle 100 \rangle$ crystallographic direction[33].

Such a structure is said to possess a fibre texture.

Problems with inspections of such grain structure

in the weldments were essentially related to the methods

and apparatus being used.   Different techniques have been

already employed to investigate the variations of the

elastic properties with the grains structure of the

weldments, all based on the use of commercial ultrasonic

probes[33,36,94,99]. These operate by generating and sending

ultrasonic compression waves through the structure.   Their

propagation is influenced by the grain, structure.

These techniques are regarded to be difficult due

to the high level of scattering from the coarse grain

structure and consequently the attenuation present in such

materials.

Joint research work has been carried out with the

Department of Metallurgy and Materials Engineering of

the University of Aston in Birmingham, to investigate the longitudinal velocity in the weldments. They were provided with two types of weld geometries to be measured. These were:-

    (a) Double-U 316 austenitic weld

    (b) Single-V 316 austenitic weld

their macrographs are shown in the publication given in Appendix B.

    The signficant feature of this work is its accurate and comparable results obtained which can be easily recognised through the comparison of these measurements with the other methods.

6.6.1 Experimental Investigation of the Longitudinal Wave Velocity through Austenitic Weldments

    To investigate how the grain structure influences the wave velocity in the weld, the number of samples in shapes of thin narrow strip geometries have been machined out of the weld with grains elongated at different angles with the length of the strips. Using the method described previously, the values of the resonant frequencies for different modes were obtained for each of the five strips. The longitudinal wave velocity (rod velocity C_o) was then determined as approximate as possible, bearing in mind that the high anisotropy of the weld structure affects the mode harmonicity.

The measured values of the rod velocity, as a function of the grains angle corresponding to the length of the strip for the two welds, are given in Table 6.5. This shows that the maximum value of the rod velocity occurs when the grains have an angle of about 45 degrees. This has two minimum values at zero and 90 degrees respectively, (see Appendix B). In this respect it is similar to steel (B).

Assuming that the curve of the rod velocity is symmetr*ical* about $\theta = 0^\circ$ and $\theta = 90^\circ$, where θ is the grain direction with respect to the plate length. The variation of the rod velocity can be then expressed as:-

$$C_\theta = C_o + C_1 \cos 2\theta + C_2 \cos 4\theta + C_3 \cos 6\theta + C_4 \cos 8\theta \qquad (6.5)$$

where C_o, C_1, C_2, C_3 and C_4 are constants which can be determined from the experimental values given for each weld in the Table 6.5. By entering the values of θ from 0° to 360° a plot of C_o, as a function of θ for each of these two welds, is obtained. This is clearly shown in Fig. 6.8.

It is vital to emphasise at the end of this section that this work has shown recognised measured values for both welds with comparable results to the experimental and the theoretical investigations already reported[33,36,94,99]. The results have been fully *described* in a publication which is shown in Appendix B.

6.7 FINAL COMMENTS AND RECOMMENDATION FOR FURTHER INVESTIGATIONS

The method of determining the longitudinal rod velocity of the rectangular plate geometries shows its sensitivity towards the anisotropy of the materials. This is clearly demonstrated by measuring the longitudinal modes of strips machined out of the rolled metal sheets. These can be considered as moderately anisotropy since the rolling process direct the grains obviously at certain dimension of the plate. The angle of the grains direction can be considered with respect to the length of the axis of the plate.

Clearly the variation of the modal resonant frequencies with their harmonic orders is evident from the graphical plot which was used to find the rod velocity (C_o) by extrapolating the curve.

This curve could be less smooth if the material is highly anisotropy. While the smooth variation of the curve is only obvious when the material is isotropic.

The investigation could well be extended for further work related with non-metallic materials where the grains are elongated toward certain axis of the body, e.g. wood, graphite cut from the sheet plate and other carbon fibre composites. This is important in determining their elastic constants and consequently their physical properties.

-174-

The method of exciting the resonant vibration of the plate is quite suitable and no modification is required for the range of the frequencies used to excite the resonant spectra of the body.

(A)

Disk Mode (1,2)
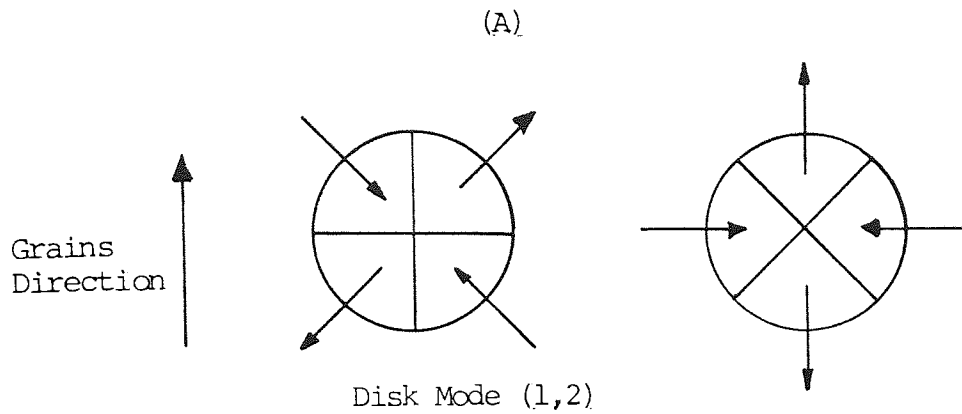
The anisotropy removes the mode degeneracy and the mode becomes double
(The frequency difference was found to be about 8% in shim steel metal
sheet).

(B)

Square Plate
The Flexural Mode
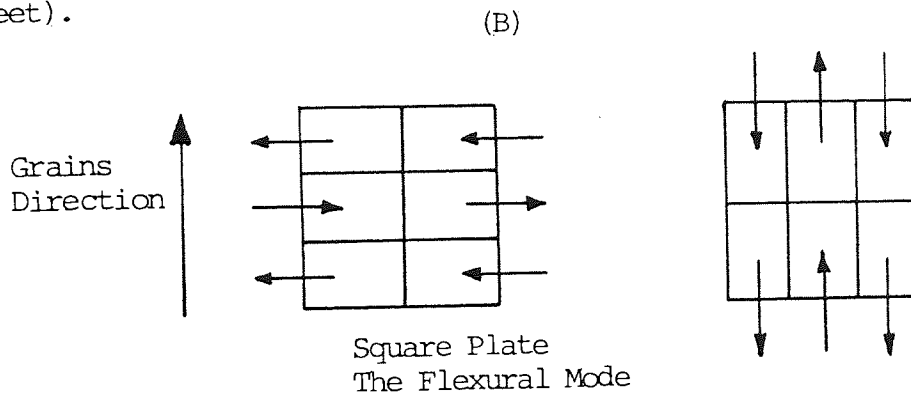
The anisotropy again removes the degeneracy of this mode which becomes
double. (The frequency difference was found to be about 3% in shim
steel metal sheet).

(C)

Rectangular Strip
The Fundamental Mode
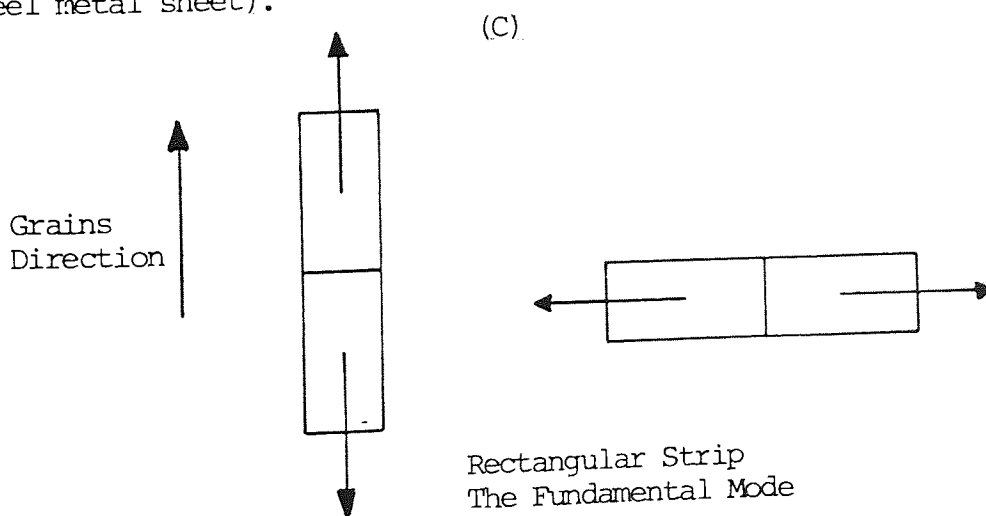
The anisotropy is effecting the mode frequency. No split in mode is
expected. The results give the   elasticity parallel and perpendicular
to the direction of roll.

FIG. 6.1   The effects of grain orientation on different modes of
various resonators.

-176-
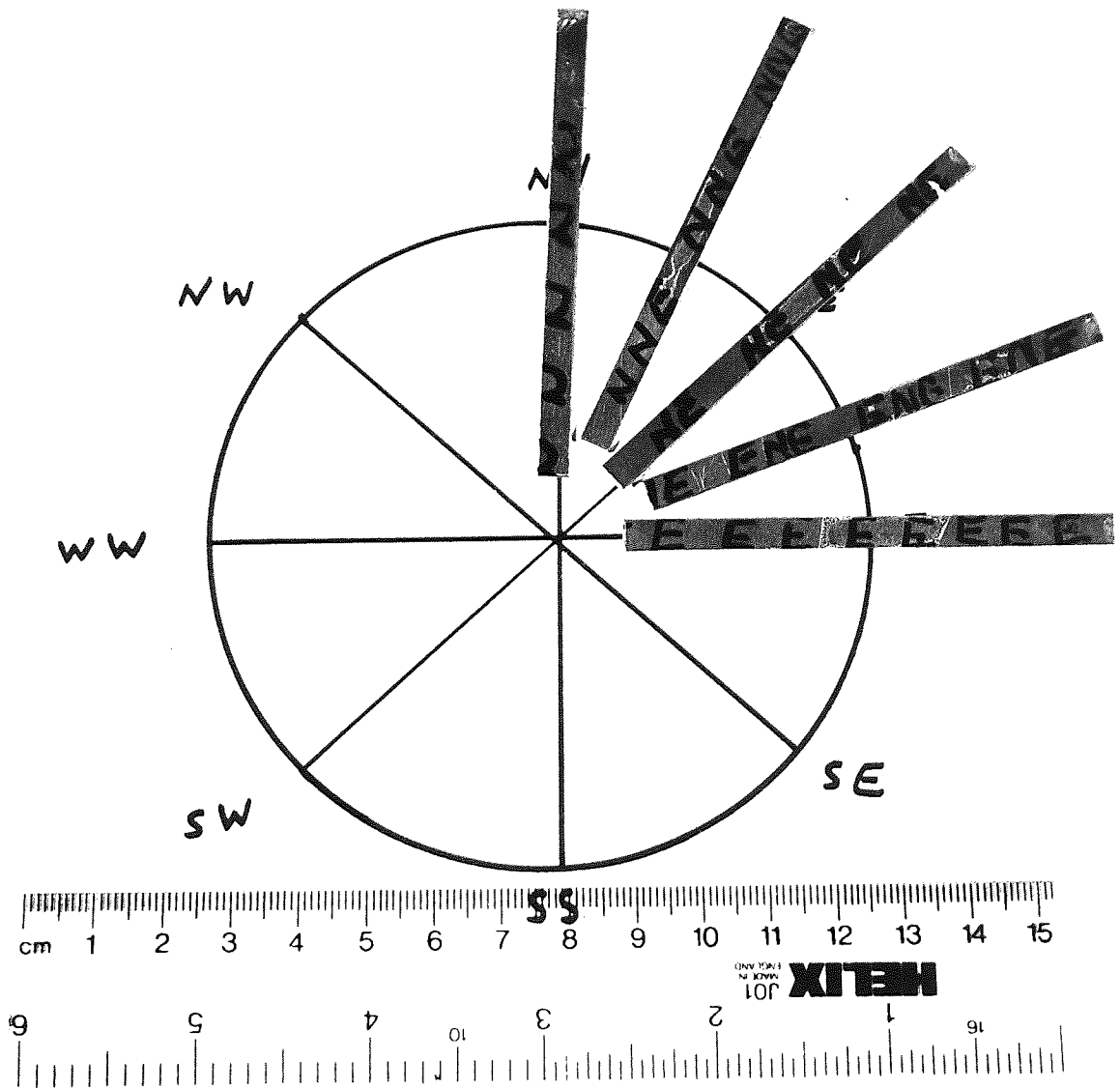
Fig. 6.2   A photographical display showing the samples

prepared with different grains direction angle.

Here the grains considered to be oriented to

the North when they are parallel to the length of

the strip.   That, with the grains across the

length, are considered to be oriented to the East.
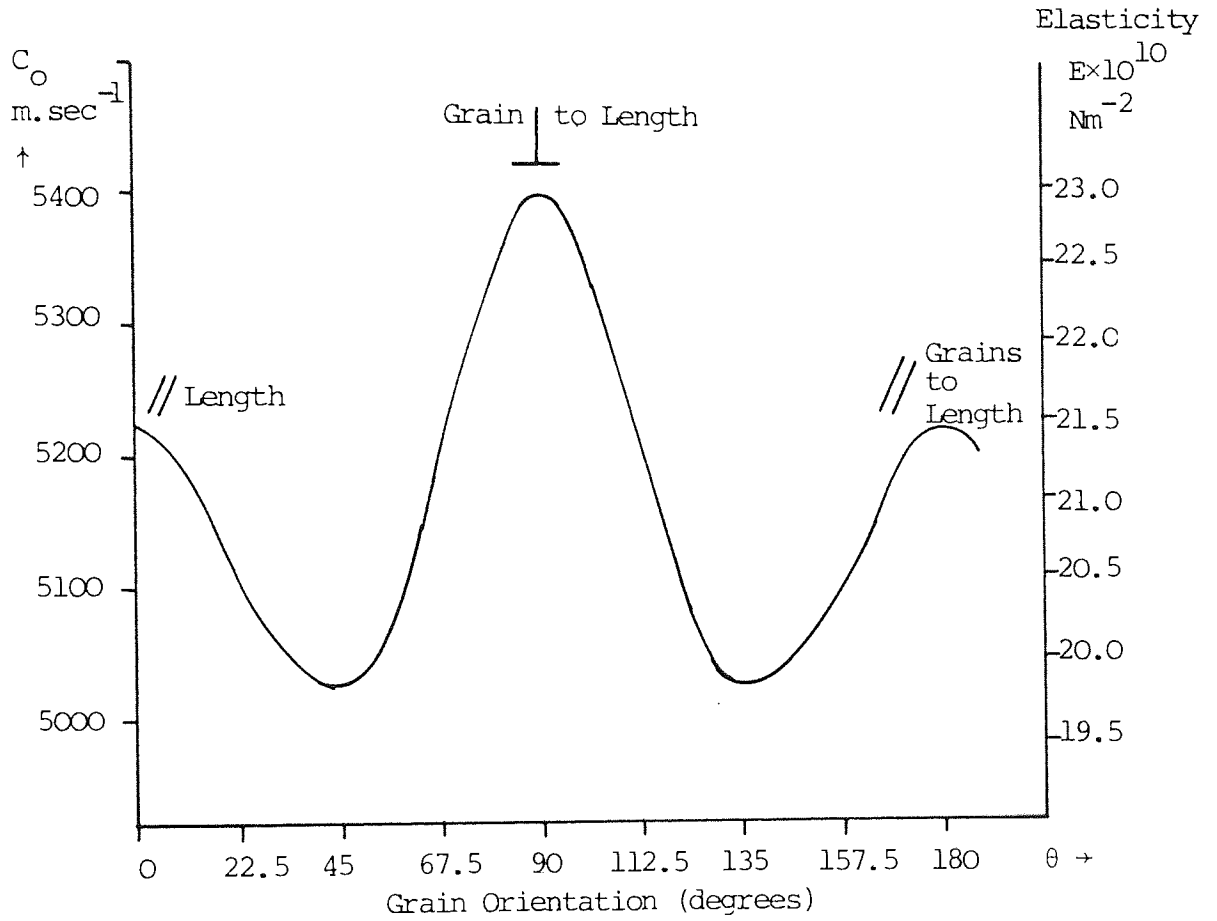
Fig. 6.3 Shows the variations of the rod velocity (C_o) and the elastic constant of shim steel with the grains orientation (θ).

Elasticity
$E \times 10^{10}$
Nm^{-2}

SHIM STEEL AND STEEL (A)

+ Experimental values

— —Values obtained from
    expression (6.2)

Steel (A)

Shim Steel

23.0

22.0

21.0

20.0

19.0

O   22½   45   67½   90   112½   135   157½   180 θ^{o}

Grains Orientation *in degree*

	Shim Steel	Steel (A)
E_O	21.0435	21.4000
E_1	−0.7185	−0.3900
E_2	1.1573	−0.6700
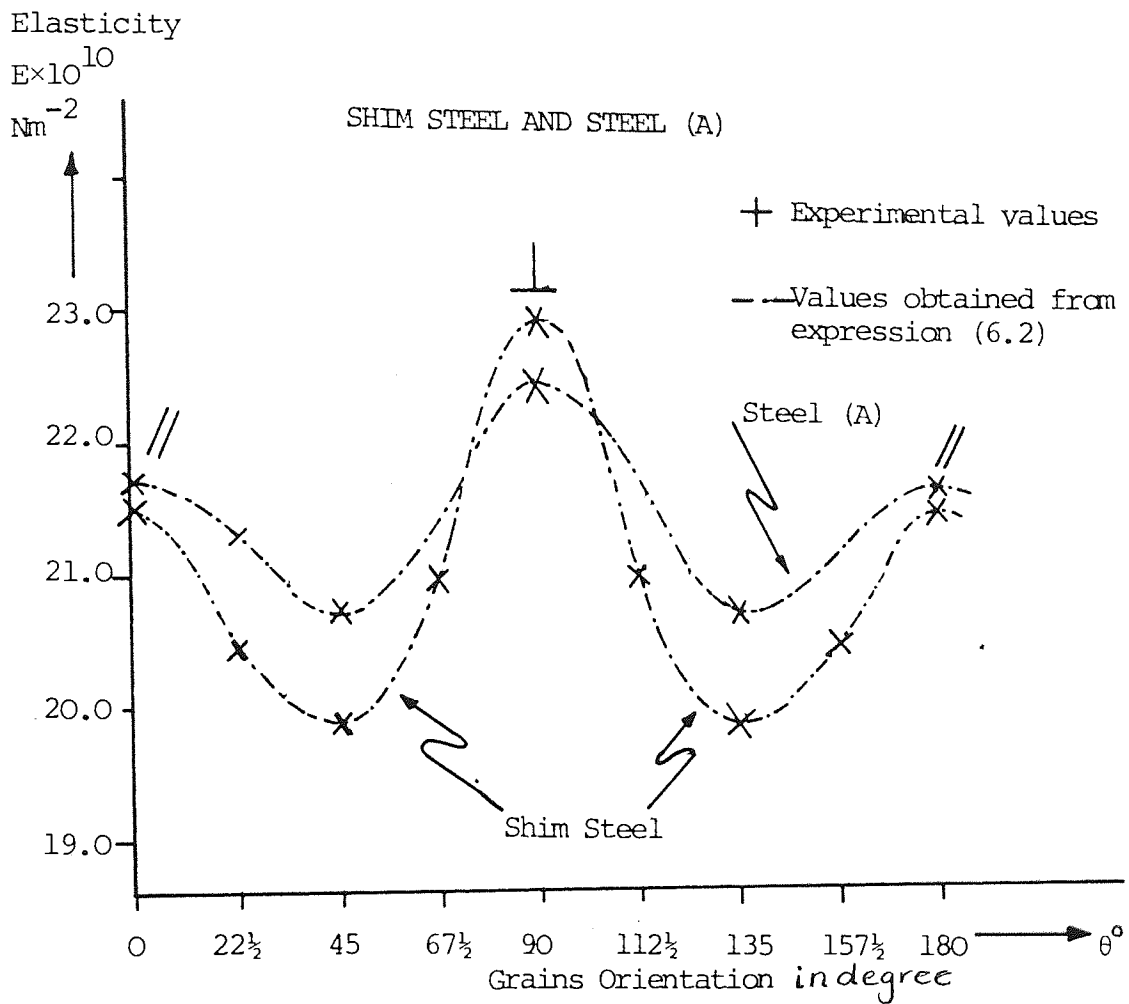
$\times 10^{10}$
Nm^{-2}

Fig. 6.4   The graphical representation of the variations of Young's
modulus as a function of the grains orientation in shim
steel and steel (A). The curve is symmetry about $\theta = 0^{o}$
and $\theta = 90^{o}$.

-179-

Elasticity
$E \times 10^{10}$
Nm^{-2}

STEEL (B)

$$E_\theta = E_o + E_1 \cos 2\theta + E_2 \cos 4\theta$$

23.5 –

23.0 –

22.5 –

22.0 –

⊥ to Length

21.5 –

// to Length

21.0 –

// to Length

O   22½   45   67½   90   112½   135   157½   180 θ —→

Grain direction in degrees

E_o	22.012
E_1	−0.242
E_2	−0.655
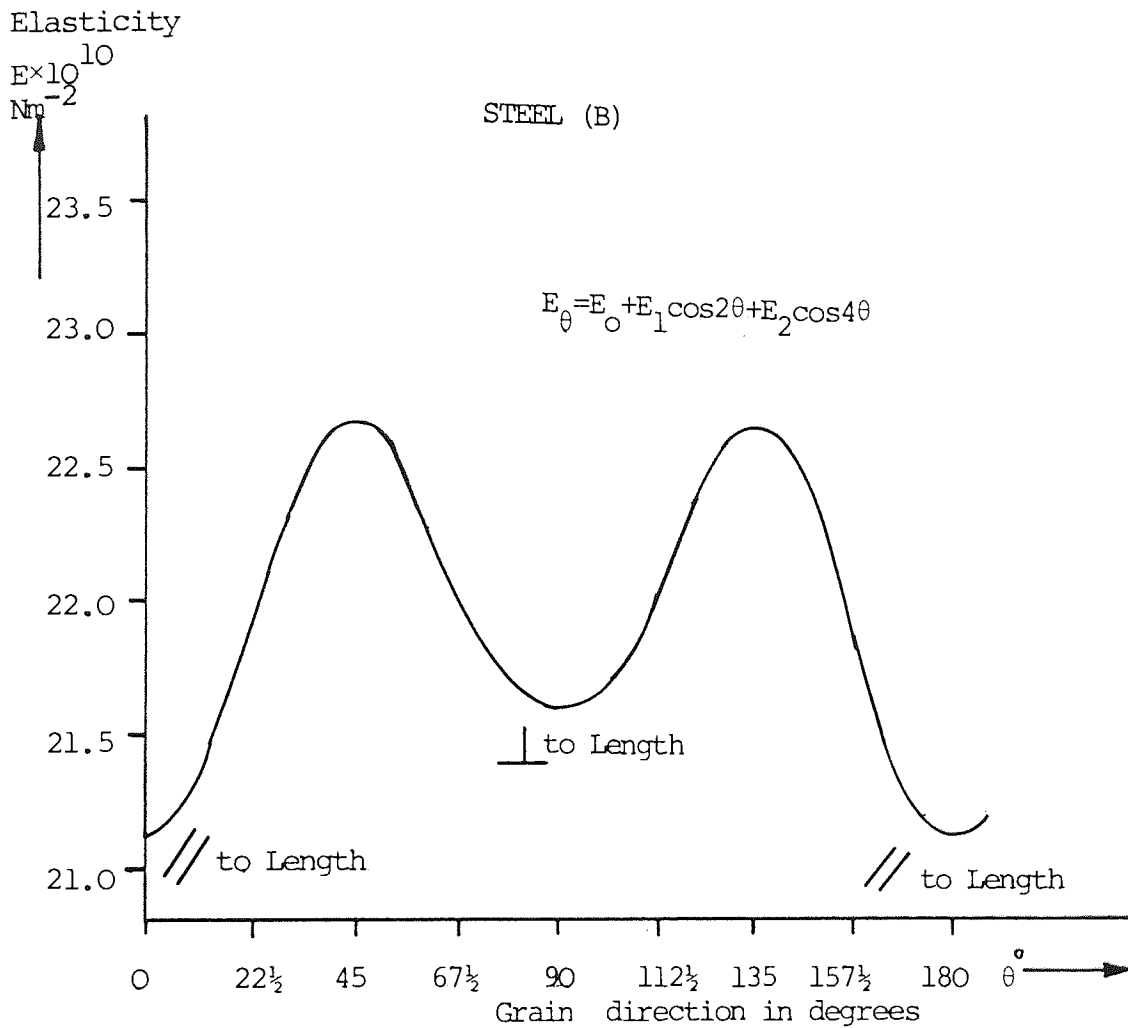
$\times 10^{10}$
Nm^{-2}

Fig. 6.5   The graphical plot of Young's modulus variations with the grains angle corresponds to the length of the plate for steel of type (B).

Elasticity

$E \times 10^{10}$
Nm^{-2}

ALUMINIUM ROLLED SHEET

7.3

Grains
// to Length

Grains $\perp$ to Length

Grains // to Length

7.2

7.1

7.0

6.9

O   22½   45   67½   90   112½   135   167½   180 θ°

Grain direction in degrees

E_O	7.0533
E_1	-0.0055
E_2	0.1863
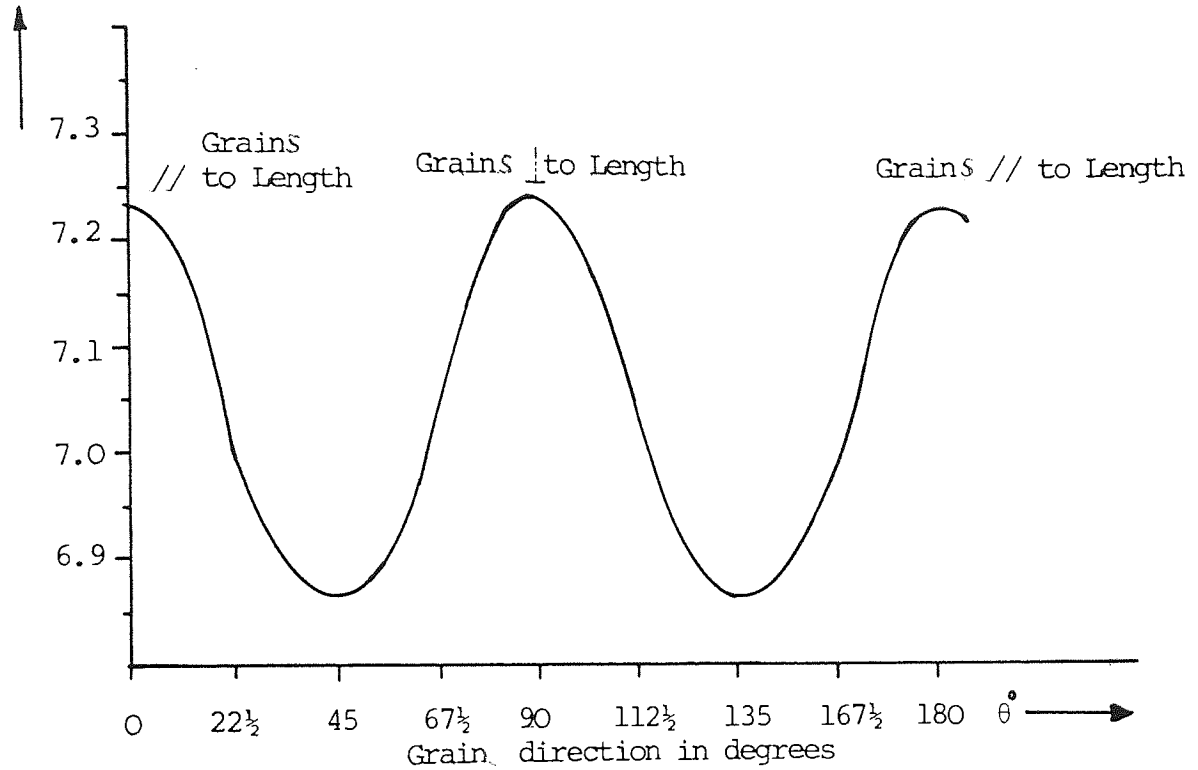
$\times 10^{10}$
Nm^{-2}

Fig. 6.6 The variations of the Young's modulus with the grains
angle corresponds to the length of the aluminium strips.
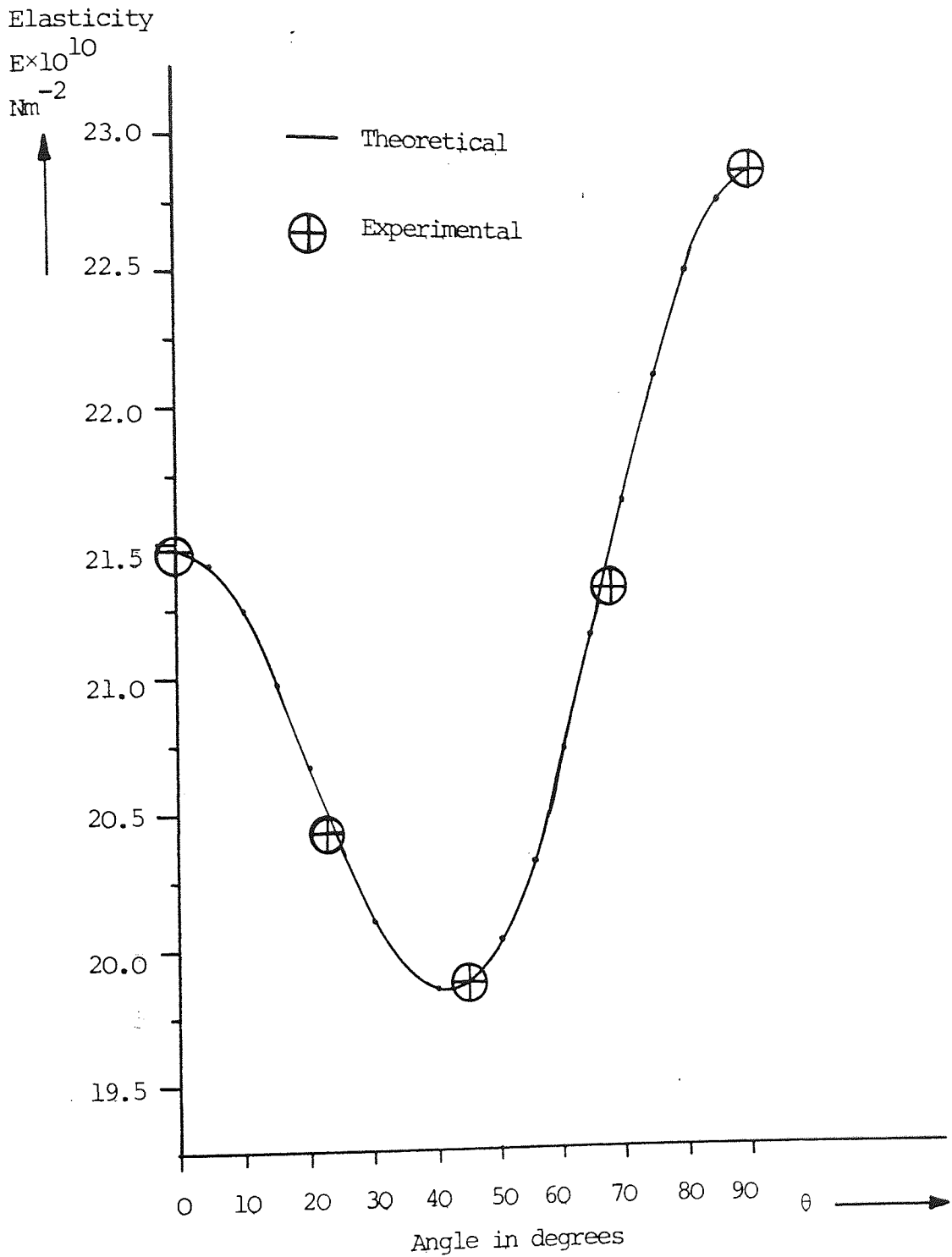
Fig. 6.7 The theoretical and experimental plot of the shim steel elastic constant variations with the grain direction. (Zero degrees grains parallel to the length, 90 degrees grains perpendicular).
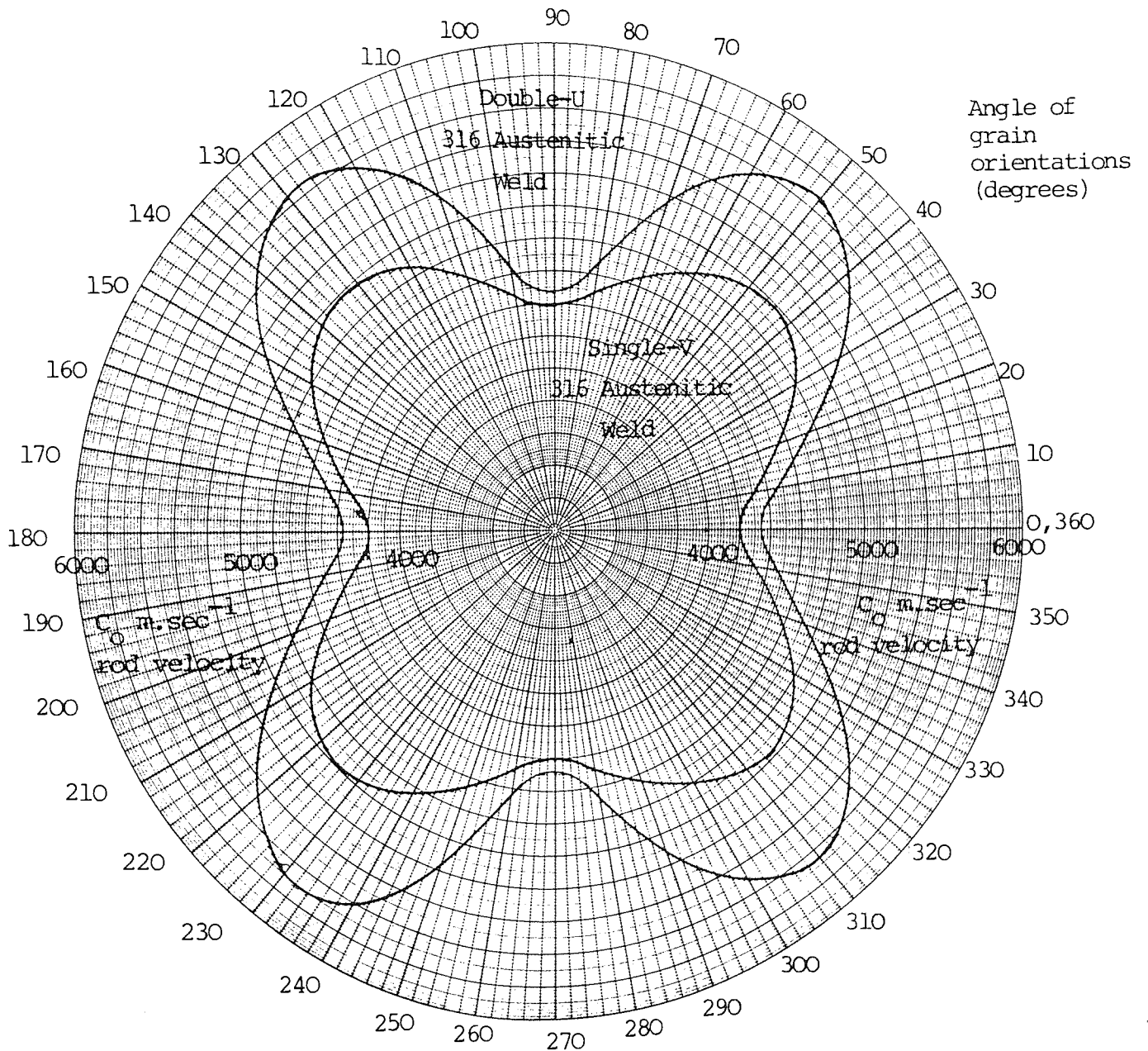
Fig. 6.8   The variations of the rod wave velocity (C_o) with respect to the grain direction for the two types of welds.

TABLE 6.1

SHIM STEEL

(Density $\rho = 7860$ Kgm.m^{-2})

Grain Direction	Direction	Angle with Length in Degrees	Length mm	Frequency KHz	$C_o = 2\ell f$ msec^{-1}	Elasticity $E \times 10^{10}$ N m^{-2}
//	N	0	75.16	34.779	5228	21.483
	NNE	22.5	75.30	33.865	5100	20.444
	NE	45	75.15	33.466	5030	19.886
	ENE	67.5	75.0	34.733	5210	21.335
⊥	E	90	75.25	35.880	5400	22.920

The experimental measurement results of shim steel. The rod velocity is shown for each sample and the Young's modulus have been determined using formula (6.1).

TABLE 6.2

STEEL TYPE (B)

(Density ρ = 7860 Kgm.m^{-3})

Grain Direction		Strip Length mm	Frequency in KHz	Rod Velocity C_o in m.msec^{-1}	Elasticity $E_\theta \times 10^{10}$ N.m^{-2}
Direction	Angle with Length in Degrees				
// N	0	75.20	34.62	5183	21.115
NNE	22.5	75.25	34.10	5283	21.934
NE	45	75.10	35.75	5370	22.666
ENE	67.5	75.20	35.17	5294	22.029
$\perp$ E	90	75.10	34.90	5242	21.598

The experimental measurement results for steel type (B). The rod velocity and elasticity for each strip having specific grain direction has been determined.

TABLE 6.3

Aluminium

(Density $\rho = 2700$ Kgm.m^{-3})

Grain Direction		Length mm	Frequency KHz	C_o m.sec^{-1}	$E \times 10^{10}$ N.m^{-2}
Direction	Angle with Length in Degrees				
// N	0	75.28	34.378	5176	7.234
NNE	22½	75.13	33.868	5089	6.992
NE	45	75.37	33.455	5043	6.867
ENE	67½	75.10	34.028	5111	7.053
⊥ E	90	75.38	34.359	5180	7.245

The experimental measurement results of Aluminium shows the rod velocity and the elasticity for different grains angle with the length of the plate. The elasticity at zero degrees and 90 degrees are very close.

TABLE 6.4

$$E_\theta = E_o + E_1\cos2\theta + E_2\cos4\theta$$

Sample	$E_o \times 10^{10}$ $N.m^{-2}$	$E_1 \times 10^{10}$ $N.m^{-2}$	$E_2 \times 10^{10}$ $N.m^{-2}$
SHIM STEEL	21.0435	-0.7185	1.1575
STEEL - A	21.4000	-0.3900	0.6700
STEEL - B	22.0113	-0.2415	-0.6547
ALUMINIUM	7.0533	-0.0055	0.1863

The values of the constants of equation (6.2) for four different samples. These constants have been obtained from the experimental results, shown earlier, of each sample. The elasticity at any angle can be obtained theoretically by introducing these constants in the equation above.

TABLE 6.5

Grains Direction	DOUBLE U TYPE				SINGLE V TYPE			
	Length mm	Width mm	f kHz	C_0 msec^{-1}	Length mm	Width mm	f kHz	C_0 msec^{-1}
0	21.43	4.68	98.161	4207	66.62	5.78	32.68	4354
22½	21.20	4.05	112.222	4758	53.60	5.95	45.10	4835
45	19.30	4.27	128.545	4962	58.08	6.30	48.21	5600
67½	9.30	3.23	253.799	4721	49.74	5.95	53.44	5316
90	17.20	3.29	128.896	4403	60.64	5.75	36.63	4443

The experimental measurements of the longitudinal rod velocity for the strips machined from the two austenitic weldments at various grains structures orientation.

APPENDIX A

RAYLEIGH-LAMB PHASE VELOCITY CORRECTION

TO THE ROD VELOCITY

$$R = \frac{C_\phi}{C_o} = \phi\{2(1+\sigma)\}^{-\frac{1}{2}}$$

σ \\ w/λ	0.025	0.05	0.075
-0.50	0.9997425	0.9989642	0.9976472
0.49	0.9997527	0.9990050	0.9977397
0.48	0.9997627	0.9990451	0.9978305
0.47	0.9997725	0.9990844	0.9979193
0.46	0.9997820	0.9991228	0.9980064
0.45	0.9997914	0.9991605	0.9980916
0.44	0.9998005	0.9991973	0.9981750
0.43	0.9998095	0.9992333	0.9982566
0.42	0.9998183	0.9992684	0.9983364
0.41	0.9998268	0.9993028	0.9984143
0.40	0.9998351	0.9993363	0.9984903
0.39	0.9998433	0.9993690	0.9985646
0.38	0.9998512	0.9994009	0.9986370
0.37	0.9998589	0.9994320	0.9987075
0.36	0.9998665	0.9994622	0.9987762
0.35	0.9998738	0.9994916	0.9988430
0.34	0.9998809	0.9995202	0.9989080
0.33	0.9998878	0.9995480	0.9989711
0.32	0.9998945	0.9995749	0.9990323
0.31	0.9999010	0.9996011	0.9990917
0.30	0.9999072	0.9996264	0.9991493
0.29	0.9999133	0.9996508	0.9992050
0.28	0.9999192	0.9996745	0.9992587
0.27	0.9999249	0.9996973	0.9993106
0.26	0.9999303	0.9997193	0.9993607
0.25	0.9999356	0.9997405	0.9994088
0.24	0.9999406	0.9997608	0.9994551
0.23	0.9999455	0.9997803	0.9994995
0.22	0.9999501	0.9997990	0.9995421
0.21	0.9999545	0.9998168	0.9995827
0.20	0.9999588	0.9998339	0.9996215
0.19	0.9999628	0.9998500	0.9996583
0.18	0.9999666	0.9998654	0.9996933
0.17	0.9999702	0.9998800	0.9997265
0.16	0.9999736	0.9998937	0.9997577
0.15	0.9999768	0.9990654	0.9997870
0.14	0.9999798	0.9999186	0.9998145
0.13	0.9999826	0.9999298	0.9998400
0.12	0.9999852	0.9999402	0.9998637
0.11	0.9999897	0.9999585	0.9999053

σ \ w/λ	0.025	0.05	0.075
0.10	0.9999897	0.9999585	0.9999053
0.09	0.9999934	0.9999663	0.9999233
0.08	0.9999934	0.9999734	0.9999394
0.07	0.9999959	0.9999796	0.9999576
0.06	0.9999963	0.9999850	0.9999659
0.05	0.9999974	0.9999896	0.9999763
0.04	0.9999983	0.9999933	0.9999849
0.03	0.9999991	0.9999963	0.9999915
0.02	0.9999996	0.9999983	0.9999962
0.01	0.9999999	0.9999996	0.9999990
0.0	1.0000000	1.0000000	1.0000000
-0.01	0.9999999	0.9999996	0.9999990
-0.02	0.9999996	0.9999983	0.9999962
-0.03	0.9999991	0.9999963	0.9999915
-0.04	0.9999984	0.9999934	0.9999849
-0.05	0.9999974	0.9999896	0.9999763
-0.06	0.9999964	0.9999850	0.9999659
-0.07	0.9999959	0.9999796	0.9999537
-0.08	0.9999934	0.9999734	0.9999395
-0.09	0.9999917	0.9999664	0.9999234
-0.10	0.9999907	0.9999585	0.9999055

σ \ w/λ	0.10	0.125	0.15
0.50	0.9957613	0.9932621	0.9900894
0.49	0.9959270	0.9935235	0.9904699
0.48	0.9960896	0.9937800	0.9908438
0.47	0.9962490	0.9940317	0.9912108
0.46	0.9964051	0.9942785	0.9915710
0.45	0.9965581	0.9945204	0.9919244
0.44	0.9967078	0.9947573	0.9922708
0.43	0.9968544	0.9949893	0.9926102
0.42	0.9969977	0.9952163	0.9929425
0.41	0.9971377	0.9954383	0.9932677
0.40	0.9972745	0.9956552	0.9935858
0.39	0.9974081	0.9958671	0.9938967
0.38	0.9975384	0.9960739	0.9942003
0.37	0.9976653	0.9962756	0.9944966
0.36	0.9977890	0.9964722	0.9947856
0.35	0.9979095	0.9966636	0.9950671
0.34	0.9980266	0.9968498	0.9953412
0.33	0.9981403	0.9970309	0.9956079
0.32	0.9982508	0.9972067	0.9958670
0.31	0.9983580	0.9973774	0.9961185
0.30	0.9984618	0.9975425	0.9963624
0.29	0.9985622	0.9977028	0.9965987
0.28	0.9986593	0.9978577	0.9968273
0.27	0.9987531	0.9980072	0.9970481
0.26	0.9988435	0.9981514	0.9972613
0.25	0.9989305	0.9982903	0.9974666
0.24	0.9990142	0.9984238	0.9976640
0.23	0.9990944	0.9985520	0.9978537
0.22	0.9991713	0.9986748	0.9980355
0.21	0.9992448	0.9987922	0.9982093
0.20	0.9993150	0.9989043	0.9983752
0.19	0.9993817	0.9990109	0.9985332
0.18	0.9994450	0.9991121	0.9986831
0.17	0.9995049	0.9992079	0.9988251
0.16	0.9995613	0.9992982	0.9989590
0.15	0.9996145	0.9993831	0.9990849
0.14	0.9996641	0.9994626	0.9992027
0.13	0.9997104	0.9995366	0.9993125
0.12	0.9997532	0.9996051	0.9994141
0.11	0.9997926	0.9996682	0.9995077
0.10	0.9998286	0.9997258	0.9995931
0.09	0.9998612	0.9997779	0.9996704
0.08	0.9998903	0.9998245	0.9997396
0.07	0.9999160	0.9998656	0.9998006
0.06	0.9999383	0.9999014	0.9998536
0.05	0.9999572	0.9999315	0.9998983
0.04	0.9999726	0.9999561	0.9999349
0.03	0.9999846	0.9999753	0.9999634
0.02	0.9999931	0.9999890	0.9999837
0.01	0.9999983	0.9999973	0.9999959
0.0	1.0000000	1.0000000	1.0000000
-0.01	0.9999983	0.9999973	0.9999959
-0.02	0.9999932	0.9999890	0.9999838
-0.03	0.9999846	0.9999754	0.9999635
-0.04	0.9999726	0.9999562	0.9999351
-0.05	0.9999572	0.9999316	0.9998987
-0.06	0.9999384	0.9999016	0.9998541
-0.07	0.9999162	0.9998661	0.9998016
-0.08	0.9998906	0.9998251	0.9997410
-0.09	0.9998615	0.9997788	0.9996724
-0.10	0.9998291	0.9997270	0.9995958

σ \ w/λ	0.175	0.20	0.225
0.50	0.9861651	0.9813908	0.9756449
0.49	0.9866895	0.9820846	0.9765344
0.48	0.9872052	0.9827678	0.9774115
0.47	0.9877120	0.9834401	0.9782761
0.46	0.9882099	0.9841014	0.9791278
0.45	0.9886988	0.9847516	0.9799663
0.44	0.9891785	0.9853903	0.9807914
0.43	0.9896490	0.9860175	0.9816028
0.42	0.9901101	0.9866329	0.9824001
0.41	0.9905618	0.9872364	0.9831830
0.40	0.9910040	0.9878279	0.9839514
0.39	0.9914364	0.9884070	0.9847049
0.38	0.9918592	0.9889738	0.9854432
0.37	0.9922722	0.9895279	0.9861661
0.36	0.9926751	0.9900693	0.9868732
0.35	0.9930682	0.9905978	0.9875643
0.34	0.9934511	0.9911132	0.9882392
0.33	0.9938239	0.9916153	0.9888975
0.32	0.9941863	0.9921041	0.9895390
0.31	0.9945384	0.9925793	0.9901635
0.30	0.9948801	0.9930410	0.9907707
0.29	0.9952113	0.9934887	0.9913603
0.28	0.9955319	0.9939225	0.9919322
0.27	0.9958419	0.9943422	0.9924860
0.26	0.9961412	0.9947477	0.9930215
0.25	0.9964296	0.9951388	0.9935386
0.24	0.9967072	0.9955155	0.9940371
0.23	0.9969739	0.9958776	0.9945166
0.22	0.9972297	0.9962251	0.9949770
0.21	0.9974744	0.9965577	0.9954182
0.20	0.9977080	0.9968754	0.9958399
0.19	0.9979305	0.9971782	0.9962420
0.18	0.9981418	0.9974659	0.9966244
0.17	0.9983419	0.9977384	0.9969867
0.16	0.9985308	0.9979957	0.9973290
0.15	0.9987083	0.9982377	0.9976511
0.14	0.9988746	0.9984644	0.9979529
0.13	0.9990294	0.9986755	0.9982342
0.12	0.9991729	0.9988712	0.9984950
0.11	0.9993049	0.9990514	0.9987351
0.10	0.9994256	0.9992160	0.9989545
0.09	0.9995347	0.9993650	0.9915312
0.08	0.9996324	0.9994983	0.9993309
0.07	0.9997186	0.9996159	0.9994878
0.06	0.9997933	0.9997179	0.9996238
0.05	0.9998565	0.9998041	0.9997388
0.04	0.9999082	0.9998747	0.9998329
0.03	0.9999484	0.9999295	0.9999061
0.02	0.9999771	0.9999687	0.9999583
0.01	0.9999943	0.9999922	0.9999896
0.0	1.0000000	1.0000000	1.0000000
-0.01	0.9999943	0.9999922	0.9999896
-0.02	0.9999771	0.9999688	0.9999584
-0.03	0.9999485	0.9999298	0.9999066
-0.04	0.9999085	0.9998753	0.9998341
-0.05	0.9998571	0.9998054	0.9997411
-0.06	0.9997944	0.9997200	0.9996276
-0.07	0.9997204	0.9996193	0.9994939
-0.08	0.9996351	0.9995034	0.9993400
-0.09	0.9995386	0.9993722	0.9991660
-0.10	0.9994309	0.9992259	0.9989722

σ \ w/λ	0.25	0.275	0.30
0.50	0.9687823	0.9606354	0.9510217
0.49	0.9698930	0.9619906	0.9526392
0.48	0.9709904	0.9633325	0.9542452
0.47	0.9720741	0.9646606	0.9558386
0.46	0.9731436	0.9659742	0.9574187
0.45	0.9741985	0.9672728	0.9589848
0.44	0.9752384	0.9685556	0.9605360
0.43	0.9762628	0.9693222	0.9620715
0.42	0.9772712	0.9710717	0.9635904
0.41	0.9782633	0.9723037	0.9650918
0.40	0.9792386	0.9735173	0.9665748
0.39	0.9801966	0.9747121	0.9680385
0.38	0.9811370	0.9758872	0.9694820
0.37	0.9820591	0.9770420	0.9709042
0.36	0.9829627	0.9781759	0.9723043
0.35	0.9838473	0.9792882	0.9736812
0.34	0.9847123	0.9803781	0.9750339
0.33	0.9855575	0.9814451	0.9763614
0.32	0.9863824	0.9824885	0.9776628
0.31	0.9871865	0.9835075	0.9789369
0.30	0.9879694	0.9845015	0.9801828
0.29	0.9887308	0.9854699	0.9813995
0.28	0.9894702	0.9864120	0.9825859
0.27	0.9901872	0.9873279	0.9837410
0.26	0.9908815	0.9882148	0.9848638
0.25	0.9915526	0.9890741	0.9859532
0.24	0.9922002	0.9899047	0.9870084
0.23	0.9928240	0.9907059	0.9880282
0.22	0.9934236	0.9914771	0.9890118
0.21	0.9939986	0.9922177	0.9899583
0.20	0.9945488	0.9929273	0.9908666
0.19	0.9950739	0.9936053	0.9917360
0.18	0.9955736	0.9942512	0.9925656
0.17	0.9960476	0.9948645	0.9933545
0.16	0.9964956	0.9954449	0.9941021
0.15	0.9969174	0.9959918	0.9948075
0.14	0.9973129	0.9965049	0.9954701
0.13	0.9976817	0.9969839	0.9960893
0.12	0.9980238	0.9974283	0.9966644
0.11	0.9983389	0.9978380	0.9971950
0.10	0.9986270	0.9982126	0.9976806
0.09	0.9988877	0.9985520	0.9981207
0.08	0.9991212	0.9988559	0.9985150
0.07	0.9993273	0.9991242	0.9988632
0.06	0.9995059	0.9993568	0.9991651
0.05	0.9996571	0.9995536	0.9994206
0.04	0.9997806	0.9997145	0.9996295
0.03	0.9998767	0.9998395	0.9997918
0.02	0.9999452	0.9999288	0.9999076
0.01	0.9999863	0.9999822	0.9999769
0.0	1.0000000	1.0000000	1.0000000
-0.01	0.9999864	0.9999823	0.9999770
-0.02	0.9999455	0.9999292	0.9999083
-0.03	0.9998775	0.9998410	0.9997942
-0.04	0.9997826	0.9997179	0.9996352
-0.05	0.9996609	0.9995602	0.9994317
-0.06	0.9995126	0.9993681	0.9991843
-0.07	0.9993379	0.9991422	0.9988935
-0.08	0.9991369	0.9988826	0.9985600
-0.09	0.9989101	0.9985899	0.9981844
-0.10	0.9986575	0.9982644	0.9977676

σ \ w/λ	0.325	0.350	0.375
0.50	0.9397614	0.9267074	0.9917898
0.49	0.5416496	0.9288599	0.9141812
0.48	0.9435296	0.9310096	0.9165772
0.47	0.9454004	0.9331558	0.9189770
0.46	0.9472612	0.9352974	0.9213797
0.45	0.9491110	0.9374334	0.9237844
0.44	0.9509488	0.9395628	0.9261901
0.43	0.9527736	0.9416843	0.9285958
0.42	0.9545842	0.9437689	0.9310004
0.41	0.9563796	0.9458992	0.9334026
0.40	0.9581586	0.9479899	0.9358011
0.39	0.9599200	0.9500676	0.9381945
0.38	0.9616625	0.9521308	0.9405813
0.37	0.9633849	0.9541780	0.9429600
0.36	0.9650860	0.9562077	0.9453287
0.35	0.9667642	0.9582180	0.9476866
0.34	0.9684183	0.9602073	0.9500288
0.33	0.9700468	0.9621737	0.9523562
0.32	0.9716483	0.9641153	0.9546656
0.31	0.9732214	0.9660301	0.9569545
0.30	0.9747644	0.9679162	0.9592205
0.29	0.9762760	0.9697712	0.9614609
0.28	0.9777545	0.9715932	0.9636730
0.27	0.9791984	0.9733798	0.9658638
0.26	0.9806061	0.9751288	0.9680002
0.25	0.9819761	0.9768377	0.9701089
0.24	0.9833678	0.9785043	0.9721766
0.23	0.9845966	0.9801260	0.9741997
0.22	0.9858439	0.9817005	0.9761748
0.21	0.9870473	0.9832252	0.9780979
0.20	0.9882052	0.9846977	0.9799653
0.19	0.9893162	0.9861156	0.9817730
0.18	0.9903788	0.9874764	0.9835170
0.17	0.9913915	0.9887777	0.9851933
0.16	0.9923530	0.9900172	0.9867978
0.15	0.9932622	0.9911926	0.9883267
0.14	0.9941178	0.9923017	0.9897759
0.13	0.9949185	0.9933425	0.9911416
0.12	0.9956634	0.9943131	0.9924201
0.11	0.9963515	0.9952115	0.9936080
0.10	0.9969819	0.9960361	0.9947019
0.09	0.9975539	0.9967856	0.9956990
0.08	0.9980667	0.9974585	0.9965964
0.07	0.9985200	0.9980538	0.9973920
0.06	0.9989130	0.9985705	0.9980837
0.05	0.9992457	0.9990080	0.9986701
0.04	0.9995178	0.9993659	0.9991500
0.03	0.9997291	0.9996440	0.9995228
0.02	0.9998797	0.9998421	0.9997885
0.01	0.9999700	0.9999606	0.9999473
0.0	1.0000000	1.0000000	1.0000000
-0.01	0.9999702	0.9999609	0.9999478
-0.02	0.9998810	0.9998442	0.9997923
-0.03	0.9997332	0.9996511	0.9995357
-0.04	0.9995275	0.9993827	0.9991802
-0.05	0.9992646	0.9990407	0.9987286
-0.06	0.9989455	0.9986266	0.9981840
-0.07	0.9985712	0.9981422	0.9975495
-0.08	0.9981428	0.9975894	0.9968286
-0.09	0.9976615	0.9969702	0.9960249
-0.10	0.9971286	0.9962869	0.9951422

w/λ σ	0.400	0.425	0.450
0.50	0.8950651	0.8767509	0.8572230
0.49	0.8976502	0.8794685	0.8600054
0.48	0.9002479	0.8822058	0.8628127
0.47	0.9028574	0.8849626	0.8656449
0.46	0.9054784	0.8877387	0.8685024
0.45	0.9081102	0.8905341	0.8713852
0.44	0.9107521	0.8933483	0.8742937
0.43	0.9134034	0.8961812	0.8772280
0.42	0.9160633	0.8990323	0.8801881
0.41	0.9187309	0.9019014	0.8831742
0.40	0.9214050	0.9047879	0.8861864
0.39	0.9240847	0.9076911	0.8892247
0.38	0.9267687	0.9106106	0.8922891
0.37	0.9294556	0.9135455	0.8953796
0.36	0.9321440	0.9164950	0.8984961
0.35	0.9348322	0.9194580	0.9016383
0.34	0.9375184	0.9224335	0.9048062
0.33	0.9402008	0.9254202	0.9079993
0.32	0.9428771	0.9284165	0.9112172
0.31	0.9455450	0.9314209	0.9144594
0.30	0.9482019	0.9344314	0.9177253
0.29	0.9508452	0.9374460	0.9210139
0.28	0.9534717	0.9404621	0.9243243
0.27	0.9560782	0.9434771	0.9276552
0.26	0.9586611	0.9464879	0.9310052
0.25	0.9612166	0.9494910	0.9343724
0.24	0.9637405	0.9524826	0.9377548
0.23	0.9662284	0.9554582	0.9411499
0.22	0.9686754	0.9584129	0.9445544
0.21	0.9710766	0.9613413	0.9479650
0.20	0.9734264	0.9642372	0.9513772
0.19	0.9757191	0.9670937	0.9547860
0.18	0.9779486	0.9699032	0.9581853
0.17	0.9801086	0.9726573	0.9615678
0.16	0.9821924	0.9753468	0.9649251
0.15	0.9841934	0.9779615	0.9682469
0.14	0.9861045	0.9804906	0.9715212
0.13	0.9879187	0.9829221	0.9747337
0.12	0.9896290	0.9852436	0.9778677
0.11	0.9912285	0.9874419	0.9809036
0.10	0.9927106	0.9895034	0.9838190
0.09	0.9940689	0.9914145	0.9865878
0.08	0.9952976	0.9931615	0.9891814
0.07	0.9963913	0.9947316	0.9915682
0.06	0.9973456	0.9961127	0.9937153
0.05	0.9981566	0.9972945	0.9955895
0.04	0.9988216	0.9982682	0.9971599
0.03	0.9993387	0.9990279	0.9984006
0.02	0.9997071	0.9995698	0.9992915
0.01	0.9999271	0.9998931	0.9998244
0.0	1.0000000	1.0000000	1.0000000
-0.01	0.9999280	0.9998951	0.9998298
-0.02	0.9997145	0.9995856	0.9993339
-0.03	0.9993633	0.9990807	0.9985390
-0.04	0.9988794	0.9983912	0.9974755
-0.05	0.9982681	0.9975291	0.9961754
-0.06	0.9975354	0.9965070	0.9946700
-0.07	0.9966874	0.9953382	0.9929888
-0.08	0.9957307	0.9940355	0.9911587
-0.09	0.9946719	0.9926117	0.9892038
-0.10	0.9935178	0.9910792	0.9871450

w/λ σ	0.475	0.500	0.525
0.50	0.8369663	0.8164966	0.7962854
0.49	0.8397503	0.8192319	0.7989381
0.48	0.8425617	0.8219949	0.8016171
0.47	0.8454010	0.8247861	0.8043228
0.46	0.8482685	0.8276059	0.8070556
0.45	0.8511646	0.8304548	0.8098160
0.46	0.8482685	0.8276059	0.8070556
0.45	0.8511646	0.8304548	0.8098160
0.44	0.8540899	0.8333333	0.8126043
0.43	0.8570448	0.8362420	0.8154211
0.42	0.8600297	0.8391813	0.8182668
0.41	0.8630450	0.8421519	0.8211419
0.40	0.8660912	0.8451543	0.8240467
0.39	0.8691688	0.8481889	0.8269819
0.38	0.8722782	0.8512565	0.8299477
0.37	0.8754198	0.8543577	0.8329448
0.36	0.8785942	0.8574929	0.8359736
0.35	0.8818017	0.8606630	0.8390345
0.34	0.8850429	0.8638684	0.8421281
0.33	0.8883180	0.8671100	0.8452549
0.32	0.8916277	0.8703883	0.8484153
0.31	0.8949722	0.8737041	0.8516098
0.30	0.8983519	0.8770580	0.8548389
0.29	0.9017672	0.8804509	0.8581029
0.28	0.9052183	0.8838835	0.8614025
0.27	0.9087056	0.8873565	0.8647379
0.26	0.9122293	0.8908708	0.8681096
0.25	0.9157895	0.8944272	0.8715180
0.24	0.9193861	0.8980265	0.8749632
0.23	0.9230192	0.9016696	0.8784457
0.22	0.9266885	0.9053575	0.8819655
0.21	0.9303936	0.9090909	0.8855228
0.20	0.9341337	0.9128709	0.8891174
0.19	0.9379081	0.9166985	0.8927492
0.18	0.9417152	0.9205746	0.8964178
0.17	0.9455533	0.9245003	0.9001226
0.16	0.9494199	0.9284767	0.9038625
0.15	0.9533116	0.9325048	0.9076361
0.14	0.9572240	0.9365858	0.9114415
0.13	0.9611509	0.9407209	0.9152758
0.12	0.9650844	0.9449112	0.9191355
0.11	0.9690136	0.9491580	0.9230154
0.10	0.9729234	0.9534626	0.9269084
0.09	0.9767936	0.9578263	0.9308051
0.08	0.9805959	0.9622504	0.9346922
0.07	0.9842908	0.9667365	0.9385510
0.06	0.9878236	0.9712859	0.9423555
0.05	0.9911186	0.9759001	0.9460683
0.04	0.9940746	0.9805807	0.9496359
0.03	0.9965652	0.9853293	0.9529823
0.02	0.9984514	0.9901475	0.9560023
0.01	0.9996148	0.9950372	0.9585593
0.0	1.0000000	1.0000000	0.9604990
-0.01	0.9996400	0.9966137	0.9616896
-0.02	0.9986391	0.9932694	0.9620765
-0.03	0.9971312	0.9899664	0.9617096
-0.04	0.9952437	0.9867042	0.9607159
-0.05	0.9930813	0.9834824	0.9592450
-0.06	0.9907233	0.9803004	0.9574294
-0.07	0.9882279	0.9771576	0.9553721
-0.08	0.9856373	0.9740535	0.9531476
-0.09	0.9829818	0.9709875	0.9508087
-0.10	0.9802836	0.9679592	0.9483927

w/λ a	0.55	0.75	1.00
0.50	0.7767124	0.6592038	0.5911544
0.49	0.7792635	0.6610465	0.5926686
0.48	0.7818386	0.6628997	0.5941902
0.47	0.7844381	0.6647630	0.5957194
0.46	0.7870622	0.6666365	0.5972559
0.45	0.7897113	0.6685200	0.5987966
0.44	0.7923857	0.6704133	0.6003506
0.43	0.7950857	0.6723162	0.6019087
0.42	0.7978115	0.6742285	0.6034737
0.41	0.8005634	0.6761500	0.6050456
0.40	0.8033418	0.6780804	0.6066243
0.39	0.8061469	0.6800194	0.6082095
0.38	0.8089789	0.6819668	0.6098010
0.37	0.8118382	0.6839222	0.6113989
0.36	0.8147249	0.6858852	0.6130028
0.35	0.8176392	0.6878555	0.6146126
0.34	0.8205813	0.6898326	0.6162281
0.33	0.8235515	0.6918160	0.6178490
0.32	0.8265496	0.6938052	0.6194751
0.31	0.8295760	0.6957998	0.6211062
0.30	0.8326306	0.6977989	0.6227419
0.29	0.8357132	0.6998022	0.6243821
0.28	0.8388239	0.7018087	0.6260263
0.27	0.8419624	0.7038179	0.6276743
0.26	0.8451285	0.7058289	0.6293258
0.25	0.8483216	0.7078409	0.6309804
0.24	0.8515416	0.7098528	0.6326376
0.23	0.8547874	0.7118639	0.6342972
0.22	0.8580581	0.7138729	0.6359586
0.21	0.8613527	0.7158788	0.6376215
0.20	0.8646698	0.7178805	0.6392854
0.19	0.8680075	0.7198766	0.6409497
0.18	0.8713638	0.7218658	0.6426140
0.17	0.8747359	0.7238467	0.6442778
0.16	0.8781207	0.7258179	0.6459405
0.15	0.8315143	0.7277777	0.6476015
0.14	0.8849116	0.7297244	0.6492601
0.13	0.8883070	0.7316565	0.6509159
0.12	0.8916931	0.7335720	0.6525680
0.11	0.8950612	0.7354690	0.6542159
0.10	0.8984005	0.7373457	0.6558589
0.09	0.9016979	0.7391999	0.6574961
0.08	0.9049376	0.7410296	0.6591269
0.07	0.9081003	0.7428326	0.6607504
0.06	0.9111627	0.7446066	0.6623660
0.05	0.9140973	0.7463495	0.6639727
0.04	0.9168720	0.7480590	0.6655697
0.03	0.9194500	0.7497327	0.6671563
0.02	0.9217913	0.7513684	0.6687314
0.01	0.9238542	0.7529636	0.6702943
0.0	0.9255986	0.7545162	0.6718440
-0.01	0.9269903	0.7560240	0.6733797
-0.02	0.9280054	0.7574846	0.6749003
-0.03	0.9286338	0.7588962	0.6764051
-0.04	0.9288808	0.7602566	0.6778930
-0.05	0.9287657	0.7615640	0.6793632
-0.06	0.9283192	0.7628165	0.6808147
-0.07	0.9275781	0.7640128	0.6822467
-0.08	0.9265819	0.7651514	0.6836582
-0.09	0.9253690	0.7662310	0.6850483
-0.10	0.9239751	0.7672506	0.6864163

σ \ w/λ	1.25	1.50	1.75
0.50	0.563034	0.550587	0.544692
0.45	0.570202	0.557630	0.551721
0.40	0.577552	0.564862	0.558946
0.35	0.585074	0.572279	0.566364
0.30	0.592757	0.579872	0.573970
0.25	0.600581	0.587628	0.581751
0.20	0.608522	0.595529	0.589692
0.15	0.616547	0.603548	0.597771
0.10	0.624612	0.611652	0.605958
0.05	0.632663	0.619798	0.614212
0.0	0.640637	0.627932	0.622485
-0.05	0.648458	0.635991	0.630716
-0.1	0.656044	0.643902	0.638835

σ \ w/λ	2.0	2.25	2.50
0.50	0.541747	0.540218	0.539400
0.45	0.548795	0.547289	0.546492
0.40	0.556043	0.554565	0.553796
0.35	0.563491	0.562043	0.561296
0.30	0.571132	0.569719	0.568999
0.25	0.578957	0.577584	0.576894
0.20	0.586951	0.585622	0.584965
0.15	0.595092	0.593813	0.593191
0.10	0.603353	0.602129	0.601544
0.05	0.611694	0.610531	0.609986
0.0	0.620068	0.618972	0.618469
-0.05	0.628414	0.62739	0.626932
-0.01	0.636663	0.635719	0.635305

PUBLICATION

This paper has been published in the British Journal of
Non-Destructive Testing; Volume 23, No. 6, November, 1981.

BIBLIOGRAPHY

1. Ambati, G.
    "An experimental and theoretical investigation into
    the acoustic spectra of solids having cylindrical
    symmetry",
    Ph.D. thesis, Dept. of Elect. and Electro. Eng.,
    The University of Aston in Birmingham, 1976.

2. Auld, B. and Tsao, E. M.
    "A variational analysis of edge resonance in a semi-
    infinite plate",
    IEEE Trans. on Sonics and Ultrasonics, Vol. SU-24(5),
    pp. (317-326), Sept. 1977.

3. Baerwald, H. A. and Libove, C.
    "Breathing vibrations of planary isotropic square plates"
    Clevite Research Centre, Cleveland, Ohio, Contract
    Nonr-1055(OO), Tech. report 8, 12th Dec. 1955.
    (This report is generally not available, but it is
    reproduced in reference (31)).

4. Bancroft, D.
    "The velocity of longitudinal waves in cylindrical bars",
    J. Physics Review, Vol. 59, pp.(588-593), April 1941.

5. Bell, J. F. W.
    "Ultrasonic thermometry using resonance techniques",
    Fifth symposium on temperature, Washington D.C. 1971.

6. Bell, J. F. W.
    "A solid acoustic thermometer",
    Ultrasonic, Vol. 6, pp(11-14), 1968.

7. Bell, J. F. W.
    "The velocity of sound in metals at high temperatures",
    Phil. Mag.,Vol. 2, pp.(1113-1120), 1957.

8. Bell, J. F. W., Chen, J. Y. F. and Chaplain, K. R.
    "The elastic constants of refractory metals at high
    temperatures",
    Proceedings of the first international symposium on
    Ultrasonic Materials Characterisation held at NBS,
    Gaithersurg, Mid-June, 1978, Issued Nov. 1980.

9. Bell, J. F. W., Chen, J. Y. F. and Chaplain, K. R.
    "Ultrasonic characterisation of refractories at high
    temperature",
    Journal of NDT International, Vol. 13(6), pp. (301-304),
    Dec. 1980.

10. Bell, J. F. W., Chen, J. Y. F., Steel, G. K. and Sanders,
    S. A. C.
    "A model for a two dimensional distributed resonator",
    J. Sound and Vibration, Vol. 68(1), pp. (45-58), 1980.

11. Bell, J. F. W. and Kalmarczie, P. J.
    "The end resonance of strips and plates",
    J. Physics Letters, Vol. 61A(2), pp. (91-93), April, 1977

12. Bell, J. F. W. and Pelmore, J. M.
    "An instrument for internal friction measurement at
    high temperatures",
    J. Physics E: Scientific Instruments,Vol. 10, pp(1145-
    1149), 1977.

13. Bell, J. F. W. and Sharp, J. C. K.
    "The precision measurement of the elastic constants
    of isotropic solids over wide temperature ranges",
    Rev. Int. Htes. Temp. et Réfract. t. 12, pp.(40-43),
    1975.

14. Bell, J. F. W., Johnson, A. C. and Sharp, J. C. K.
    "Pulse-echo method of investigating the properties
    of mechanical resonators",
    J. of the Acoustical Soc. of America, Vol.57(5),
    pp. (1085-1093), 1975.

15. Bell, J. F. W., Noble, A. E. and Seth, T. N.
    "Graphical displays of acoustic properties of solids",
    J. Ultrasonics, pp.(178-181), July 1973.

16. Booker, R. E. and Sagar, F. H.
    "Velocity dispersion of the lowest-order longitudinal
    mode in infinite rods of circular cross-section",
    J. of the Acoustical Soc. of America, Vol. 49(5),
    pp.(1491-1498), 1971.

17. Cady, W. G.
    "Piezoelectricity"
    McGraw-Hill Book Co., London, 1946.

18. Chaplain, K. R.
    "Elastic constant measurements at high temperatures",
    Ph.D. thesis, Dept. of Elect. and Electro. Eng.,
    University of Aston in Birmingham, 1980.

19. Chen, J. Y. F.
    "Surface wave technique for the study of engineering
    structures and materials",
    Ph.D. thesis, Dept. of Elect. and Electro. Eng.,
    University of Aston in Birmingham, 1979.

20. Cohen, H.
    "Wave propagation in elastic plates",
    J. Elasticity, Vol. 6(3), pp.(245-259), 1976.

21. EerNisse, E. P.
    "Coupled -mode approach to elastic-vibration analysis",
    J.. of the Acoustical Soc. of America, Vol. 40(5),
    pp.. (1045-1050), 1966.

22. Ekstein, H..
    "Free vibrations of anisotropic bodies",
    J. of Physics Review, Vol. 66(55 and 6), pp.(108-118),
    1944.

23. Fleury, W. H., Rosinger, H. E. and Ritchie, I. G.
    "A finite element computer program for the calculation
    of the resonant frequencies of anisotropic materials",
    Whitehall Nuclear Research Establishment, Pinawa,
    Manitoba, Sept. 1975.

24. Gazis, D. C. and Mindlin, R. D.
    "Extensional vibrations and waves in a circular disk
    and a semi-infinite plate",
    Trans. of the ASME, pp.(541-547), 1960.

25. Glandus, J. C., Platon, F. and Boch, P.
    "Measurements of the elastic moduli of ceramics",
    J. Materials in Engineering Applications, Vol. 1,
    June, 1979.

26. Graff, K. F.
"Waves motion in elastic solids",
Clarendon Press - Oxford, (Chapter Eight), 1975.

27. Grinchenko, V. T. and Meleshko, V. V.
"Peculiarities of energy distribution in a thin
rectangular plate with end resonance",
Dopovidi-An Ukrainskoi RSR SERIYA A, Vol. 1976,
pp. (612-616), 1976.

28. Hafner, E.
"Crystal resonators"
IEEE Trans. on Sonics and Ultrasonics, Vol. SU-21(4),
Oct. 1974.

29. Hearmon, R.F.S.
"An introduction to applied anisotropy",
Oxford University Press, 1961.

30. Holland, R.
"Numerical studies of elastic-disk contour modes
lacking axial symmetry",
J. of the Acoustical Soc. of America, Vol. 40, pp.
(1051-1057), 1966.

31. Holland,R.
"Contour extensional resonant properties of
rectangular peizoelectric plates",
IEEE Trans. on Sonic and Ultrasonics, Vol. SU-15 (2),
pp. (97-105), April, 1968.

32. Holland, R. and Roark, A. L.
"Computer program for analysing free, rectangular
piezoelectric plates",
Sandia Corp., Albuquerque, N. Mex.,Research Report
SC-RR-67-524, August, 1967.

33. Hudgell, R. J. and Steel, H.
"Ultrasonic longitudinal waves examination of
austenitic welds",
British J. of NDT, Vol. 22(2), pp. (78-85), 1980.

34. Jones, O. E.
"Longitudinal strain pulse propagation in wide
rectangular bars", Part I and II.
Trans. of the ASME, pp. (51-69), 1963.

35. Jumonji, H.
"Analysis of characteristics of multiple-mode
resonators vibrating in longitudinal and flexural
modes",
J. Electronics and Communications in Japan, Vol. 53-A,
(4), pp. (15-23), 1970.

36. Juva, A. and Lenkkeri, J.
"The effects of anisotrophy on the propagation of
ultrasonic waves in austenitic stainless steel",
Presented at CSNI - Specialist Meeting on Reliability
of Ultrasonic Inspection of Austenitic Stainless
Steel Components, Brussels, Belgium, 29-30 June 1980.

37. Kagawa, Y., and Yamabuchi, T.
"Finite element simulation of two-dimensional
electro-mechanical resonators",
IEEE Trans. on Sonics and Ultrasonics, Vol. SU-21(4),
pp. (275- 283), 1974.

38. Kalmarczie, P. T.
"Energy trapped resonance in solid structures",
Ph.D. thesis, Dept. of Elect. and Electro. Eng.,
University of Aston in Birmingham, 1976.

39. Kapranos, P. A., Al-Helaly, M. M. H., and Whittaker, V.N
"Ultrasonic velocity measurements in 316 Austenitic
Weldments",
British Journal of NDT, Vol. 23(6), pp. (288-292),
Nov. 1981.

40. Kapur, K..K.
"Vibrations of a tomoshenko beam, using finite-element
approach",
J. Acoustical Soc. of America, Vol. 40(5), pp. (1058-
1063), 1966.

41. Knibbs, R. H. and Morris, J. B.
"The effects of fibre orientation on the physical
properties of composites",
J. of Composites, Vol. 5, pp. (209-218), Sept. 1974.

42. Kolsky, H.
"Stress waves in solids",
Dover publication, 1965.

43.   Lamb, H.
      "On the flexure of an elastic plate"
      Proc. of London Math. Soc., Vol. 21, pp.(85), 1889.

44.   Lamb, H.
      "On waves in an elastic plate",
      Proceedings of the Royal Society, London, Ser. A.,
      Vol. 93, pp.(114-128), 1917.

45.   Lamé, M. G.
      "Lecons sur la théorie mathématique de l'élasticité
      des corps solides"
      Second edition, 1866, pp. (166-172). (It has been
      quoted by some authors as 1886).

46.   Lee, P. C. Y.
      "Extensional, flexural and width vibrations of thin
      rectangular plates",
      Proc. AFCS, Vol. 25, pp. (63-69), 1971.

47.   Leissa, A. W.
      "The free vibration of rectangular plates",
      J. of Sound and Vibration, Vol. 31(3), pp. (257-293),
      1973.

48.   Lloyd, P. and Redwood, M.
      "Finite-difference method for investigations of the
      vibrations of solids and the evaluation of the
      equivalent-circuit characteristics of piezoelectric
      resonators, Parts I and II",
      J. Acoustical Soc. of America, Vol. 39(2), pp.(346-361),
      1966.

49.   Lloyd, P. and Redwood, M.
      "Finite-difference method for investigation of the
      vibrations of solids and the equivalent-circuit
      characteristics of piezoelectric resonators, Part III",

      J. Acoustical Soc. of America, Vol. 40(1), pp.(82-85),
      1966.

50.   Love, A. E.
      "A treatise on mathematical theory of elasticity",
      Cambridge University Press, 4th edition, 1927.

51. Mähly, H. and Trösch, A.
    "Shear modes of square plates",
    Helv. Phys. Acta, Vol. 20, pp.(253-255), 1947.

52. Mason, W. P.
    "Piezoelectric crystals and their application to
    ultrasonics",
    D. Van Nostrand Co., New York, 1950.

53. Mason, W. P.
    "The motion of bar velocity in flexural, including
    the effects of rotary and lateral inertia",
    J. Acoust. Soc. of America, Vol. (6), pp. (246-249),
    1935.

54. Mason, W. P.
    "A new crystal plate designated the GT",
    Proc. IRE, Vol. 28, pp. (220-223), 1940.

55. Mason, W. P. and Sykes, R. A.
    "Low frequency Quartz crystal cuts having low
    temperature coefficients",
    (Quartz crystal for electrical circuit) Edited by
    R. A. Heising, Van Nostrand, New York, pp.(537-554),
    1946.

56. McMahon, G. H.
    "Finite-difference analysis of the vibrations of solid
    cylinders",
    J. Acoust. Soc. of America, Vol. 41(1), pp.(307-312),
    1970.

57. McMahon, G. H.
    "Experimental study of the vibrations of solid,
    isotropic, elastic cylinders",
    J. Acoust. Soc. of America, Vol. 36,(1), pp. (85-92),
    1964.

58. McSkimin, H. J.
    "Notes and references for the measurement of elastic
    moduli by means of ultrasonics waves",
    J. Acoustical Soc. of America, Vol. 33 (5), pp. (606-
    615), 1961.

59. McSkimin, H. J.
"Theoretical analysis of modes of vibration for isotropic rectangular plates",
(Quartz crystals for electrical circuits), Edited by R. A. Heising, Van Nostrand, New York, 1946.

60. Medick, M. A. and Poa, Y.
"Extensional vibrations of thin rectangular plates",
J. Acoust. Soc. of America, Vol. 37 (1), pp. (59-65), 1965.

61. Meitzler, A. H.
"Backward-Wave transmission of stress wave pulses elastic cylinder and plates",
J. Acoustical Soc. of America, Vol. 37, pp. (835-842), 1966.

62. Mindlin, R. D.
"Waves and vibrations in isotropic, elastic plates",
Proc. 1st Symposium on Naval Structure Mechanics,
In Structural Mechanics (Ed: J. N. Goodier and N. Hoff), pp. (199-232), 1960.

63. Mindlin, R. D.
"Vibrations of an infinite, elastic plate at its cut-off frequencies",
Proc. of the 3rd National Congress of Applied Mechanics, pp. (225-226), 1958.

64. Mindlin, R. D.
"Simple modes of vibration of crystals",
J. Applied Physics, Vol. 27 (12), pp. (1462-1466) Dec. 19

65. Mindlin, R. D.
"Influence of rotary inertia and shear on flexural motion of isotropic elastic plates",
J. Applied Mechanics, Vol. 18 (1), pp. (31-38), 1951.

66. Mindlin, R. D. and Fox, E. A.
"Vibrations and waves in elastic bars of rectangular cross section",
J. Applied Mechanics, Trans. of the ASME, Vol. 27, pp. (152-158), 1960.

67. Mindlin, R. D. and Gazis, D. G.
    "Extensional vibrations and waves in a circular disk
    and a semi-infinite plate",
    J. Applied Mechanics, Vol. 27, pp. (542-547), 1960.

68. Mindlin, R. D. and Herrmann, G.
    "A one-dimensional theory of compressional waves in
    an elastic rod",
    Proc. 1st, U.S. National Congress of Applied Mechanics,
    pp.(187-191), 1950.

69. Mindlin, R. D. and Medick, M. A.
    "Extensional vibrations of elastic plates",
    J. Applied Mechanics, Trans. of the ASME, Vol. 26,
    pp. (562-569), 1959.

70. Mindlin, R. D. and McNiven, H. D.
    "Axially symmetric waves in elastic rod",
    J. Applied Mechanics, Trans. of the ASME, Vol. 27,
    pp. (145-151), 1960.

71. Morse, P. M.
    "Vibration and Sound".
    McGraw-Hill Book Co., pp. (162), 1948.

72. Morse, P. M. and Freshbach, H.
    "Method for theoretical physics",
    McGraw-Hill, New York, 1953.

73. Morse, R. W.
    "Velocity of compressional waves in rods of rectangular
    cross section",
    J. Acoust. Soc. of America, Vol. 22(2), pp. (219-223),
    1950.

74. Morse, R. W.
    "Dispersion of compressional waves in isotropic rods
    of rectangular cross section",
    J. Acoust. Soc. of America, Vol. 20 (6), pp. (833-838),
    1948.

75. Oliver, J.
    "Elastic wave dispersion in cylindrical rod by a
    wide-band short-duration pulse technique",
    J. Acoust. Soc. of America, Vol. 29(2), pp. (189-194),
    1957.

76. Onoe, M.
"Contour vibrations of isotropic circular plates",
J. of the Acoustical Soc. of America, Vol. 28(6),
pp(1158-1162), 1956.

77. Onoe, M.
"Gravest contour vibration of thin anisotropic
circular plates",
J. of the Acoustical Soc. of America, Vol. 30(7),
pp. (634-638), 1956.

78. Onoe, M.
"Contour vibrations of thin rectangular plates",
J. of the Acoustical Soc. of America, Vol. 30(12),
pp.(1159-1162), Dec. 1958.

79. Onoe, M.
"Frequency of edge mode of isotropic thin rectangular
plate, circular disk and rod",
J. of the Acoustical Soc. of America, Vol. 33,
pp. (1627), 1961.

80. Onoe, M., McNiven, H. D. and Mindlin, R. D.
"Dispersion of axially symmetric waves in elastic rods",
J. of Applied Mechanics, Trans. of ASME, pp.(729-734),
1962.

81. Onoe, M. and Pao, Y. H.
"Edge mode of thin rectangular plate of Barium Titanate"
J. of the Acoustical Soc. of America, Vol. 33, pp.(1628)
1961.

82. Onoe, M. and Tiersten, H. F.
"Resonant frequencies of finite piezoelectric ceramic
vibrators with high electromechanical coupling",
IEEE Trans. on Ultrasonic Engineering, Vol. EV-10 (1),
pp. (32-39), 1963.

83. Onoe, M., Tiersten, H. and Heitzler, A. H.
"Shift in the location of resonant frequencies caused
by large electromechanical coupling in thickness-mode
resonators",
J. of the Acoustical Soc. of America, Vol. 35 (1),
pp. (36-40), 1963.

84. Papadakis, E. P. and Bernstein, H.
"Elastic moduli of Pyrolytic Graphite",
J. of the Acoustical Soc. of America, Vol. 35(4),
pp. (521-524), 1963.

85. Poisson, S. D.
"Memoire sur l'equilibre et le mouvement des corps
elastiques",
Momoire de l'Academic de Paris, Vol. 8, 1829.

86. Pollard, H. F.
"Resonant behaviour of an acoustic transmission line",
Anst. J. Physics, Vol. 15, pp. (513-526), 1962.

87. Ramanamurty, P. V. and Ramamurti, V.
"Longitudinal elastic wave propagation in rods - a
review",
J. of Aeronautical Society of India, Vol. 28(2),
pp.(207-212), 1976.

88. Rayleigh, Lord.
"Theory of sound",
2nd Edition, Dover Publication, New York, 1945.

89. Rayleigh, Lord.
"On the free vibrations of an infinite plate of
homogeneous isotropic elastic matter",
Proc. of London Math. Soc., Vol. 20, pp. (225-234), 1889

90. Rayleigh, Lord.
"On waves propagated along the plane surfaces of an
elastic solid",
Proc. of London Math. Soc., vol. 17, pp. (4-11), 1855.

91. Reynolds, W. N. and Wilkinson, S. J.
"The analysis of fibre-reinforced porous composite
materials by the measurement of ultrasonic wave
velocities",
Ultrasonic, Vol. 16, pp. (159-163), July, 1978.

92. Sharp, J. C. K.
"A theoretical and experimental investigation into
the spectra of selected resonators",
Ph.D. thesis, Dept. of Elect. and Electro. Eng.,
University of Aston in Birmingham, 1974.

93. Shaw, A. E. G.
"On the resonant vibrations of thick Barium Titanate disks",
J. of the Acoustical Soc. of America, Vol. 28,
pp. (38-50), 1956.

94. Silk, M. G., Lidington, B. H. and Hammond, G. F.
"A time domine approach to crack location and sizing in austenitic welds",
British J. of NDT, Vol. 22(2), pp. (55-61), 1980.

95. Southwell, R. V.
"An introduction to the theory of elasticity for engineers and physicists",
2nd Edition, Clarendon Press, Oxford, 1941.

96. Sykes, R. A.
"Modes of motion in Quartz crystals, the effect of coupling and methods of design",
Quartz Crystals for Electrical Circuits, Edited by R. A. Heising, Van Nostrand, New York, pp.(205-248), 1946.

97. Tiersten, H. F.
"Wave propagation in an infinite piezoelectric plate",
J. of Acoustical Soc. of America, Vol. 35(2),
pp. (234-239), 1963.

98. Tiersten, H. F.
"Thickness vibrations of piezoelectric plates",
J. of Acoustical Soc. of America, Vol. 35(1),
pp. (53-56), 1963.

99. Tomlinson, J. R., Wagg, A. R. and Whittle, M. J.
"Ultrasonic inspection of austenitic welds",
British J. of NDT, Vol. 22(3), pp. (119-127), 1980.

100. Viktorov, I. A.
"Rayleigh and Lamb waves",
Plenum Press, New York, 1967.

101. Young, D.
"Vibration of rectangular plates by the Ritz method",
J. of Applied Mechanics, Vol. 17, pp. (448-453), 1950.